Aus dem Frauenklinik

Molekularbiologie und Biochemie der Reproduktionsmedizin

der Medizinischen Fakultät

der Universität des Saarlandes, Homburg/Saar

Human sperm chromatin condensation assessment using Raman spectroscopy and its impact on ICSI induced fertilization and embryonic development

Dissertation zur Erlangung des Grades eines Doktors der Naturwissenschaften

der Medizinischen Fakultät

der UNIVERSITÄT DES SAARLANDES

2020

vorgelegt von: Mohammadalaa Al-Dean Younis Jahmani

geb. am: 23.08.1979 in Jordan

Tag der Promotion: 10.12.2020

Dekan: Prof. Dr. Med. Michael D. Menger

Berichterstatter: Prof. Dr. Mohamed Hammadeh

Prof. Dr. Gabriela Krasteva-Christ

Dr. Stephan Maxeiner

Abstract

The status of human sperm chromatin has become an important parameter in male fertility evaluation. Chromatin condensation of the sperm genome is necessary for the reproduction process. It causes inactivation of most of the spermatid's genes and protects DNA from chemical and physical damage. It is evident that the typical composition of sperm chromatin is fundamental to maintain DNA integrity and therefore its ability to fertilize the egg. Fertilization with sperm that possess improper chromatin condensation may have a negative effect on early embryonic growth or lead to the development of genetic diseases. Chromatin condensation evaluation using the current methods is based on staining procedures, rendering the assessed sample unusable for assisted reproductive technology procedures. The current study aims to evaluate the ability of Raman spectroscopy as a non-invasive technique to detect any chemical changes in the normal morphology sperm that are usually selected and used during the intracytoplasmic sperm injection (ICSI) procedure. In addition, the protamine deficiency, histone retention, DNA fragmentation, ICSI outcomes and semen parameters were also assessed and tested for correlation with the obtained Raman spectral data or Raman quantitative parameters. Sperm samples of 85 donors were evaluated. Donor consent and approval from an Ethics Committee were given.

The Raman peaks at 1098 cm^{-1}, 1334 cm^{-1}, 1372 cm^{-1} and 1532 cm^{-1} show a significant difference between the fertile and sub-fertile groups. The Raman peaks at 670 cm^{-1}, 731 cm^{-1}, 785 cm^{-1}, 1062 cm^{-1}, 1098 cm^{-1}, 1185 cm^{-1}, 1372 cm^{-1}, 1424 cm^{-1}, 1450 cm^{-1}, 1532 cm^{-1}, 1618 cm^{-1} and 1673 cm^{-1} show a significant difference between the CMA3≤41 and CMA3>41 groups. The Raman peaks at 670 cm^{-1}, 731 cm^{-1}, 1062 cm^{-1}, 1098 cm^{-1}, 1185 cm^{-1}, 1372 cm^{-1}, 1424 cm^{-1}, 1618 cm^{-1} and 1673 cm^{-1} show a significant difference between the CMA3<28, 28≤CMA3≤50 and CMA3>50 groups. The CMA3-numbers indicate the percentage of stained cells.

The relative DNA content, DNA/protein ratio and protein content standard deviation show a significant difference between the fertile and sub-fertile groups. The relative protein content, relative DNA content, DNA/protein ratio and protein standard deviation show a significant difference between the CMA3≤41 and CMA3>41 groups. The relative protein content, relative DNA content, DNA/protein ratio and protein standard deviation show a significant difference between the CMA3<28, 28≤CMA3≤50 and CMA3>50 groups.

Protamine deficiency, evaluated by chromomycin A3 staining, was significantly correlated with the relative protein content, relative DNA content, DNA/protein ratio and protein standard deviation. Histone retention, evaluated by aniline blue staining, was significantly correlated with the relative protein content, relative DNA content, DNA/protein ratio, protein standard deviation, DNA standard deviation and DNA/protein

ratio standard deviation. DNA fragmentation that was evaluated by acridine orange staining was significantly correlated with the relative protein content, relative DNA content, DNA/protein ratio, protein standard deviation, DNA standard deviation and DNA/protein ratio standard deviation.

The fertilization rate was significantly correlated with the relative protein content, relative DNA content, DNA/protein ratio, protein standard deviation, DNA standard deviation and DNA/protein ratio standard deviation. The cleavage score was significantly correlated with the relative DNA content and protein content standard deviation. The embryo development score was significantly correlated with the relative protein content and relative DNA content.

In conclusion, the Raman spectroscopic measurements, both the individual Raman peak analysis or the Raman quantitative parameter analysis, represent a promising diagnostic tool that has the ability to label-free detect sperm with chromatin abnormalities, such as improper chromatin condensation and DNA fragmentation to a certain degree similar to that of the existing staining techniques at the individual cell level. Furthermore, it has the ability to predict estimated ICSI outcomes. The Raman spectral analysis and the Raman quantitative parameters, obtained from normal morphology sperm, showed great differences and variation indicating that Raman spectroscopy has the ability to detect the presence of immature sperm and even some hidden abnormalities resulting from disturbances during spermatogenesis.

Zusammanfassung

Der Zustand des Chromatins im menschlichen Spermium wird ein immer wichtigerer Parameter in der Diagnostik der männlichen Fertilität. Die Kondensation der DNS des Spermiengenoms in das Chromatin ist ein notwendiger Vorgang für den Fortpflanzungsprozess. Es deaktiviert die meisten Gene im Spermatid und schützt die DNS vor schädlichen chemischen und physikalischen Einflüssen. Es ist offensichtlich, dass die typische Zusammensetzung des Chromatins des Spermiums von großer Bedeutung für die Integrität des Genoms und damit für die spätere Fähigkeit zur Befruchtung ist. Eine Befruchtung durch ein Spermium mit fehlerhafter Chromatinstruktur kann negative Auswirkungen auf die frühe embryonale Entwicklung haben oder zu genetischen Defekten führen. Heutzutage basiert die Untersuchung der Kondensation des Chromatins auf Färbemethoden, die aber die untersuchten Zellen für eine Weiterverwendung zum Zwecke der künstlichen Befruchtung unbrauchbar machen. Diese Arbeit hat daher zum Zwecke die Raman-Spektroskopie als eine nichtinvasive Methode zur Untersuchung der chemischen Zusammensetzung des Chromatins von morphologisch normalen Spermien, wie man sie zur künstlichen Befruchtung mit Hilfe der ICSI einsetzt, zu evaluieren. Zusätzlich wurden Protamindefizienz, Histonrückhaltung, DNS-Fragmentierung, ICSI Erfolg sowie Sperma-Parameter aus dem Spermiogramm untersucht und auf Korrelation mit ramanspektroskopischen Daten oder den Parametern eines quantitativen parametrischen Modells der Spektren getestet. Es wurden Spermien von 85 Versuchsteilnehmern untersucht. Die Spender haben der Teilnahme zugestimmt. Es liegt positives Votum der zuständigen Ethikkommission vor.

Die Raman Peaks bei 1098 cm^{-1}, 1334 cm^{-1}, 1372 cm^{-1} und 1532 cm^{-1} zeigen einen signifikanten Unterschied zwischen der fertilen und der subfertilen Spendergruppe. Die Ramanpeaks bei 670 cm^{-1}, 731 cm^{-1}, 785 cm^{-1}, 1062 cm^{-1}, 1098 cm^{-1}, 1185 cm^{-1}, 1372 cm^{-1}, 1424 cm^{-1}, 1450 cm^{-1}, 1532 cm^{-1}, 1618 cm^{-1} und 1673 cm^{-1} zeigen einen signifikanten Unterschied zwischen der CMA3≤41 und der CMA3>41 Spendergruppe. Die Ramanpeaks bei 670 cm^{-1}, 731 cm^{-1}, 1062 cm^{-1}, 1098 cm^{-1}, 1185 cm^{-1}, 1372 cm^{-1}, 1424 cm^{-1}, 1618 cm^{-1} und 1673 cm^{-1} zeigen einen signifikanten Unterschied zwischen den Spendergruppen CMA3<28, 28≤CMA3≤50 und CMA3>50. Die CMA3-Zahlen entsprechen dem prozentualen Anteil an CMA3-gefärbten Zellen der jeweiligen Spender der Gruppe.

Der relative DNS-Gehalt, DNS-zu-Protein-Verhältnis, sowie die Standardabweichung des Protein-Gehalts zeigen einen signifikanten Unterschied zwischen der fertilen und der subfertilen Spendergruppe. Der relative Protein-Gehalt, relativer DNS-Gehalt, DNS-zu-Protein-Verhältnis, sowie die Standardabweichung des Protein-Gehalts zeigen einen signifikanten Unterschied zwischen der CMA3≤41 und der CMA3>41 Spendergruppe. Der relative Protein-Gehalt, relativer DNS-Gehalt, DNS-zu-Protein-Verhältnis, sowie die Standardabweichung des Protein-Gehalts zeigen einen signifikanten Unterschied zwischen den CMA3<28, 28≤CMA3≤50 und CMA3>50 Spendergruppen.

Protamindefizienz, untersucht mit einer Chromomycin-A3-Färbung, korreliert signifikant mit dem relativen Protein-Gehalt, relativem DNS-Gehalt, DNS-zu-Protein-Verhältnis, sowie der Standardabweichung des Protein-Gehalts. Histonrückhaltung, untersucht mit einer Anilin-Blau-Färbung, korreliert signifikant mit dem relativen Protein-Gehalt, relativem DNS-Gehalt, DNS-zu-Protein-Verhältnis, der Standardabweichung des Protein-Gehalts, der Standardabweichung des DNS-Gehalts, sowie der Standardabweichung des DNS-zu-Protein-Verhältnisses. DNS-Fragmentierung, untersucht mit einer Acridin-Orange-Färbung, korreliert signifikant mit dem relativen Protein-Gehalt, relativem DNS-Gehalt, DNS-zu-Protein-Verhältnis, der Standardabweichung des Protein-Gehalts, der Standardabweichung des DNS-Gehalts, sowie der Standardabweichung des DNS-zu-Protein-Verhältnisses.

Die Befruchtungsrate korreliert signifikant mit dem relativen Protein-Gehalt, relativem DNS-Gehalt, DNS-zu-Protein-Verhältnis, der Standardabweichung des Protein-Gehalts, der Standardabweichung des DNS-Gehalts, sowie der Standardabweichung des DNS-zu-Protein-Verhältnisses. Der Teilungsscore korreliert signifikant mit dem relativem DNS-Gehalt, sowie der Standardabweichung des Protein-Gehalts. Der Embryonenscore korreliert signifikant mit dem relativem Protein-Gehalt sowie dem relativen DNS-Gehalt.

Zusammenfassend lässt sich sagen, dass die Ramanspektroskopie, sowohl in Form einer einfachen Peakanalyse als auch in Form eines quantitativen parametrischen Modells, eine vielversprechende Methode darstellt, die ähnlich zu den etablierten Färbemethoden in der Lage ist Veränderungen im Chromatin einzelner Spermien ohne vorherige Markierung zu untersuchen. Zusätzlich ist sie in der Lage den Erfolg einer ICSI-Behandlung vorab abzuschätzen. Die Raman-Spektren und die Parameter des quantitativen parametrischen Modells morphologisch normaler Spermien weisen eine große Varianz und deutliche Unterschiede auf. Dies deutet darauf hin, dass die Ramanspektroskopie in der Lage ist, unreife Spermien sowie verdeckte Anomalitäten auf Grund von Störungen während der Spermatogenese zu detektieren.

Dedication

To my parents

Table of Contents

List of figures

List of tables

Abbreviations

AB	Aniline Blue
ABP	Androgen-Binding Protein
AO	Acridine Orange
ART	Assisted Reproductive Technology
CCD	Charge-Coupled Device
CMA3	Chromomycin A3
DGC	Density Gradient Centrifugation
DNA	Deoxyribonucleic Acid
FSH	Follicle-Stimulating Hormone
GnRH	Gonadotrophin-Releasing Hormone
HA	Hyaluronic Acid
HOS	Hypo-Osmotic Swelling
ICSI	Intracytoplasmic Sperm Injection
IMSI	Intracytoplasmic Morphologically Selected Sperm Injection
IR	Infrared
IVF	In Vitro Fertilization
LH	Luteinizing Hormone
MACS	Magnetic-Activated Cell Sorting
Micro-TESE	Microdissection Testicular Sperm Extraction
mRNA	Messenger Ribonucleic Acid
MSOME	Motile Sperm Organellar Morphology Examination
P1	Protamine 1
P2	Protamine 2
PBS	Phosphate-Buffered Saline
PIXE	Particle Induced X-ray Emission
Pre-P2	Protamine 2 Precursors
PS	Phosphatidylserine
ROC	Receiver Operating Characteristics
ROS	Reactive Oxygen Species
TUNEL	Terminal Deoxynucleotidyl transferase dUTP Nick End Labeling
UV	Ultraviolet
WHO	World Health Organization
ZP	Zona Pellucida

1 Introduction

1.1 Male infertility

According to the World Health Organization (WHO)'s criteria, infertility is the inability of couples of a reproductive age to achieve pregnancy during one year in spite of unprotected intercourse (Evgeni *et al*., 2014; Zegers-Hochschild *et al*., 2009; Gurunath *et al*., 2011). Roughly, 10 to 15 percent of couples worldwide have infertility problems. Female factors account for 35-40% of cases, and male factors for about 20-40% of cases, while 20-30% of cases are assumed to be caused by both partners or due to unexplained reasons in the remaining cases (de Kretser, 1997; Jose-Miller *et al*., 2007).

1.1.1 Etiology of male infertility

Male infertility can be caused by several factors that can be categorized into two major types obstructive infertility and non-obstructive infertility (Nardelli *et al*., 2014). Obstructive infertility, representing 40% of the cases, it occurs as a result of physical blockage in the sperm delivery duct. Normal sperm are being produced during normal spermatogenesis, accompanied by normal luteinizing hormone (LH) and follicle-stimulating hormone (FSH) functions (Baker and Sabanegh, 2013; Hamada *et al*., 2013; Wosnitzer *et al*., 2014). In general, obstructive infertility can be occurred as a result of several factors, including sexual problems as premature ejaculation (Lotti *et al*., 2012), genetic diseases such as cystic fibrosis, structural problems such as testicle blockage, obstruction of ejaculatory tract, damage to the any part of the male reproductive organs or inflammation of the epididymis, prostate or seminal vesicles (Wosnitzer *et al*., 2014). Non-obstructive infertility is responsible for 60% of the cases. It occurs as a result of problems associated with sperm production and function, accompanied by abnormal LH and FSH levels (Kumar, 2013; Wosnitzer *et al*., 2014). Non-obstructive infertility can be occurred as a result of several factors, including genetic defects, developmental problems, cryptorchidism, radiation, chemotherapy, infections or varicoceles (Wosnitzer *et al*., 2014). Male infertility can also be occurred as a result of several other factors including obesity (Fode *et al*., 2012; Harlev *et al*., 2015), or wearing tight underwear that increases scrotum temperature (Jung and Schuppe 2006), Cigarette smoking, alcohol consumption, anabolic steroids abuse (Naz and Kamal, 2017) or increased exposure to environmental factors, including pesticides and radiation (Jensen *et al*., 2006; Pizent *et al*., 2012). However, more than 30% of male infertility with reduced semen parameter values remains unexplained and is diagnosed as idiopathic (Naz and Kamal, 2017).

1.1.2 Diagnosis of male infertility

Male infertility diagnosis includes case history, physical examination and semen analysis. Regardless of the imperfections of semen analysis, it is still the fundamental diagnostic procedure in male infertility evaluation (Barratt, 2007). The diagnostic process to assess all semen parameters in the ejaculated sample

has to be carried out according to strict standards (WHO 2010). Despite the fact that this test provides valuable data for the initial assessment of infertile men, it is not a good assay for fertility because it does not provide any valuable data about the ability of the sperm to fertilize the oocyte (Jequier, 2010). According to the World Health Organization (WHO 2010) guidelines, semen analysis mainly includes the evaluation of the main semen parameters, including sperm morphology, concentration and motility in addition to semen volume, viscosity and pH (Patil *et al*., 2013; Vasan, 2011). Distinguishing between fertile and infertile men is based on standard threshold values for each of the semen parameters. An ejaculate should yield semen parameters above these standard thresholds in order to be classified as normal (fertile). If any values are below their corresponding threshold, the patient will be classified according to different pathological conditions depending on the affected parameters, as illustrated in Table 1.1. The determination of semen parameters, according to the WHO, is based on the analysis of 100-200 sperms using light microscopy. Consequently, it is a biased procedure with high levels of variation within and between laboratories (Cooper *et al*., 1992; Neuwinger *et al*., 1990). These issues reduce the predictive potential of the WHO analysis, as seen in several cases that showed normal spermograms but were actually infertile (Singh and Jaiswal, 2011; Bonde *et al*., 1998). Another disadvantage of the diagnostic procedure, according to WHO standards, is that it does not evaluate all the relevant sperm quality aspects (Guzick *et al*., 2001; Bonde *et al*., 1998).

Table 1.1: Semen parameters according to WHO 2010
Pathological conditions related to standard threshold values of the semen parameters.

Pathological condition	Standard threshold
Oligozoospermia	Sperm concentration less than $15*10^6$/ml; Total sperm count less than $39*10^6$
Asthenozoospermia	Progressive motility less than 32%
Teratozoospermia	Normal morphology sperm less than 4%
Oligo-astheno-teratozoospermia	Presence of the above three conditions
Azoospermia	Absence of sperm in the ejaculate
Cryptozoospermia	Absence of sperm in the fresh ejaculate, but found in the centrifuged pellet
Aspermia	Absence of ejaculate

1.2 Spermatogenesis

In humans, as in any other mammals, sperms are produced by a unique, multistep and complex process called spermatogenesis (D'Occhio *et al*., 2007). This process includes physiological, biochemical and morphological modifications that turn diploid spermatogonial cells into completely differentiated haploid sperm (D'Occhio *et al*., 2007). Sperm are highly specialized cells that carry on the male chromatin during sexual reproduction. They can fertilize the oocyte and transfer the male chromatin to the next generation (Boe-Hansen *et al.,* 2006; Cebesoy *et al.,* 2006; Bungum *et al.,* 2007). Spermatogenesis occurs in the testis seminiferous tubules. It is a continuous process that lasts throughout the reproductive age. It is maintained

by a special population of spermatogonial cells, called type A spermatogonia or spermatogonial stem cells. These are adult stem cells that do not exhibit heterochromatin (De Rooij and Russell, 2000).

The spermatogenesis process is controlled mainly by two hormones, secreted from the interior pituitary gland, namely, the luteinizing hormone (LH) and the follicle-stimulating hormone (FSH). These hormones are secreted under the control of the hypothalamus through the gonadotrophin-releasing hormone (GnRH). The luteinizing hormone (LH) induces testosterone production in the Leydig cells that are found in the interstitial space (Payne *et al*., 1980; Ewing and Keeney, 1993). The follicle-stimulating hormone (FSH) induces the Sertoli cells in the seminiferous tubule lining to secrete the androgen-binding protein (ABP). ABP binds to testosterone and increases its concentration in the seminiferous tubules and stimulates the spermatogonial cell to divide and finally produce mature sperm (Griswold, 1995; Ma *et al*., 2015).

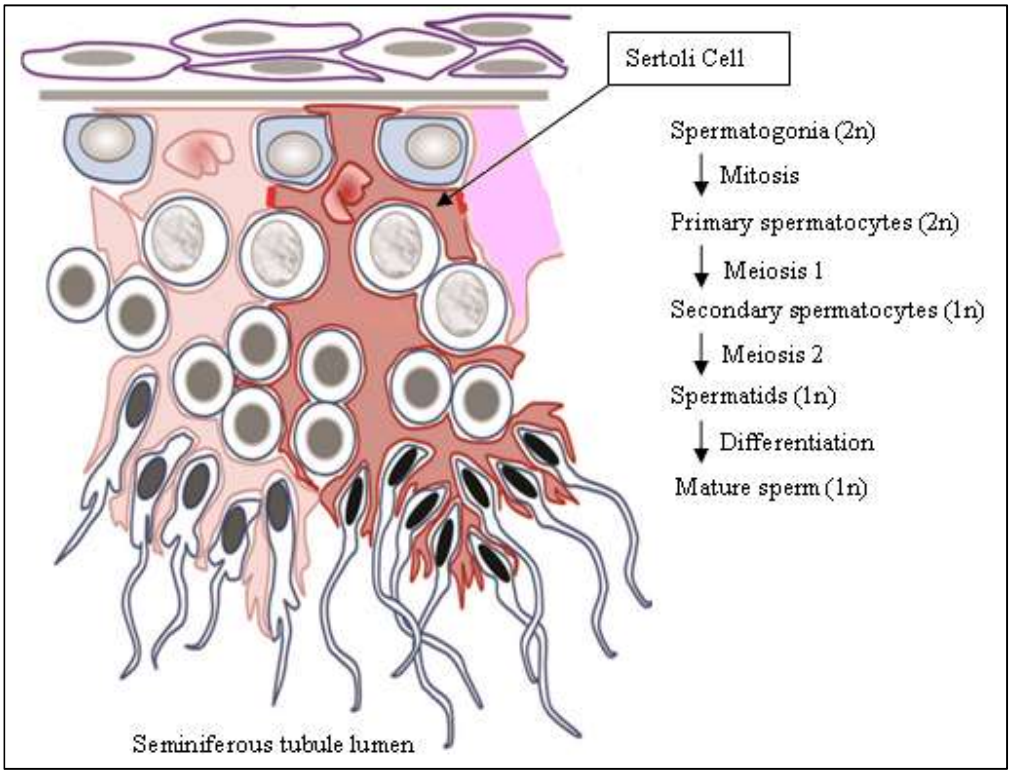

Figure 1.1: Diagrammatic Representation of Spermatogenesis. (Adapted from Hunter *et al.,* 2012).

Spermatogenesis is mainly divided into the following three phases: spermatocytogenesis, meiosis and spermiogenesis (D'Occhio *et al*., 2007). As illustrated in Figure 1.1 spermatocytogenesis includes the mitotical division of the undifferentiated type A spermatogonial cells to replace themselves and to produce cells called type B spermatogonia. These proceed to the next stage of spermatogenesis. The last spermatogonial division result in cells, called primary spermatocytes, which undergo meiosis to produce the secondary spermatocytes by meiosis 1 and spermatids by meiosis 2. The resulting spermatids can be categorized into the following types according to their maturation levels: an early spermatid with a circular

nucleus, an intermediate spermatid with an elongated nucleus and a mature spermatid with a condensed nucleus (Dadoune, 2003). The final phase of spermatogenesis is called spermiogenesis. It includes the morphological conversion of the early circular spermatids into completely differentiated functional sperm. In these, the nucleus is relatively inactive at the transcriptional level and most of the cytoplasm is discarded as a residual body (Sakkas *et al*., 2002). It starts immediately after the completion of meiosis and involves several morphological changes, including the development of the Golgi complex, mitochondria and the tail. During maturation, the acrosomal vesicle, proximal centriole and axial filament are formed (Sharma, 2007). The chromatin also undergoes a maturation process, starting with the substitution of histone proteins by transitional proteins and finally, through protamine deposition, resulting in sperm with highly condensed chromatin (Kumaroo *et al.,* 1975; Goldberg *et al.,* 1977; Poccia, 1986). This remodeling in the packaging of the sperm genome is necessary for the reproduction process. It causes inactivation of most of spermatid's genes and it is an important stage in the preparation of the male genome for its introduction into the egg (Oliva, 2006).

1.3 Sperm chromatin structure

The chromatin structure and composition of mature sperm completely differ from that of somatic cells (Ward, 1993; Haaf and Ward, 1995; Evenson *et al*., 2002). During the spermatogenesis until the end of meiotic division yielding round spermatids, chromatin packaging in sperm is similar to that of somatic cells and it is made up of histone proteins and DNA organized in the ordinary nucleosome (Evenson, 1999; Balhorn, 2011).

As the spermatocytes start going through meiosis and proceed to the early stages of spermiogenesis, they start to synthesize new, DNA-binding proteins that bind to DNA. This process induces several remodelling steps, changing the organization and the activity of sperm chromatin (Balhron, 2011). This remodelling includes the removal of histone proteins from spermatocytes and early spermatid chromatin and replacing them with transition proteins. Finally, the transition proteins are then removed and replaced with protamines. Protamines are relatively small arginine-rich proteins that are essential in maintaining the final packaging status of sperm chromatin, resulting in a highly condensed and stabilized structure, as illustrated in Figure 1.2 (Kistler *et al*., 1996; Prigent *et al*., 1996; Steger, 1999; Kierszenbaum, 2001; Zhao *et al*., 2001).

The interaction between sperm DNA and protamines occurs in a unique pattern in which sperm DNA is coiled to form a special structure, called toroid or doughnut loops. Each toroidal subunit contains about 50 kb. At the end of the spermiogenesis, the completely mature packed sperm contain around 50000 toroidal subunits (Ward and Coffey, 1991; Balhorn *et al*., 1999; Ward, 2011). The unique coiling of sperm chromatin in the toroidal subunits results in at least a six times higher compaction, compared to that of

somatic cells (Conwell *et al.,* 2003; Hammoud *et al.,* 2009). The unique pattern of sperm chromatin condensation is essential for sperm functioning. It protects the sperm DNA from physical and chemical factors during its journey until reaching the oocyte (Fuentes-Mascorro *et al.,* 2000; D'Occhio *et al.,* 2007).

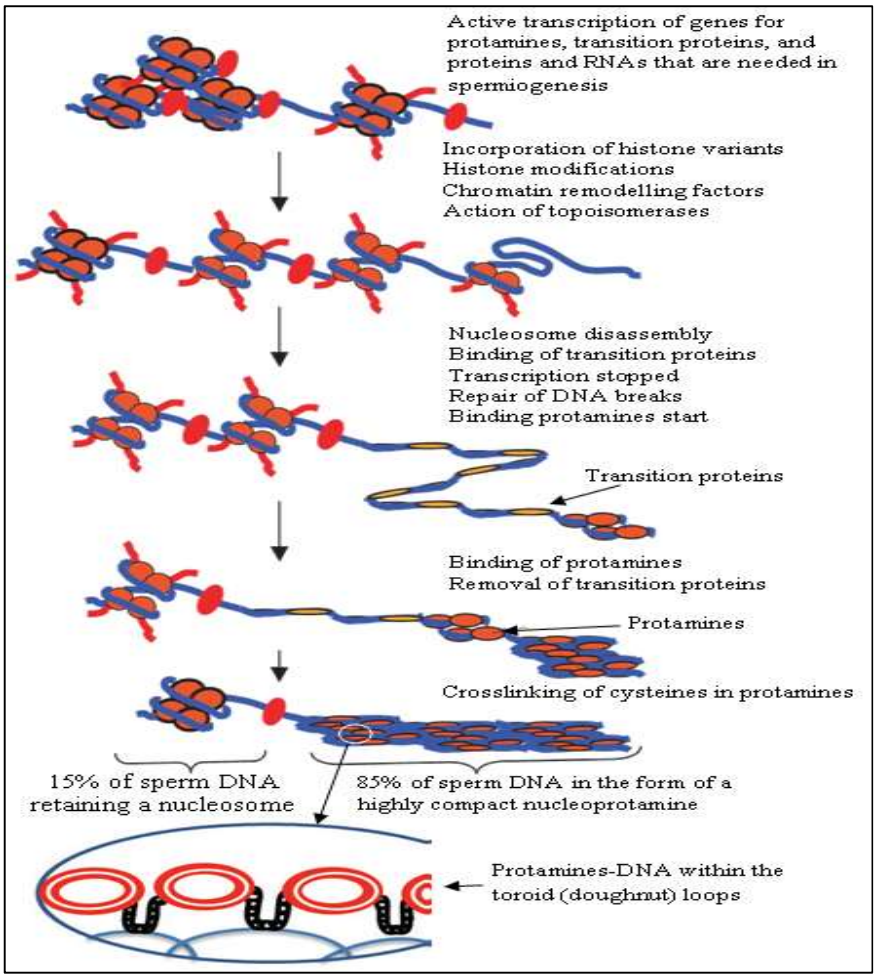

Figure 1.2: Histones replacement by protamine.
Diagrammatic illustration of the major alteration that occur during spermiogenesis, in which the nucleohistone (top) in the form of nucleosome as somatic cells undergoes several modifications resulting in nucleoprotamine complex, in addition to the toroid loops model (Adapted from Oliva, 2006; Rahman *et al*., 2013).

The exact interaction between sperm DNA and protamines is not yet fully understood. However, there are several suggestions to explain this interaction. Pogany suggested protamine links to the major groove of the DNA helix (Pogany *et al*., 1981), while D'Auria proposed protamines linking major and minor grooves (D'Auria *et al*., 1993), and Bianchi described protamines being linked electrostatically to the negatively charged phosphate group of the DNA (Bianchi *et al*., 1994). All of these suggestions share the premise that the positively charged protamines permit the neutralization of negatively charged DNA. Protamines constitute about 85% of the total proteins in the mature sperm nucleus. Two main types of protamines are

found in the sperm nucleus, namely, protamines 1 and 2. Protamines 1 and 2 are expressed in a ratio approximately equal to 1 in fertile men (Bench *et al.,* 1996; Carrell and Liu, 2001; Torregrosa *et al.,* 2006; Oliva, 2006). The remaining 15% of mature sperm nuclear proteins are retained histones. Histones are a less basic protein compared to protamine but they nevertheless play an essential role in reducing the compaction of sperm chromatin and initiate the decondensation of sperm chromatin after fertilization. The retained histones are therefore essential for sperm functioning and for early embryo development (Wykes and Krawetz, 2003; Rajender *et al.,* 2011).

1.4 The importance of sperm chromatin condensation in male fertility

The status of human sperm chromatin becomes an important parameter in male fertility evaluation. Chromatin packaging of the sperm genome is necessary for the reproduction process. It causes inactivation of most of the spermatid's genes and it is an important stage in the preparation of the male genome to be introduced into the egg (Oliva, 2006). This unique packaging also protects DNA from chemical and physical damage, which makes the male genome unreachable by the reactive oxygen species (ROS), or by any other internal or external factors (Barone *et al*., 1994; Braun, 2001). Nowadays, it is evident that the typical composition of sperm chromatin is fundamental in maintaining the DNA integrity (Cho *et al*., 2003). Any defect in sperm chromatin will probably have a severe effect on sperm DNA integrity and its ability to participate in the fertilization process. Fertilization with sperm that possess improper DNA packaging may have a negative result on early embryonic growth or lead to the development of genetic diseases. However, in 50 to 70% of the cases, the sperm of infertile males contains improperly packaged DNA (De Yebra *et al*., 1993). Sperm chromatin quality is clearly necessary for sperm function and later normal embryonic development. As a result, any abnormalities in the sperm chromatin structure are associated with natural reproductive failure, such as spontaneous miscarriage and also failure of assisted reproduction procedures (Boe-Hansen *et al*., 2006; Cebesoy *et al*., 2006; Bungum *et al*., 2007). Semen samples showing a high level of chromomycin A3 (CMA3) stained sperm are negatively correlated with the fertilization rate during the intracytoplasmic sperm injection (ICSI) procedure (Sakkas *et al*., 1998). It has also been demonstrated that CMA3 staining is a valuable predictor of the *in vitro* fertilization (IVF) outcome (Tarozzi *et al*., 2009). It has also been reported that the chromatin condensation evaluation by aniline blue staining can predict the IVF outcome (Hammadeh *et al*., 1998).

1.5 Abnormal chromatin packaging

Spermiogenesis ends up with the production of fully packed sperm chromatin. However, abnormalities can occur at any stage of this process; the most widely recognized issues are due to an abnormal DNA loop domain or the replacement of histones by protamines (D'Occhio *et al*., 2007).

1.5.1 Abnormal DNA loop domain

An abnormal DNA loop domain occurs as a normal step during the sperm maturation process. This is because the toroid formation develops torsional stress, which is reduced by DNA strand nicks (Marcon and Boissonneault, 2004). These strand nicks are created mainly during the developmental stages from round to elongated spermatids. They facilitate the histone replacement by transition proteins and later by protamines. Strand nicks occur and are ligated by a specific enzyme, called topoisomerase II (Sakkas *et al*., 1999; Henkel *et al*., 2004; McPherson and Longo, 1993). Consequently, any factors that affect topoisomerase II activity, such as inhibitors, could result in abnormal chromatin condensation and increase the probability of DNA breaks in the mature sperm (Lewis and Aitken, 2005). Thus, the presence of DNA strand nicks in mature sperm can be considered as an indication of both incomplete sperm maturation and abnormalities during chromatin packaging at spermiogenesis (Manicardi *et al*., 1995).

1.5.2 Replacement of histones by protamines

As mentioned before, two main types of protamines are expressed in human sperm, protamines 1 and 2. The ratio of these two proteins is a key factor for sperm fertilization capability (Aoki *et al*., 2006a; Carrell *et al*., 2007). Protamine 2 precursors (pre-P2) are assumed to play a central role in maintaining this ratio. Any change in the expression levels of pre-P2 leads to anomalous sperm morphogenesis and decreased sperm motility and affects the sperm fertilization capability (Torregrosa *et al*., 2006; Tseden *et al*., 2007). Furthermore, the number of disulfide bonds between the sulfhydryl (SH) group of neighbouring protamine chains plays a role in the sperm chromatin stability (D'Occhio *et al*., 2007; Dadoune, 2003). This stabilization of sperm chromatin is initiated in the testis and is maintained during its transit through the epididymis (Dadoune, 2003). During sperm migration through the epididymis, the cysteine SH-group gradually oxidizes to disulfide bonds, leading to a more stabilized and more compacted DNA protamine complex (Love and Kenney, 1999; Brewer *et al*., 2002, 2003). Consequently, defects at any stage of this process may result in abnormal sperm packaging.

Actually, one of the most significant consequences of abnormal sperm chromatin packaging is increased susceptibility to DNA fragmentation (Carrell *et al*., 2007). This has been confirmed in several studies that have shown there is indeed a correlation between protamine deficiency as an indicator of abnormal chromatin packaging with the presence of fragmented sperm DNA (Aoki *et al*., 2005; Nasr-Esfahani *et al*., 2005; Aoki *et al*., 2006b; Torregrosa *et al*., 2006). This observation is particularly important, because both DNA fragmentation and abnormal chromatin packaging are associated with reduced male reproductive potential, both in natural and in assisted reproduction (Oliva, 2006; and Tarozzi *et al*., 2007).

1.6 Assay of sperm chromatin integrity

Several laboratory tests to assess sperm chromatin integrity (Erenpreiss *et al*., 2004; Chan *et al*., 2001) have been described. These tests are considered to be valuable diagnostic tools for fertilization rate prediction, both in assisted reproductive technology (ART) methods and in natural reproduction (Sadeghi *et al*., 2009). These tests depend on the staining of sperm with a fluorescent or non-fluorescent dye, followed by a light or fluorescent microscopy assessment to determine the fraction of stained or unstained sperm (Hekmatdoost *et al*., 2009). However, observational assessments by researchers seem to show high variations, resulting in controversial results regarding the correlation between sperm chromatin integrity and the fertilization rate (Sadeghi *et al*., 2009; Hodjat *et al*., 2008). Several studies, based on ICSI procedure, indicate that abnormal sperm chromatin integrity affects fertilization rate and embryo development (Shoukir *et al*., 1998; Larson *et al*., 2000; Razavi *et al*., 2003; Velez *et al*., 2008). Other studies, also based on ICSI, show that abnormal sperm chromatin integrity does not affect either fertilization rates or embryo development (Hammadeh *et al*., 1996; Lin *et al*., 2008).

1.6.1 Chromomycin A3 staining

Chromomycin A3 (CMA3) is a natural fluorochrome produced by the bacterium *Streptomyces griseu*, which binds specifically to the guanine-cytosine-rich sequences in the DNA molecule. It is used to estimate the protamine deficiency in sperm chromatin indirectly, because it competes with protamines to bind to specific binding sites in the DNA sequence. CMA3 binds to the minor groove in the guanine-cytosine-rich sequence in the absence of protamines, specifically it binds the DNA as the Mg^{+2}-coordinated dimer. This binding triggers a conformational disturbance in the DNA sequence, creating a shallower but wider minor groove in the binding site (Gao and Patel, 1990; Gao *et al*., 1992). The assessment of CMA3 staining is performed by differentiating the sperm that is a fluorescent bright yellow versus that which is a dull yellow, and then determining the percentage of stained sperm (bright yellow) in the sample under analysis. High levels of Chromomycin A3 staining are consequently considered to be a strong indication of protamine deficiency (Manicardi *et al*., 1995). The disadvantage of this staining method is that it estimates the protamine deficiency but without distinguishing between P1 and P2. Polyacrylamide gel electrophoresis can address this problem (Oliva, 2006).

1.6.2 Aniline blue staining

Aniline blue (AB) is an acidic stain, that used to differentiate between sperm with mature chromatin having an arginine/cysteine-rich protamines and sperm with immature chromatin having lysine-rich histones (Hofmann and Hilschler, 1991). This differentiation is based on the ability of this stain to react and bind specifically to the lysine amino-acid in the histones. Histones have a high lysine content, and protamines have a high arginine and cysteine content. As the nucleus of immature sperm is rich in histones, it will

preferentially bind with the blue stain due to the abundance of lysine. The nucleus of mature sperm is rich in protamines with a low lysine content but a high arginine and cysteine content, yielding an unstained nucleus (Hammadeh *et al.,* 2001).

1.6.3 Acridine orange staining

Acridine orange (AO) is a fluorochrome, which intercalates with sperm double-stranded DNA in a monomeric form, while it binds to sperm single-stranded DNA in an aggregated form. Acridine orange is a metachromatic dye, based on this property this dye is used to detect the integrity of sperm DNA by distinguishing between the normal sperm with double-stranded DNA (intact DNA) and abnormal sperm with single-stranded DNA (fragmented DNA) (Tejada *et al*., 1984). The binding of the acridine orange monomeric form with native normal double-stranded DNA results in green fluorescence, while the acridine orange aggregated form binds to the denatured single-stranded DNA, resulting in a fluorescent colour range from yellow to red. During the acridine orange procedure sperm is treated with acidic pH, resulting in thiols dissociating from the DNA, which leads to an increase in the susceptibility of the DNA to denaturation and to the subsequently acridine orange subsequently competing for anionic binding sites by avoiding nonspecific aggregation (Angelopoulos *et al*., 1998). Using acridine orange is an inexpensive and simple staining technique, but it is important to take into consideration that colour fading occurs in a relatively short time, and therefore immediate evaluation is required (Duran *et al*., 1998).

1.7 Sperm selection methods:

In natural fertilization fully mature sperm with proper chromatin condensation are selected during their movement through the female reproductive tract (Sadeghi *et al*., 2009). Regardless of the great successes of the intracytoplasmic sperm injection (ICSI) technique in achieving pregnancy in couples suffering from infertility problems (Palermo *et al*., 1992; Tarlatzis *et al*., 1998), it eliminates the natural selection of the mature sperm by bypassing all the physiological barriers through injecting the sperm inside the mature oocyte. Embryologists select the good sperm based mainly on morphology and motility. However, according to the results from several studies, sperm parameters, such as morphology and motility, are actually not a predictor of sperm function or chromatin condensation (Sills *et al*., 2004; Bianchi *et al*., 1996). Based on this selection approach, sperm with hidden anomalies, such as abnormal chromatin condensation or DNA fragmentation, could be inadvertently selected and thereby given the opportunity to participate in fertilization, resulting in negative effects on the early embryonic growth or potentially leading to the development of genetic disease (Huser *et al*., 2009; Sadeghi *et al*., 2009). Based on these findings, it is recommended that sperm should be carefully selected during ICSI.

Depending on the functional characteristics of the sperm, it seems to be mainly the morphology and membrane characteristics that are associated with chromatin integrity. Several methods have been

developed to increase the chance of selecting high quality sperm with mature chromatin. These methods, together with the ICSI procedure, have been used to minimize any inverse effect that may result due to inadvertent oocyte injection with abnormal immature sperm. Nasr-Esfahani *et al*., (2011) summarized the following selection methods:

1.7.1 The hyaluronic acid binding method

Mature sperm that result from normal spermatogenesis express a high number of hyaluronic acid (HA) binding receptors on their membranes. The principle of this method is depending on the ability of the fully developed sperm to bind to a solid HA (Huszar *et al*., 2003). Several studies have investigated the capability of this principle to differentiate between the fully developed and immature sperm. Based on these studies, sperm that bind to solid HA are mature and characterized by normal morphological head, motile, low DNA fragmentation, and condensed chromatin, and they are also able to show acrosomal reaction (Parmegiani *et al*., 2010; Huszar *et al*., 2003; Nasr-Esfahani *et al*., 2011).

1.7.2 The cumulus oophorus passing method

In natural fertilization the fully developed sperm can penetrate the cumulus oophorus complex that surrounds the oocyte, then pass and penetrate the zona pellucida (ZP). The principle of this method is based on this penetration capability. Cumulus oophorus cells are placed in a capillary tube, and sperm that have undergone swim-up are placed in oil and allowed to pass into the opposite side of the capillary tube through the cumulus oophorus cells; the passed sperm can be obtained and used for ICSI procedure (Hong *et al*., 2004). Sperm selected by this method show higher percentage of normal head morphology and a higher protamine content than the unselected sperm (Hong *et al*., 2004; Rijsdijk and Franken, 2007). Furthermore, other studies found that chromatin condensation, acrosome reaction and binding to zona pellucida (ZP) are better in selected sperm compared to unselected sperm (Hong *et al*., 2004; Rijsdijk and Franken, 2007; Franken and Bastiaan, 2009).

1.7.3 The zona pellucida binding method

The principle of this selection method is based on the ability of the fully developed sperm to undergo an acrosomal reaction and its ability to penetrate the zona pellucida (ZP), resulting in successful fertilization (Bastiaan *et al*., 2003; Franken and Oehninger, 2006). In normal ejaculate, only low percentages of sperm have this ability. This percentage is further reduced in the ejaculate of infertile men (Liu *et al*., 2003). In this method, an ICSI needle is used to place the sperm near the oocyte and induce the initial physical contact. In this condition, the mature functional sperm bind to the zona pellucida, and then the ZP-bound sperm are restored and used in the ICSI procedure (Braga *et al*., 2009; Black *et al*., 2010; Liu *et al*., 2011). ICSI outcomes were improved in studies using this method, resulting in an increase in the number of embryos

with a high-quality score (Braga *et al*., 2009; Liu *et al*., 2011), and a good implantation rate (Liu *et al*., 2011).

1.7.4 The motile sperm organellar morphology examination (MSOME) method

The principle of this method is based on a strict morphological assessment of the normal morphology with good motility sperm that are usually selected during the ICSI procedure. This assessment is carried out at a high magnification power (6600X). The acrosome, post-acrosomal lamina, neck, mitochondria, and tail are evaluated as being morphologically normal or abnormal. The nucleus morphological assessment also includes the shape and the chromatin content (Bartoov *et al*., 2002). The combination of this method with the ICSI procedure resulted in a procedure known as Intracytoplasmic Morphologically Selected Sperm Injection (IMSI) (Bartoov *et al*., 2002; Berkovitz *et al*., 2006). Using this method, Nadalini found that the embryo quality and pregnancy rate were enhanced, and the miscarriage rate was decreased (Nadalini *et al*., 2009). Bartoov found that the fertilization and pregnancy rate are highly correlated with the normal sperm nucleus (Bartoov *et al*., 2002).

1.7.5 The zeta potential selection method

The principle of this method is based on the electrical potential of the solid-to-liquid interface of particles due to surface charges. This potential is called 'the zeta potential'. The plasma membrane of the fully developed sperm characterized by zeta potential ranged between -16 to -20 millivolt, which results from the existence of negatively charged sialoglycoproteins. These sialoglycoproteins are added to the sperm membrane through the epididymis maturation process (Ishijima *et al*., 1991; Kirchhoff and Hale, 1996). In this method, sperm are selected by an instrument called a Sperm Sorter, which permits sperm to flow into a plate electrode covered by a porous membrane driven by electrophoresis (Ainsworth *et al*., 2005).

Sperm that are selected by this method show that the normal morphology, chromatin maturation and DNA integrity percentages were higher compared to sperm that are prepared by density gradient centrifugation (DGC) (Chan *et al*., 2006; Kheirollahi-Kouhestani *et al*., 2009; Razavi *et al*., 2010). Ainsworth demonstrated an increased percentage of viability, motility and normal morphology, and a decreased DNA fragmentation in sperm that are selected by the Sperm Sorter instrument (Ainsworth *et al*., 2005). Moreover, a clinical study used density gradient centrifugation, accompanied by this method, to select sperm during the ICSI procedure. They observed a significant increase in fertilization, implantation and pregnancy rate (Kheirollahi-Kouhestani *et al*., 2009).

1.7.6 The membrane integrity assessment method

The principle of this method is based on the plasma membrane integrity and its selective permeability. Plasma membrane integrity is assessed by hypo-osmotic swelling (HOS) procedure. It involves the

incubation of sperm in a hypo-osmotic medium, and then water will cross the intact plasma membrane and enter the sperm until an osmotic equilibrium is reached. Fluids will influx into the sperm with intact membrane resulting in tail bending, a condition known as 'tail curling'. This effect cannot be observed in sperm with an inactive membrane (Jeyendran *et al*., 1984). This method has been used to distinguish between viable and non-viable sperm during the ICSI procedure; the results indicated that the ICSI outcome, including the fertilization and pregnancy rates were correlated with swelling degree (Check *et al*., 2001; Kordus *et al*., 2008). Stanger found that the swelling degree is correlated with DNA fragmentation (Stanger *et al*., 2010).

1.7.7 The magnetic-activated cell sorting (MACS) method

This method can separate intact sperm from those that possess the apoptotic membrane marker phosphatidylserine (PS). Phosphatidylserine is an internal membrane marker of intact sperm but which translocates to the outer membrane in sperm undergoing apoptosis (Martin *et al*., 1995). Based on the external presence of Phosphatidylserine (PS) on the sperm plasma membrane, apoptotic sperm can be selected using superparamagnetic annexin V-conjugated microbeads. Annexin V has a high affinity to PS (Said *et al*., 2006a). A sperm population characterized by a decreased percentage of sperm with external PS and fragmented DNA was selected using this method, accompanied by density gradient centrifugation (Said *et al*., 2006b).

1.8 Raman spectroscopy

1.8.1 Fundamentals of Raman spectroscopy

Raman spectroscopy is a vibrational spectroscopic technique, which depends on the Raman effect. Light can be scattered either due to elastic or inelastic scattering (Raman and Krishnan 1928). The discovery of the Raman Effect was made by the Indian physicist C. V. Raman, who won the Nobel Prize for Physics in 1930 for this discovery. Raman spectroscopy became a widespread technique, which is now commonly used in analytical chemistry for the identification and characterization of molecules from different sources, such as food, minerals and biological samples (Long, 2001; Gregoriou and Braiman, 2005).

When a photon interacts with a particle or a molecule smaller than the incident photon wavelength, it will be scattered in two different ways. The majority of the scattered light known as Elastic or Rayleigh scattering. It has an equal energy and frequency as incident light. No energy exchange between the matter and the incident light is observable after the scatter event. The second category is called inelastic or Raman scattering. The scattered photons are of a different frequency from that of the incident photons due to an energy exchange between the scattering matter and the incident photons. Some photons increase in energy, some decrease. Raman Scattering is very weak. Raman scattered light represents only about 10^{-6} of the total scattered light (Atkins, 2002). This makes is challenging to observe and contributed to its late discovery.

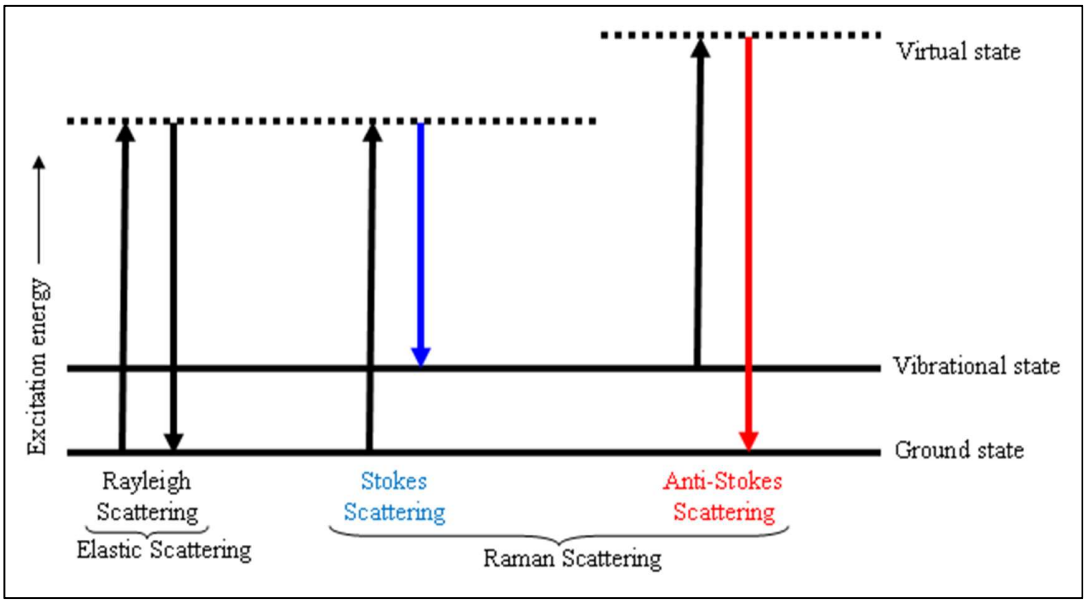

Figure 1.3: Illustrations of Raman scattering.

The exchanged energy should be equivalent to the energy difference between the molecule's excited and ground states. Thus, the photon energy shift represents an alteration in the rotational or vibrational energy of the molecule. If photons are emitted with lower energy and frequency, compared to the incident photons, the scattering is called a Stokes scattering. Stokes scattering occurs when the incident photon loses energy to the molecule situated in the ground state. This energy excites the molecules into a higher virtual state, followed by relaxation to a vibrational level on the ground state. Thus, the emitted photon will be with reduced energy and frequency. If photons are emitted with higher energy and frequency, compared to the incident photon, the scattered light is called Anti-stokes scattering. Anti-stokes scattering are restricted for the molecules that already in the excited vibrational state. Upon the scatter event the molecule will transfer energy to the scattered photon and relax back to its ground state. Thus, the emitted photon will be with higher energy and frequency (Asher, 1993; Banwell and McCash, 2013). These three types of light scattering are illustrated in Figure 1.3.

At room temperature, anti-stokes scattering is less abundant when compared to stokes scattering, because the likelihood of the molecule being in the excitation state is much lower than it being in the ground state. Therefore, stokes photons are the most commonly collected and analyzed photons in Raman scattering. Regardless of the rareness of anti-stokes photons, they are sometimes better suited to analysis because they lack the fluorescence interference. Fluorescence is considered a central problem for Raman spectroscopy. Fluorescence differs from Raman scattering, in which the incident photon is completely absorbed and changes the electronic energy state of the molecule. Later, normally in the order of nanoseconds, the

fluorescence photons are emitted from the molecule when it relaxes to the lower energy state. while the Raman scattered photon is emitted instantly (Szymanski 1967).

If a diatomic molecule is irradiated by incident light, the nuclei with positive charge are pulled to the negative pole, and oppositely the negatively charged electrons are pulled towards the positive pole resulting in an induced dipole moment. and the molecule is polarized. A Raman spectrum is obtained by an irradiated molecule if the polarizability changed during the molecular vibration, and the molecule is said to be a Raman active. Ideal strong Raman scatterer molecules contain a moiety with distributed electron clouds, such as C=C double bonds. The double bond's π-electron cloud is readily deformed when exposed to external energy, resulting in a change in the electron distribution of the bond and causing a high change in the induced dipole moment. Molecules with a high polar moiety, such as O-H bond has a permanent dipole, in such molecules, the external energy does not induce a high change in the dipole moment, consequently, these molecules are weak Raman scatterers. Therefore, water is considered as a weak Raman scatterer and is preferred as a solvent during biological sample Raman spectroscopy. Its Raman spectrum is largely featureless and very weak in the wavenumber range typically employed in most biological studies. Water hardly interferes with the resulting Raman spectra of the studied samples. (Gelder *et al*., 2007; Vašková, 2011). The normal vibrational mode is an independent movement of atoms in the molecule that occurs without leading to the movement of other modes. The number of normal vibrational modes is only 1 for diatomic molecule "stretching". While for the polyatomic molecules, it can be determined by the vibrational degrees of freedom. The number of normal vibrational modes is 3N-6 for non-linear molecules, such as the H_2O molecule, and 3N-5 for linear molecules, such as the CO_2 molecule (N represents the number of atoms in the molecules). As illustrated in Figure 1.4, these vibrational modes can be symmetric stretching, antisymmetric stretching and bending (Ferraro and Nakamoto, 2012). Typically, Raman spectroscopy is based on the energy difference between the incident and the scattered photons and is known as the Raman shift. This difference is totally dependent on the chemical constitution of the scattering molecules and independent of the incident photon. Raman shift is usually in wavenumber with a unit of inverse length (cm^{-1}). Raman scattering intensity (photons per square centimeter per second) is proportional to the change in polarizability of the scattering molecules (Haynes *et al*., 2005).

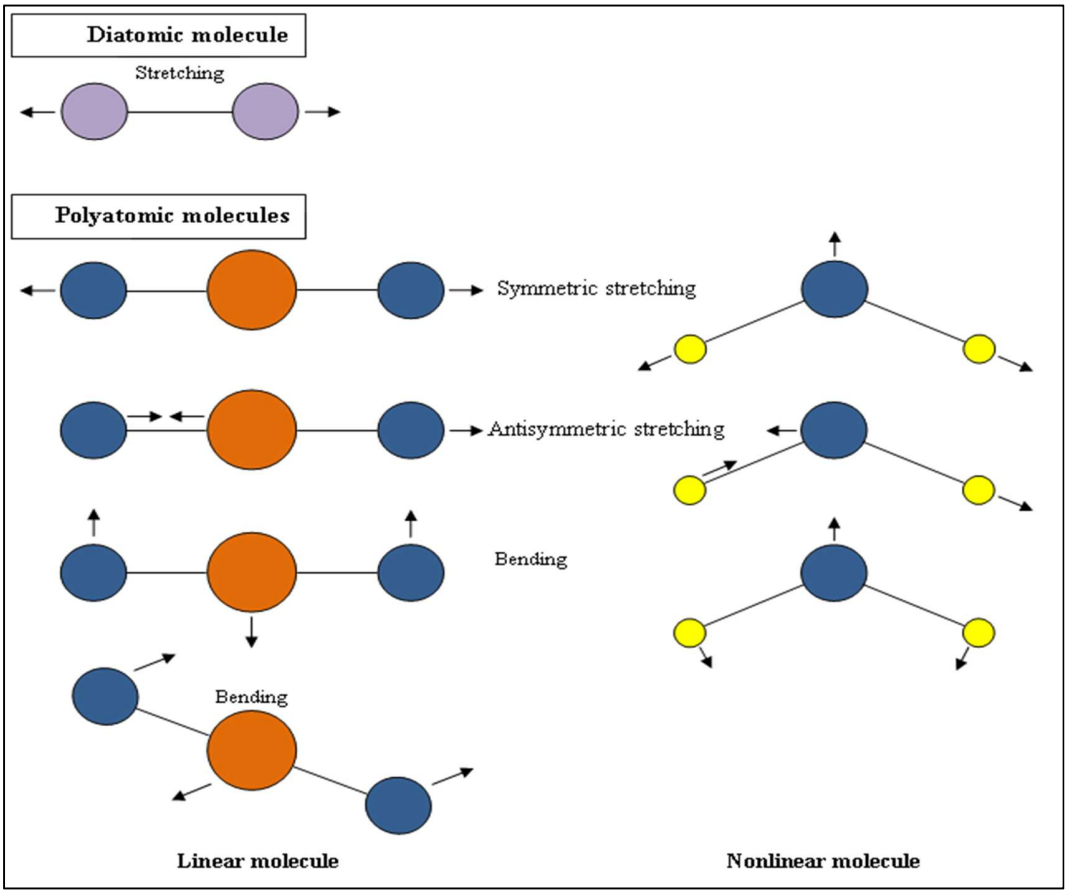

Figure 1.4: Normal vibrational modes of diatomic and polyatomic molecules. (Adapted from Ferraro and Nakamoto, 2012)

1.8.2 Raman spectrometer

The typical Raman instrument (Figure 1.5) consists of the following main components, which are essential to obtain Raman spectra:

1. **Light source**: the Raman spectrometer uses a laser as a light source because the light emitted by a laser has a highly monochromatic nature. For Raman spectroscopy special lasers are employed that even further minimize the emission of other frequencies, so-called side lines. This is an important feature because Raman scattering is very weak (1000-fold weaker) compared to Rayleigh scattering. Any emissions of the laser within the examined wave number range deteriorate the signal to a noise ratio. A Raman spectrometer commonly operates in the visible light range (400-785 nm). The disadvantage of using laser with such range during the measurement of a biological sample is the emission of fluorescence. Fluorescence emission could be produced from some molecules in the cells and the sample damaged due to the absorption of visible laser light. Fluorescence generally produces a strong background signal that can mask the Raman spectrum. Longer excitation wavelengths commonly reduce fluorescence but can also affect the signal intensity.

2. **Microscope**: it is an important part to collect light during Raman spectroscopy of the microscopic samples. The microscopic objective focuses the laser into a tiny spot and maximizes the photon collection capability of the Raman scattered photons.
3. **Monochromator**: separates the Raman scattered light into light of different wavelengths using two concave mirrors and a reflective diffraction grating. The scattered Raman light enters into the spectrometer, is collected by the collection mirror and redirected towards the reflective diffraction grating. Then, the diffracted light is collected by the focusing mirror and redirected to the charge-coupled device (CCD) detector.
4. **Charge-coupled device (CCD) detector**: it is a silicon-based photosensitive microchip device, essentially a digital camera chip, which receives the scattered Raman photons generating electrical charges and translating them into digital values.

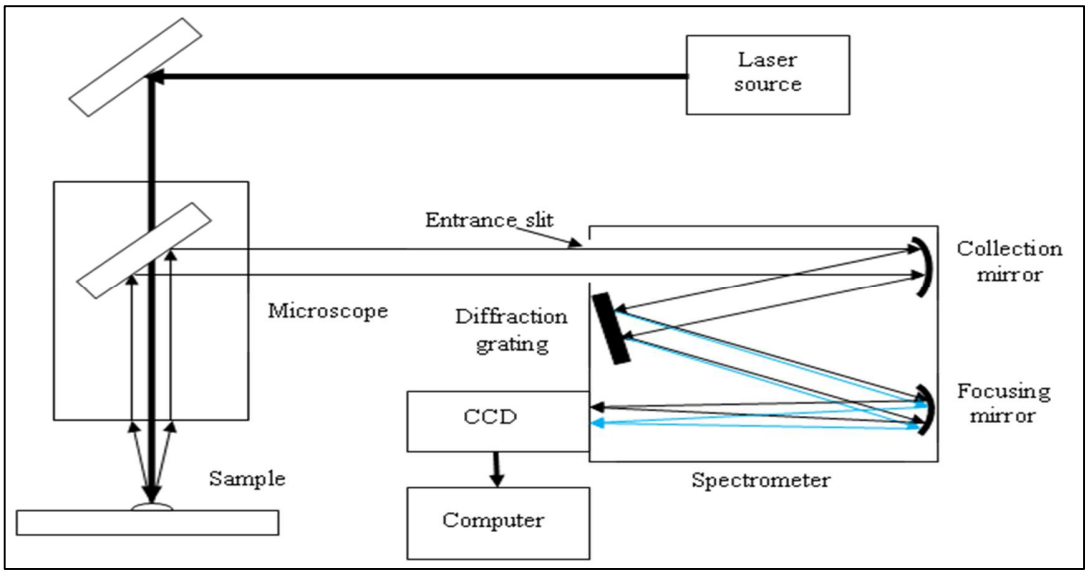

Figure 1.5: Diagrammatic representation of the Raman instrument.

1.8.3 Raman spectra

During Raman spectroscopy, the scattered photons are detected as a count on the CCD. A grating diffracts the photons with different energy and leads them into different positions on the CCD. Therefore, the Raman spectrum X-axis represents the energy of photon on, and the Y-axis represents the photon counts. In other words, the Raman spectrum is a plot presenting the scattered light intensity versus the wavenumber (1/wavelength). The x-axis of the Raman spectrum is called the Raman shift (cm^{-1}), which can be obtained using the following formula (Settle, 1997).

Raman shift (cm^{-1}) = ($10^7/ \lambda_{incident} - 10^7/ \lambda_{scattered}$)

Where $\lambda_{incident}$ represents the incident light wavelength (nm), and $\lambda_{scattered}$ represents the scattered light wavelength (nm), the Raman shift does not depend on the incident light wavelength, because the wavenumber and the energy of both incident and scattered light are linearly correlated (Xu *et al*., 2018).

With commercial instruments, Raman spectra can typically be acquired between 10 cm^{-1} to 4000 cm^{-1}. For organic molecules the range between 400 cm^{-1} to 4000 cm^{-1} is commonly analyzed. Each normal vibrational mode of the molecules represents a peak in the Raman spectrum. The peaks are collected from the Raman spectrometer and provide detailed information about the molecule under analysis as illustrated in Figure 1.6. The peak positions correspond to the structure or functional groups and can be considered as a fingerprint of the molecule. Band intensity represents the molecule or functional group concentration. Band position shifting provides information about the effect on and the interaction with the environment, such as temperature, pressure, stress and deformation. Variation in crystallinity or order can be obtained by the full width at half-maximum. The more ordered the structure and the less molecules interact, the narrower the peaks get.

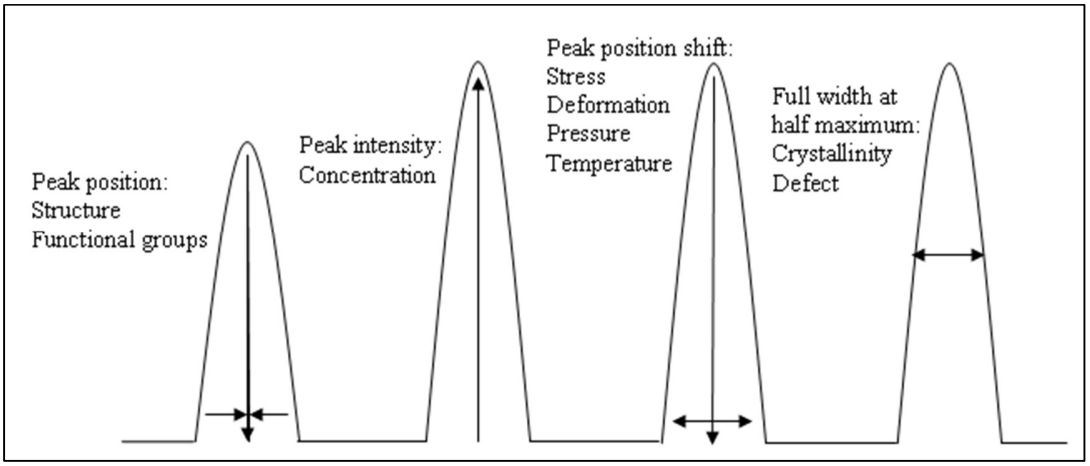

Figure 1.6: Typical Raman peak (Adapted from Xu *et al*., 2018).

1.8.4 Raman Spectroscopy Substrates

Raman spectroscopic measurements require a suitable substrate to support the sample under analysis. Commonly, the examined samples are thin and easily penetrated by the incident photons. This allows the incident photons to scatter on the substrate supporting the sample. This interaction will yield a spectral background, which affects the measurement. Therefore, the correct selection of the substrate is an important factor. A proper selection minimizes the background spectral features in the spectral region of interest and results in high quality Raman spectra (Bonnier *et al*., 2010). Currently, quartz, calcium fluoride, zinc selenide, stainless steel and low-emissivity microscopic slides are used as substrates during Raman measurements. Plastic Petri dishes, calcium fluoride, quartz and zinc selenide were investigated as substrates for the Raman measurement of living cells. The results indicate a toxicity in zinc selenide

rendering this substrate material not applicable for the Raman measurements of living cells. Plastic dishes yield a very intense Raman spectrum, which hides the Raman cell spectrum. The results also indicate that calcium fluoride and quartz produce Raman spectra with a high spectral quality. According to these results, quartz was considered to be the most appropriate substrate and it also does not affect both cell growth and morphology (Draux *et al*., 2009).

1.8.5 Raman versus Infrared spectroscopy

Raman and infrared spectroscopy are similar and complementary methods, but they are based on different principles. Both methods provide information about the vibrational and rotational transitions in the molecule under analysis. They are therefore considered to be identification methods (Wartewig and Neubert, 2005). But their results are ruled by different principles, because each method depends on different modes of photon interaction with the studied samples. Raman spectroscopy is a scattering method, based on changes in the polarizability. Infrared spectroscopy is an absorption method, based on the changes in the permanent dipole. Raman spectroscopy identifies the molecular structure; based on the interaction between the molecule and the incident light, resulting in emission spectra that are a characteristic feature of the molecule. On the other hand, infrared spectroscopy identifies the molecular structure, based on the molecules absorbing specific frequencies, resulting in absorption spectra. Regarding the identification of molecular composition in the mixture, Raman is the preferred method because its bands are narrower compared to IR (Smith and Clark, 2004). The spatial resolution of the IR method is low because this method uses long wavelength excitation (Zumbusch *et al*., 1999); it is reported to be between 2.5 and 25 μm. Moreover, the strong water absorption limits the studying of samples containing water with IR spectroscopy. This problem gives Raman spectroscopy an advantage because it can use visible or near IR light for excitation (Day *et al*., 2011). As a result, Raman spectroscopy has a wider applicability range because it is barely affected by air, moisture or water. The diatomic molecules can also be measured by Raman spectroscopy, but not by IR spectroscopy, because the diatomic molecules do not have a permanent dipole moment (Yeo *et al*., 2009; Smith and Clark, 2004). Regarding quantitative measurement, the Raman band intensities scale linearly with concentration, while the IR intensities scale with Beer's Law. Some molecules can produce high quality for both Raman and IR spectra. However, centrosymmetric molecules, for example, can only produce one of them. A molecule producing a strong Raman spectrum has weak IR absorption and vice-versa. Polyatomic inorganic compounds and most organic compounds have intensive Raman spectra. Small polar molecules and single-bonded compounds have intensive IR spectra. Finally, the fluorescence resulting from the photoreaction of molecules with the incident light impedes Raman spectra acquisition (Vašková, 2011).

1.8.6 Applications of Raman spectroscopy

1.8.6.1 General applications of Raman spectroscopy

After the discovery of the Raman Effect, Raman spectroscopy was used exclusively by physicists and chemists for a long period of time due to the technical challenges it involved. But during the 1970's Raman spectroscopy started to be applied in biomedical research. The use of it was modest at the beginning but it gradually became a widely used method, either in biomedical or other research fields, due to the development of new and user-friendly Raman instruments. In this field Raman spectroscopy research started with a basic evaluation of Raman spectra acquired from biological molecules, such as cytochrome c (Spiro and Strekas, 1972) and hemoglobin (Strekas and Spiro, 1972). The advances in sensitivity and spatial resolution of Raman instruments enabled the researcher to evaluate the interaction between complex molecules, such as arginine-rich histones with DNA (Mansy *et al*., 1976), to examine structures consisting of multiple sub-units, such as viruses (Hartman *et al*., 1973) erythrocyte membranes (Bulkin, 1972), or antibodies (Painter and Koenig, 1975).

Raman spectroscopy provides a flexible technique for examining a variety of sample types, including fixed, fresh or live specimens and cells. Its applications to characterize biological samples increased exponentially due to several advantages of this technique, such as it being a non-destructive and non-invasive technique, no or only minimal sample preparation being required, having a high spatial resolution that allowed measurement of single cell or even cell substructures, being rapid, and requiring only a small sample size. Raman spectra can also be obtained from aqueous samples because water is a very weak Raman scatterer (Gelder *et al*., 2007; Vašková, 2011). These advantages make Raman spectroscopy an attractive and widely used technique for biomedical analysis (Pappas *et al*., 2000). The frequency and the intensity of the Raman spectra depend on the conformations, the nature of chemical bonds, and the concentrations within the sample; it is therefore a molecule specific technique, enabling the identification of molecules within a sample (Wartewig and Neubert, 2005). Raman spectroscopy can detect at the molecular level chemical and structural resulting from diseases or pathological abnormalities (Krafft and Sergo, 2006). Due to the uniqueness of the Raman spectra of pathological samples, the resulting spectral features can be used as disease markers (Katz *et al*., 2003; Keller *et al*., 2008). Therefore, Raman spectroscopy can thus contribute to the diagnosis of several types of cancer, including bladder (De Jong *et al*., 2006), cervix uteri (Vargis *et al*., 2011), breast (Yu *et al*., 2006; Stone and Matousek, 2008), lung (Oshima *et al*., 2010), stomach (Teh *et al*., 2008), brain (Koljenović *et al*., 2002), and larynx (Bergholt *et al*., 2012).

1.8.6.2 Application of Raman spectroscopy in male infertility

1.8.6.2.1 Application in Testis

The application of Raman spectroscopy to examine testicular function and composition has been delayed, compared to other tissue types and cells, because the testicular tissue has different cell types in a complex testicular environment. There is also only a small number of testicular samples available (Liu *et al*., 2014; Mallidis *et al*., 2013). The first Raman study regarding testis was performed on frozen samples of testicular microliths obtained from patients with malignant and benign testicular tumors. The results indicated that these microliths are localized in seminiferous tubules and consisted of hydroxyapatite. Glycogen surrounded the microliths in all malignant cases but not in the benign ones (De Jong *et al*., 2004). Another study was aimed at differentiating Sertoli cells from obstructive and non-obstructive azoospermic patients, who underwent microdissection testicular sperm extraction (Micro-TESE). The results indicated that the shapes of the Raman spectrum were similar, but the statistical analysis indicated that four Raman peaks were significantly different between obstructive and non-obstructive azoospermic patients (Ma *et al*., 2013). Raman spectroscopy was also used to investigate testicular tumours using TCam-2 cells as a model. The analysis of Raman spectra provided detailed characterizations that indicated the presence of two cell populations among the TCam-2 cells, one of which had two subpopulations and was similar to some 2102EP cells (embryonic carcinoma cells). This finding provides evidence that TCam-2 is not homogeneous and contains different cell populations, one of which could have originated from embryonic carcinoma (Eppelmann *et al*., 2013).

1.8.6.2.2 Application in Sperm

Actually, sperm is the first cell that was studied using Raman spectroscopy. DNA in an aqueous solution extracted from salmon sperm was examined and compared to the synthesized model B-DNA oligomer. The resulting Raman spectra indicated that both salmon DNA and the model DNA had a B-type conformation (Kubasek *et al.,* 1986). Over two decades on from the first published study, a few Raman studies took place again concerning the application of Raman spectroscopy as a tool to investigate the different features of sperm.

Another study was carried out using confocal Raman spectroscopy to characterize different human sperm substructures including nucleus, neck, and middle piece. The effects of ultraviolet radiation on these sperm substructures were also investigated. They found a chemical compositional change in these substructures that was related to the exposure time of the ultraviolet radiation treatment. What is more, they recorded a distinct Raman spectrum from each sperm substructure due to its unique chemical components. The nucleus's spectrum was characterized by the DNA peaks, especially around 788 cm^{-1}. The ring breathing mode of the adenine and guanine around 1575 cm^{-1}, was found in both the nucleus and the middle piece

spectra. It was assumed that the 751 cm^{-1} peak was an indication of mitochondria due to the absence of this peak in the other sperm substructures (Meister *et al*., 2010).

Confocal Raman spectroscopy was used to investigate the differences between sperm, based on their ability to bind zona pellucida. Raman spectra were obtained from all sperm substructures, including the acrosome, nucleus, equatorial region, neck, middle piece, and tail. A high shift in Raman peak intensities in the 800-900 cm^{-1} and 3200-4000 cm^{-1} regions were observed only in the acrosome region of the zona pellucida bound sperm, compared with the unbound sperm. In addition to this, statistical analyses of the mean spectral intensities indicated that Raman spectroscopy can differentiate between zona pellucida bound and unbound sperm. The Raman peak intensities at 789 cm^{-1}, 810 cm^{-1}, 838 cm^{-1}, 1092 cm^{-1}, 1100 cm^{-1}, 1357 cm^{-1}, and 1421 cm^{-1} were increased, and the Raman peak intensities at 1441 cm^{-1}, 1482 cm^{-1}, 1505 cm^{-1}, 1575 cm^{-1}, 1582 cm^{-1}, and 3240 cm^{-1} were decreased in the zona pellucida bound sperm (Liu *et al*., 2013).

Three studies were performed by the same research group. They investigated the ability of Raman spectroscopy to evaluate different levels of nuclear DNA fragmentation of sperm caused by a bacterial infection, induction by ultraviolet irradiation or induction by oxidative stress. The main observation was a decrease of the PO_4 peak intensity around 1092 cm^{-1}, and an increase in the intensity of the peak around 1050 $cm^{-1,}$ regardless of the causes of the DNA fragmentation. These changes in the intensities of peaks were expressed as a ratio (1050 cm^{-1}/1092 cm^{-1}) and correlated linearly with the exposure time to the ultraviolet irradiation and the concentration of the added oxidative stress agent (Mallidis *et al*., 2011; Sanchez *et al*., 2012). They also indicated a variation in peak intensities at 980 cm^{-1}, 1250 cm^{-1}, 1483 cm^{-1}, and 1666 $cm^{-1,}$ resulting from alteration in the deoxyribose moiety of all nucleotides. The peak around 1575 cm^{-1} was increased due to the formation of 8-oxoguanosine. As the author assumed (Lang *et al*., 2013), this is the main indication of DNA fragmentation resulting from oxidative stress. The peak intensity around 1446 cm^{-1} was changed specifically in the samples that showed a high level of fragmented DNA (Sanchez *et al*., 2012). Changes in the intensities of the Raman peaks between 1400 cm^{-1} and 1600 cm^{-1} were observed. The site of DNA fragmentation was also localized by macro-mapping of the sperm nucleus (Mallidis *et al*., 2011).

Recently, another study employed Raman spectroscopy to characterize the biochemical composition of the main sperm substructures, namely, the nuclear area, the middle piece and the tail in four different species (Human (*Homo sapiens*), Monkey (*Macaca fascicularis*), Mouse (*Mus musculus*) and Sea Urchin (*Arbacia punctulata*)). They found the main spectral features remained mostly the same among the studied species, indicating that the basic biochemical components of the sperm were conserved among the studied species. They observed different Raman spectra for each substructure in all the studied species due to their different chemical compositions. The nuclear area spectrum exhibited a nucleic acid Raman peaks, which were

notable between 600 cm^{-1} and 1150 cm^{-1}. The middle piece spectrum exhibited nucleic acids, proteins and lipid Raman peaks, which were notable between 1150 cm^{-1} and 1700 cm^{-1}. This region represented the components of mitochondria and the organelles found in the middle piece. In some species (Monkey and Mouse) the middle piece spectrum exhibits a higher peak intensity of between 1400 cm^{-1} and 1700 $cm^{-1,}$ compared to the nuclear area spectrum. The tail spectrum exhibits weak protein Raman peaks, which are common with the other sperm substructures. Finally, the researchers demonstrated the presence of some Raman peaks that were conserved among all the studied species in all sperm substructures, such as 644 cm^{-1}, 850 cm^{-1}, 1447 cm^{-1} and 1660 cm^{-1} (Amaral *et al*., 2018).

Regarding sperm morphology, three studies were performed using Raman spectroscopy. The first study investigated the Raman spectral differences of sperm chromatin in regard to cell shape. They provided Raman-spectroscopic evidence that chromatin packaging in normal morphology human sperm differ from that of sperm with pear, small and double head abnormal shapes. These differences were based on a peak ratio variation of 785 cm^{-1} to 1092 cm^{-1} or 1442 cm^{-1} to 1092 cm^{-1}. They also assumed the 785 cm^{-1} peak intensity value to be an indication of chromatin packaging (Huser *et al*., 2009). The second one investigated the ability of confocal Raman spectroscopy, accompanied by multivariate analysis, to differentiate between morphologically normal and abnormal sperm in addition to being able to evaluate the nuclear DNA integrity. The spectral analyses indicated that both normal and abnormal morphology groups showed a different types of Raman spectra. Consequently, the morphological classification is partly consistent with spectral classification. The Raman spectra of normal morphology sperm show a high similarity, while the abnormal morphology sperm show a high degree of variation, especially around the 1045 cm^{-1} and 1445 cm^{-1} Raman peaks. They also indicated the ability of Raman spectroscopy to detect normal morphology sperm with fragmented DNA, based on the increased intensity of the Raman peak around 1045 cm^{-1} (Nazarenko *et al*., 2018). The third study used Raman spectroscopy, accompanied by image analysis, to identify living normal morphology sperm. The main observed result showed the importance of the intensity ratio of the Raman peaks around 1055 cm^{-1} and 1095 cm^{-1} as a predictor of DNA integrity (Huang *et al*., 2013).

Two studies were performed using Raman spectroscopy to evaluate the effect of different plant extracts to increase sperm antioxidant capability (Huang *et al*., 2014; Chen *et al*., 2014). The first study evaluated the effect of the *Herba Epimedii* extract "icariin" as an anti-oxidant agent. Sperm samples were treated with both, the $FeSO_4/H_2O_2$ to induce DNA fragmentation and the extracted icariin as an anti-oxidant agent. The spectrum of induced damaged sperm differed from that of the untreated sperm, indicating that Raman spectroscopy can indeed detect damaged DNA as shown in the change in the intensities of several Raman peaks. The Raman spectrum of the treated sperm, with both the $FeSO_4/H_2O_2$ and the icariin, also showed that the changed Raman peaks' intensity nearly recovered to normal levels, especially the mitochondrial

peaks at 860 cm^{-1}, 995 cm^{-1}, 1092 cm^{-1}, 1375 cm^{-1}, 1445 cm^{-1} and 1612 cm^{-1}. It was assumed that these Raman peaks are an indicative of mitochondrial damage (Huang *et al*., 2014). The second study evaluated the effect of the *Morinda officialis* extract "oligosaccharides" as an anti-oxidant agent. Sperm samples were treated with both, H_2O_2 to induce DNA fragmentation and the extracted oligosaccharides as an anti-oxidant agent. The Raman spectrum obtained from the treated sperm showed a high similarity with the spectrum of the untreated sperm, indicating the antioxidant effect of the extracted oligosaccharides. The intensity of many Raman peaks of sperm that were treated only with the H_2O_2, differed greatly from the Raman spectrum of the untreated sperm, especially the Raman peaks at 787 cm^{-1}, 993 cm^{-1}, 1094 cm^{-1}, 1254 cm^{-1}, 1340 cm^{-1}, 1376 cm^{-1}, 1421 cm^{-1}, 1443 cm^{-1}, 1487 cm^{-1}, 1577 cm^{-1} and 1662cm^{-1} (Chen *et al*., 2014).

Raman spectroscopy was also used to evaluate the effect of maleic acid on sperm. Raman spectra were obtained for human sperm, which was treated with varying concentrations of maleic acid. Notable changes were recorded in Raman spectra, due to structural and compositional damage induced by maleic acid, especially in the membrane and the DNA. The intensity of Raman peaks corresponding to the DNA was reduced at 787 cm^{-1}, 1094 cm^{-1}, 1337 cm^{-1} and 1421 cm^{-1}. A peak shift at 988 cm^{-1} to 973 cm^{-1} was also observed, due to the breakage of some chemical bonds in the DNA nucleotides, which may have been caused by the maleic acid. Based on a previous study that proposed the ratio of the Raman peaks at 855 cm^{-1} to 836 cm^{-1} was related to their tyrosine environment, this ratio was considered to be an indicative measure of tyrosine conformational change. The ratio for untreated sperm indicated that the tyrosine was embedded in the membrane and maintains its stability while the ratio of treated sperm indicated that the tyrosine was converted to an exposed position after the maleic acid treatment. The phenylalanine Raman peak intensity at 1004 cm^{-1} was reduced, assuming there had been damage to the protein structure (Li *et al*., 2014).

2 Aim of the study

As previously mentioned, sperm chromatin condensation is one of the main factors that affect male fertility. The selection of sperm during the intracytoplasmic sperm injection (ICSI) procedure depends solely on sperm morphology and its motility. However, there is evidence and a developing hypothesis that normal shaped sperm are not necessary to be completely functional and may have DNA that is not properly packed.

Fertilization by sperm with an abnormal shape or with improper DNA packaging may have a negative result on early embryonic growth or may lead to the development of genetic diseases. Thus, the development of a method that can non-invasively evaluate or predict the status of DNA packaging in living sperm cells would be of significant benefit and would allow for its selection and ultimate use for ICSI. All classical methods, such as chromomycin A3, methyl green, Giemsa stain and acidic aniline blue, are restricted to measuring or estimating the chromatin condensation abnormalities in an ejaculated sample are not suitable for further therapeutic use. The staining renders the assessed sample inappropriate for assisted reproductive technology procedures. Moreover, none give direct information about the status of viable sperm, nor are they able to evaluate its capacity to function properly and thus achieve pregnancy.

The objectives of the current study can be summarized as the following:

1. To investigate the ability of Raman spectroscopy to detect different levels of chromatin condensation (based on chromomycin A3 staining) in normal morphology sperm based on quantitative biochemical parameters.
2. To determine the relationship between the Raman quantitative biochemical parameters and sperm DNA fragmentation.
3. To investigate the ability of Raman quantitative biochemical parameters to predict ICSI outcomes, including fertilization rate, embryo cleavage, embryo quality and embryo development.
4. To investigate the ability of Raman quantitative biochemical parameters to distinguish between normal and abnormal semen parameters, based on WHO classification.
5. To evaluate the effect of chromatin condensation and DNA fragmentation on semen parameters.
6. To evaluate the effect of semen parameters, chromatin condensation and DNA fragmentation on ICSI outcomes.

3 Materials and methods

3.1 Materials

3.1.1 Semen Samples

Semen samples (n=85) from donors suffering from infertility problems, and enrolled in the intracytoplasmic sperm injection (ICSI) program at Prince Rashid Ben Al-Hasan Military Hospital, Irbid, Jordan were collected and included in this study.

3.1.2 Ethical approval

Semen samples were collected from donors, after they were approved to use these samples for research purposes based on the approval of the Royal Medical Services Human Research Ethics Committee number (8/2018) on 19/9/2018, (Informed consent was given by each participant). This study was carried out in the Laboratory of Biochemistry and Molecular Biology of Reproductive Medicine, Department of Obstetrics and Gynecology at the University Hospital of Saarland, Homburg, Germany, and at the Department of Informatics and Microsystems Technology, University of Applied Sciences Kaiserslautern, Campus Zweibrueken, Germany.

3.1.3 Chemicals

- Acetic Acid — Fluka, Neu-Ulm, Germany
- Acridine orange — Sigma-Aldrich, Germany
- Aniline blue — Morphisto, Germany
- Chromomycin A3 — Sigma, Munchen, Germany
- Citric acid — Sigma-Aldrich, Germany
- Deionized water — Sigma, Munchen, Germany
- Disodium hydrogenphosphate (Na_2HPO_4) — Merck, Darmstadt, Germany
- Dulbecco's Ca^{2+} -Mg^{2+} free phosphate buffer saline — Fisher scientific, UK
- Ethanol Absolute — Merck, Darmstadt, Germany
- Glutaraldehyde — Sigma, Munchen, Germany
- Glycerol — Fluka, Neu-Ulm, Germany
- Hydrochloric acid — Merck, Darmstadt, Germany
- Magnesium chloride ($MgCl_2$) — Sigma-Aldrich, Germany
- Methanol — Merck, Darmstadt, Germany

• Phosphate-buffered saline (PBS) tablet	Sigma, Munchen, Germany
• Potassium Chloride (KCl)	Merck, Darmstadt, Germany
• Potassium dihydrogen phosphate (KH_2PO_4)	Merck, Darmstadt, Germany
• Sodium Chloride (NaCl)	Merck, Darmstadt, Germany

3.1.4 Buffers and solutions

1. CMA3 Staining Solution:
    - 250 µg/ml Chromomycin A3
    - 10 mmol $MgCl_2$
    - McIlvaine buffer pH 7.0
2. Fixation Solution for CMA3 and Acridine Orange (Carnoy's solution):
    - 3X Methanol
    - 1X Glacial acetic acid
3. McIlvaine buffer pH 7.0:
    - Stock A: 0.1 M citric acid for 200 ml use 4.2g
    - Stock B: 0.2 M Na_2HPO_4 for 800 ml use 22.7g
4. Phosphate Buffer Saline (PBS), pH 7.4:
    - 137 mM Sodium Chloride (NaCl)
    - 2.7 mM Potassium Chloride (KCl)
    - 8 mM Disodium hydrogenphosphate (Na_2HPO_4)
    - 1.5 mM Potassium dihydrogen phosphate (KH_2PO_4)
5. Acridine Orange Stock Solution:
    - 1 gm of Acridine Orange powder
    - 1000 ml distilled water
6. Acridine Orange Working Solution:
    - 10 ml of acridine orange stock solution
    - 40 ml of 0.1 M citric acid
    - 2.5 ml of 0.3 M $Na_2HPO_4 \cdot 7H_2O$

3.1.5 Apparatus and Instruments

- Automatic pipettes — Eppendorf, Hamburg, Germany
- Confocal Raman microscope — Horiba Scientific Raman Workstation LabRAM Nano Evo and AIST AFM Combiscope
- Eppendorf 5414C centrifuge — Eppendorf, Hamburg, Germany
- Fluorescence microscope — Olympus, Japan
- Light compound microscope — Olympus, Japan
- Makler counting chamber — Makler Co. Sefi-Medica, Haifa, Israel
- Magnetic bars — Eppendorf, Hamburg, Germany
- Magnetic stirrer — Eppendorf, Hamburg, Germany
- pH-Meter: pH537 — Carl Roth GmbH and Co, Karlsruhe, Germany
- Stainless steel slides — Super Mirror Grade #8 polished 1.4301 stainless steel, 50mm x 20mm x 0.8mm, SG Designbleche GmbH, Germany
- Vortex — Elma GmbH, Singen, Germany

3.2 Methodology

3.2.1 Semen collection and analysis

Semen samples from 85 donors who underwent ICSI treatment were collected by masturbation, after 3-6 days of sexual abstinence in sterile plastic vials. Semen samples were allowed to be liquefied at 37°C for 30 min. Briefly, after complete liquefaction, semen parameters were determined immediately according to World Health Organization guidelines (WHO, 2010) using a Makler chamber (Sefi-Medica, Haifa, Israel). These parameters include volume, pH, sperm concentration, motility and morphology.

3.2.2 Sperm purification for Raman spectroscopy

A fraction from the raw semen samples was washed and centrifuged at 250g for 10 min in two steps: first samples were washed twice with phosphate-buffered saline (PBS). Then, the obtained sperm pellet was washed twice with deionized water. Finally, the pellet was resuspended in deionized water and stored at -20 °C until the use in the Raman measurement.

3.2.3 Sperm functional parameters assessment

3.2.3.1 Assessment of chromatin condensation (protamine deficiency) by chromomycin A3

As described by Bianchi *et al.* (1993) chromatin condensation was evaluated by chromomycin A3 (CMA3) staining. A fraction of the raw semen samples was washed with Dulbecco's Ca^{2+} -Mg^{2+} free PBS (1 volume semen: 2 volumes PBS) followed by centrifugation at 250g for 10 min. Then, the washed sperm were smeared and fixed using methanol/acetic acid, 3:1 (Carnoy's solution) at 4ºC for 5 min. Then, each slide was stained in dark for 20 min with 100 µl of CMA3 stain solution. (CMA3 stain prepared in McIlvaine buffer (pH=7.0) supplemented with 10 mM $MgCl_2$ to a final concentration of 250 µg/ml). Then, each slide was rinsed in PBS buffer, dried and mounted with buffered glycerol (1:1). The evaluation of chromatin condensation each slide was examined using a fluorescence microscope (Olympus) at 100X oil immersion magnification. 500 sperm were evaluated for each donor, by differentiating between the CMA3 positive sperm (bright yellow-stained) and CMA3 negative sperm (dull yellow-stained). The percentages of CMA3 positivity were calculated by dividing the number of sperm with positive CMA3 (protamine deficient sperm) by the total number of the evaluated sperm.

3.2.3.2 Assessment of chromatin maturity (histones retention) by aniline blue

As described by Hammadeh *et al.* (2001) Chromatin maturity was evaluated by aniline blue staining. A fraction of the raw semen samples was washed with PBS followed by centrifugation at 250g for 10 min. Then, the washed sperm were smeared and fixed for 30 min by 3% buffered glutaraldehyde in 0.2 M phosphate buffer (pH=7.2). Smears staining was performed by immersing the fixed slides for 5 min in 5% acidic aniline blue stain (pH=3.5). Chromatin maturity was evaluated by a light compound microscope using 100X oil immersion magnification. 200 sperm were evaluated for each donor by distinguishing the unstained sperm (sperm with mature chromatin) from the completely or partially blue-stained sperm (sperm with retained histones). The percentages of immature sperm were calculated dividing the number of stained sperm (sperm with retained histones) by the total number of the evaluated sperm.

3.2.3.3 Assessment of DNA fragmentation by acridine orange

As described by Tejada *et al.* (1984) DNA fragmentation was evaluated by acridine orange staining. A fraction of the raw semen samples was washed with PBS followed by centrifugation at 250g for 10 min. Then, the washed sperm were smeared and fixed using methanol/acetic acid, 3:1 (freshly prepared Carnoy's solution) for overnight at room temperature. Then, the fixated smears were allowed to air dry for a few minutes. Then, each slide was stained for 5 min by adding 2-3 ml of freshly prepared acridine orange working solution 0.19 mg/ml (10 ml of acridine orange stock solution 0.1%: 40 ml of 0.1 M citric acid: 2.5 ml of 0.3 M $Na_2HPO_4 \cdot 7H_2O$: pH=2.5). Then, slides were gently washed with deionized water and covered before drying. The evaluation of chromatin DNA integrity was performed using fluorescence microscope

(Olympus) at 100X oil immersion magnification. 200 sperm were evaluated for each donor by distinguishing the green-stained sperm (sperm with intact double-stranded DNA), from yellow- or orange- or red-stained sperm (sperm with single-stranded DNA). The percentages of the DNA fragmentation for each donor was obtained by dividing the number of yellow- or orange- or red-stained sperm (sperm with single-stranded DNA) by the total number of the evaluated sperm.

3.2.4 Sample classification

Samples were classified based on two criteria.

1. Chromomycin A3: samples were classified based on the result of sperm chromatin condensation evaluation by chromomycin A3 (CMA3) (Sakkas *et al*., 1996; Nasr-Esfahani *et al*., 2001). Using this criterion samples were classified in two different ways:
    a. Classified into two groups based on one cut-off point determined by receiver operating characteristics (ROC) curve, by applying the effect of CMA3 result on the fertilization rate.
    b. Classified into three group based on two cut-off points determined by adding and subtracting 0.5 standard deviation (SD) of the CMA3 median.
2. WHO semen parameters criterion: samples were classified into two groups, fertile and subfertile groups.

3.2.5 Intracytoplasmic sperm injection (ICSI) outcomes assessment

3.2.5.1 Fertilization rate assessment

Oocyte fertilization was assessed by examining the presence of pronuclei between 16-18 hours after sperm injection according to Scott *et al.* (2000). The fertilization rates were determined for each donor by dividing the number of fertilized oocytes (pronucleus stage) by the total number of injected oocytes.

3.2.5.2 Cleavage and embryo quality assessment

The fertilized oocytes were assessed for cleavage and embryo quality at day 3 after sperm injection. Cleavage grade was determined by counting the number of blastomeres in each fertilized oocyte (embryo) and given a number range from 1 to 4. A Score 4 contains 8 blastomeres; score 3 contains 6-7 blastomeres; score 2 contains 4-5 blastomeres; score 1 contains less than 4 blastomeres. The cleavage score was determined for each donor by dividing the sum of all cleavage scores by the total number of assessed fertilized oocytes (embryos) (Anifandis *et al*., 2010; Nasr-Esfahani *et al*., 2007).

Embryos quality was determined by examining the embryo morphology and given a number for each fertilized oocyte (embryo). Grades range from 1 to 3. Score 3 was given for grade (A) embryos that have equal-sized blastomeres and 10% fragmentation or less. Score 2 was given for grade (B) embryos that have equal-sized blastomeres and fragmentation between 10-50%. Score 1 was given for grade (C) embryos, that

have unequal-sized blastomeres and the fragmentation exceeds 50%. The embryo quality score was determined for each donor by dividing the sum of all quality scores by the total number of assessed fertilized oocytes (embryos) (Nasr-Esfahani *et al*., 2007). Also, embryos development scores were calculated, as the sum of cleavage and embryo quality scores.

3.2.6 Raman spectroscopy

3.2.6.1 Spectra acquisition

Aliquots of 20 µl of the pre-prepared sperm suspensions were smeared onto stainless steel slides and allowed to air dry. The Raman spectra of sperm were measured using a confocal Raman spectrometer (LabRAM HR, HORIBA Jobin Yvon S.A.S.), equipped with an Olympus BX41 microscope, 660 nm helium-neon laser (17 mW), motorized notch filter selector, adjustable confocal pinhole, two switchable gratings, and CCD detector. The acquisition of all spectra were performed by 8 accumulations of 5 seconds each with slit pinhole apertures of 250 µm at 600 grooves/mm diffraction grating using the Olympus X100 objective and a wavenumber range from 600 to 1850 cm^{-1} (LabSpec 6 Software). No further processing of the spectra beyond accumulation was performed on the Instrument's software. Spectra also were saved as comma separated values text files for further processing. A total of 50 normal morphology sperm per sample were chosen from different microscopic fields of view. To acquire each spectrum, the cell was centered and the laser directed at the postacrosomal region of the sperm head.

3.2.6.2 Post-acquisition analysis

The acquired raw Raman spectra (n=4250) were automatically batch processed using home written custom programs in LabVIEW software (National Instruments LabVIEW 2019). All Labview programs that applied to analyze the acquired spectra in the current study were written by Prof. Dr. Marko Baller (Department of Informatics and Microsystems Technology, University of Applied Sciences Kaiserslautern, Campus Zweibrueken, Germany).

3.2.6.2.1 Baseline correction

A baseline correction of the original spectra was performed to remove the spectral background caused by fluorescence of cell components. All acquired Raman spectra were filtered by applying a 5 points baseline model using home-written program in LabVIEW software. This program automatically subtracts the background from the raw spectra without providing a significant distortion of the Raman peaks of the measured samples resulting in virtually background-free Raman spectra. All further processing and quantitative analysis was performed with baseline corrected spectra.

3.2.6.2.2 Spectra normalization

For quantitative evaluation, spectral intensities values are rescaled for uniformity by normalization. Spectra normalization was performed by different strategies using a home-written program LabVIEW software.

1. Band intensity: in this strategy, the program normalizes the spectra according to the specific band intensity. It identifies the selected band and then the divides the whole spectrum by the intensity of this band. Several bands were used in this strategy including: 785 cm^{-1}, 1098 cm^{-1}, 1575 cm^{-1}, 1673 cm^{-1} and the highest band intensity.
2. Average intensity: in this strategy, the program normalizes the spectra by setting the lowest intensity of the spectra to zero and then dividing the whole spectrum by the average intensity of the whole spectrum. Then, multiplying the resulting spectra by 3 to arbitrarily set the maximum intensity to around 1.

3.2.6.2.3 Spectral analysis

The normalized spectra files were analyzed by home-written LabVIEW program. This program has several options that allow extracting the following data:

1. Individual cell single band intensities: this option allows extracting the intensities of the preselected bands for each sperm for each donor.
2. Individual cell all bands intensities: this option allows extracting the intensities of all bands for each sperm in each donor.
3. Percentage cells threshold: this option allows extracting the percentage of sperm above or below a preselected threshold based on preselected band.
4. Average and standard deviation band intensities: this option allows extracting the average and standard deviation of the preselected bands for each donor.
5. Average spectrum and standard deviation spectrum: this option allows extracting the average and standard deviation for each wavenumber for all spectra from the selected group of donors or all donors.
6. Group individual spectra: by using this option, the program reads all individual files, approximately 4250 spectra, and packs them into a single file. In this file, the first row represents the wavenumbers. After the first row, each row represents one sperm (one spectrum), the first number (column) represents the donor number, and the second number (column) represents the cell number followed by the intensities of all wavenumbers (493).
7. Threshold: by applying this option, spectra can be classified according to any selected intensity value of any selected Raman peak.

3.2.6.2.4 Spectra fitting model

A fitting model program in LabVIEW software was used to extract a separated Raman peaks from the original Raman spectra. This program opens the data file from the group individual spectra option (option number 6) in the previous program. Simultaneously, it opens a peak parameter list (an initial guess) which defined 62 peaks. Each peak in the list was defined with several parameters: the initial guess of the wavenumber of the maximum, the initial guess intensity, the upper and the lower limit of the intensity, an upper and a lower limit of wavenumber, an upper and a lower limit of the width. The model program uses Gaussian fit for each peak; Fitting is performed using a Levenberg–Marquardt nonlinear fitting routine (Marquardt, 1963). It tries to fit the spectrum to the sum of these 62 peaks each defined by these three parameters. A total of 186 parameters are fitted. Then, the program saves the model fit spectra, and adds to each spectrum (row) a list of parameters (wavenumber, width, and intensity) of these 62 Gaussian peaks.

3.2.6.2.5 Parameter model evaluation

The resulting model fit spectra file exported into another program in LabVIEW software 'Parameter model evaluation'. This program read the file and then resynthesizes two spectra representing the sum of proteins and DNA Raman peaks respectively. Spectra resynthesis is based peak selection list from the 62 peaks list. The program can select any of them and assign them to the two groups (proteins or DNA). It plots the resynthesized spectra of the two components, their sum, the original baseline corrected spectra and the difference between the fitted spectrum and the original baseline corrected spectrum. A scroll bar allows to manually select and display any of the thousands of spectra incl. donor number and cell number. Next, this program calculates the average height and the area of the selected DNA or protein peaks. The areas of all peaks under the curve are added up. The area under the curve represents the relative content of protein or DNA respectively. Then, the program calculates the mean, median, standard deviation and the range for each donor and displays the correlation of all these calculated statistical data with the CMA3 and fertilization rate result. It also calculates either Spearman's or Pearson's correlation coefficients and their corresponding p-values, r and r^2 values. Finally, this program correlates the height and the area of any two selected peaks.

3.2.7 Statistical analysis

Data analysis was performed using origin program (OriginPro 2020, OriginLab Corporation, Northampton, MA, USA). Data were expressed as mean ± SD, median and range. Data were tested for normality using the Anderson-Darling test. The relationship between relative protein content, relative DNA content, DNA/protein ratio, protein content SD, DNA content SD, DNA/protein ratio SD, chromomycin A3, aniline blue, acridine orange, fertilization rate, cleavage score, embryo quality score, embryo development score, sperm concentration, total motility, morphology, semen volume and donor age were analyzed using

Spearman's correlation (nonparametric) unless specifically mentioned otherwise. Also, chromatin condensation was analyzed by chemical and spectrometric methods and its effect on ICSI outcomes (fertilization rate, cleavage score, embryo quality score and embryo development score) were analyzed by nonparametric tests. The Mann-Whitney U test was used in case of comparing two groups (CMA3≤41 versus CMA3>41 and fertile versus subfertile). Kruskal-Wallis H test was used in case of comparing three groups (CMA3<28 versus 28≤CMA3≤50 versus CMA3>50), while Dunn's Post Hoc test was used to determine the differences between groups and p-values were corrected by Bonferroni test. The result was considered statistically significant when the p-value was smaller than 0.05. The effect size for the Mann-Whitney U test, $r= z / \sqrt{n}$, was calculated by dividing z by the square root of n and for Kruskal-Wallis H test, $r= chi^2/n-1$, was calculated by dividing the H (chi^2) by n-1.

4 Result

4.1 Statistical data of the studied samples

4.1.1 Conventional semen parameters

Semen parameters for all studied samples (n=85) were evaluated by determining the sperm morphology, concentration, motility and semen volume. Table 4.1 shows some descriptive statistics parameters of the data of all 5 studied semen parameters for all donors (n=85). Donor age ranged from 22 to 66 years (34.34 ± 7.21), semen volume ranged from 0.8 to 7 ml (3.14 ± 1.5), sperm concentration ranged from 0.6 to 150 $1x10^6$ /ml (36.56 ± 26.25), sperm motility percentage ranged from 2 to 90 (59.85 ± 20.8), normal sperm morphology percentage ranged from 1 to 33 (8.71 ± 7.67).

Table 4.1: Semen parameters statistical data

Parameters	Mean ± SD	Median	Minimum	Maximum
Age	34.34 ± 7.21	34	22	66
Volume	3.14 ± 1.5	3	0.8	7
Concentration ($1x10^6$ /ml)	36.56 ± 26.25	32	0.6	150
Total Motility (motile %)	59.85 ± 20.8	65	2	90
Morphology (normal %)	8.71 ± 7.67	6	1	33

4.1.2 Sperm functional parameters

Three sperm functional parameters for all studied samples (n=85) were evaluated. These parameters include chromomycin A3 (protamine deficiency), aniline blue (histones retention) staining and acridine orange (DNA fragmentation). A notable variation in the percentage of positively stained sperm in all functional semen parameters were observed. Chromomycin A3 (non-condensed chromatin: protamine deficiency) positive percentage ranged from 13 to 100 (44.95 ± 21.38) as shown in Table 4.2. The histogram Figure 4.1 shows the distribution of chromomycin A3 staining of all 85 studied donors. The distribution of chromomycin A3 seems to be bimodal with the majority of donors found between 20% and 50%, and a second mode between 70% and 90%. Few donors are found in the highly condensed category between 10% and 20%. The distribution shows one donor as an outlier. Chromomycin A3 stain binds to sperm chromatin, specifically to the DNA, resulting in bright yellow color (positive, non-condensed) in protamine deficient sperm. Normal sperm instead appear in dull yellow color (negative, condensed) because chromomycin A3 cannot bind to DNA in fully chromatin condensed sperm. Aniline blue (non-condensed chromatin: histones retention) positive percentage ranged from 11 to 82 (37.24 ± 13.26) as shown in Table 4.2. The histogram

Figure 4.1 shows the distribution of aniline blue staining of all 85 studied donors. The most frequent categories are found between 40% and 50% with most other donors found below this category. The distribution is skewed to the left with one donor as an outlier. Aniline blue stain binds specifically to the amino acid lysine in the histones resulting in a blue color (positive, non-condensed) in histones rich sperm. Normal sperm appear unstained (negative, condensed) due to the low histones content. Acridine orange (DNA fragmentation) positive percentage ranged from 9 to 90 (35.88 ± 15.51) as shown in Table 4.2. The histogram Figure 4.1 shows the distribution of Acridine orange staining of all 85 studied donors. The most frequent categories are found between 30% and 50% with most other donors found below this category. The distribution is skewed to the left with two donors as an outlier. Acridine orange stain intercalates with the double stranded DNA in normal sperm and fluoresces green (negative, intact DNA). In DNA fragmented sperm it binds to single stranded DNA to form aggregates that fluoresces yellow, orange or red (positive, fragmented DNA).

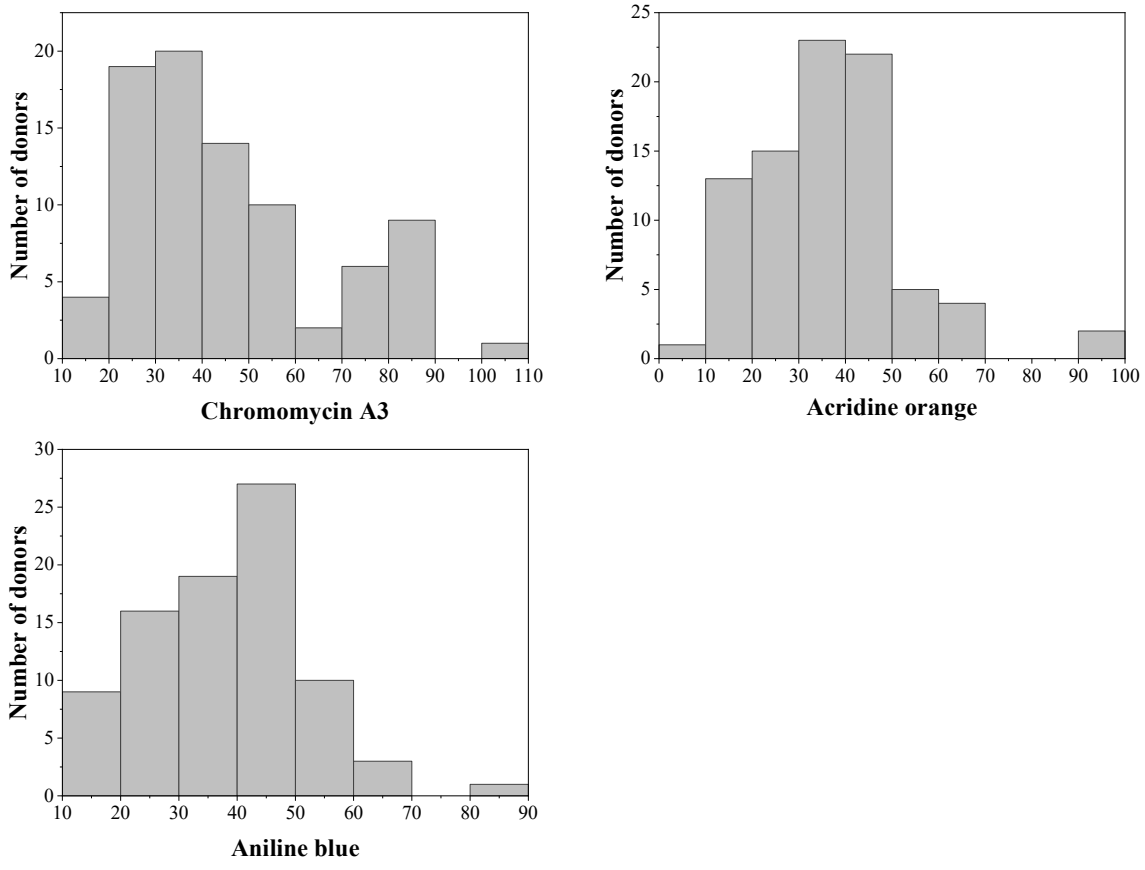

Figure 4.1: Histograms showing the distributions of all the studied sperm functional parameters. The x-axis shows the percentage intervals of the tests positivity.

Table 4.2: Sperm functional parameters statistical data

Parameters	Mean ± SD	Median	Minimum	Maximum
Chromomycin A3 (positive %)	44.95 ± 21.38	39	13	100
Aniline Blue (positive %)	37.24 ± 13.26	38	11	82
Acridine Orange (positive %)	35.88 ± 15.51	33	9	90

4.1.3 Intracytoplasmic sperm injection (ICSI) outcomes

Several ICSI outcomes were evaluated for the studied samples including fertilization rate, cleavage score, embryo quality score and embryo development score. Table 4.3 indicates the means ± standard deviations data of all studied samples (n=85 for fertilization rate, n=84 for other scores due to zero fertilization rate in one case). Fertilization rate ranged from 0 to 100 (66.44 ± 22.11), cleavage score ranged from 2 to 4 (3.38 ± 0.55), embryo quality score ranged from 1 to 3 (2.32 ± 0.42) and embryo development score ranged from 3 to 7 (5.7 ± 0.89). The histogram Figure 4.2 shows the distribution of all ICSI outcomes (n=85 for fertilization rate, n=84 for other scores). The distribution of the fertilization rate shows that the majority of donors are found within the categories between 50% and 90% with relatively few donors found between 0% and 30% with minor skewness to the left. The distribution of cleavage score seems to be bimodal with the majority of donors found between 2.8 and 3.6, and the second mode between 3.8 and 4. The distribution shows a few outlier donors between 2 and 2.2. The distribution of embryo quality score shows that the majority of donors are found within the categories between 2 and 2.8 with two outliers and minor skewness to the left. The distribution of embryo development score shows that the majority of donors are found within the categories from 5 to 7 and the distribution is skewed to the left.

Table 4.3: ICSI outcomes statistical data

Parameters	Mean ± SD	Median	Minimum	Maximum
Fertilization Rate (%)	66.44 ± 22.11	67	0	100
Cleavage Score	3.38 ± 0.55	3.47	2	4
Embryo Quality Score	2.32 ± 0.42	2.4	1	3
Embryo Development Score	5.7 ± 0.89	5.78	3	7

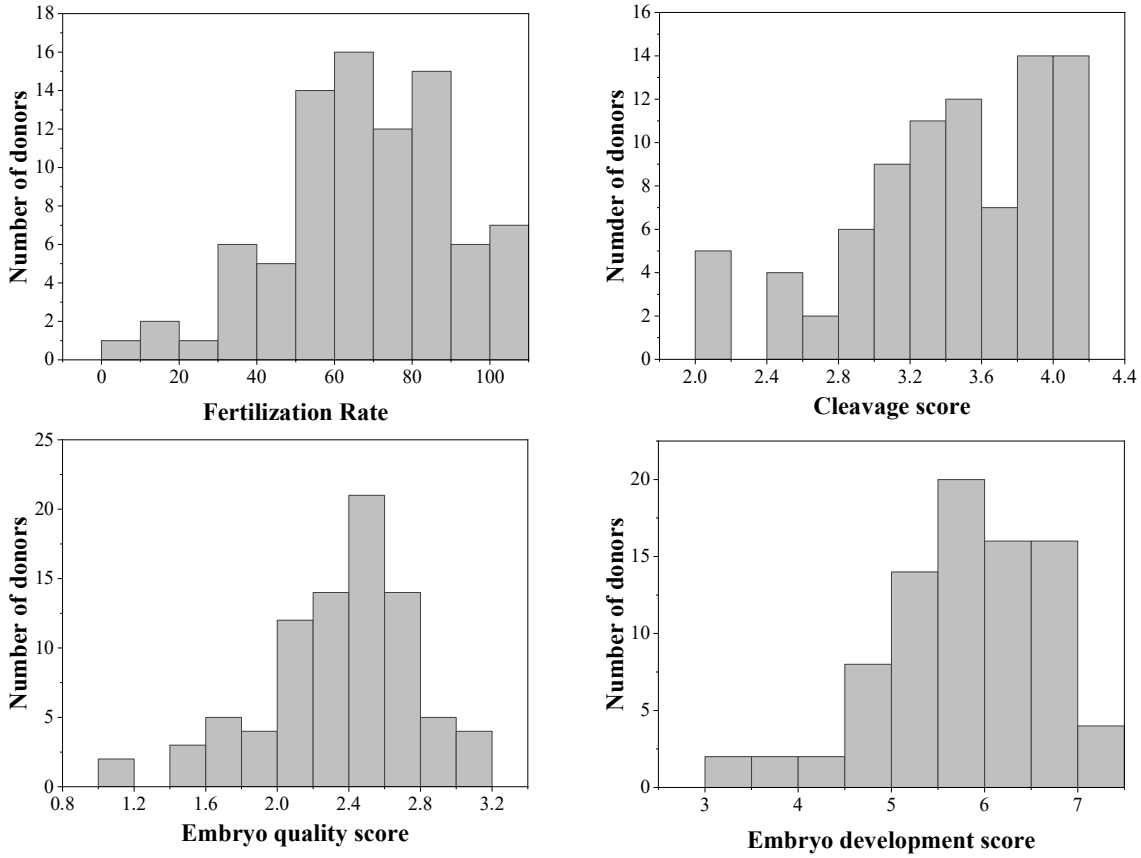

Figure 4.2: Histograms showing the distributions of all the assessed ICSI outcomes.

4.2 Correlations Analysis

4.2.1 Correlations between the assessed conventional semen parameters

Figure 4.3 shows the correlation between all conventional semen parameters in all studied samples (n=85). These parameters include age, volume, concentration, total motility, morphology. Sperm morphology was significantly positively correlated with sperm concentration ($r=0.608$, $p<0.001$) and total sperm motility ($r=0.576$, $p<0.001$), but it has not been significantly correlated with donor age ($r=-0.149$, $p=0.181$) and semen volume ($r=0.187$, $p=0.086$). Total sperm motility was significantly positively correlated with sperm concentration ($r=0.432$, $p<0.001$), but it has not been significantly correlated with donor age ($r=-0.081$, $p=0.461$) and semen volume ($r=0.193$, $p=0.076$). Sperm concentration was not significantly correlated with donor age ($r=-0.134$, $p=0.219$) and semen volume ($r=-0.106$, $p=0.334$). Finally, no significant correlation was found between donor age and semen volume ($r=-0.12$, $p=0.273$).

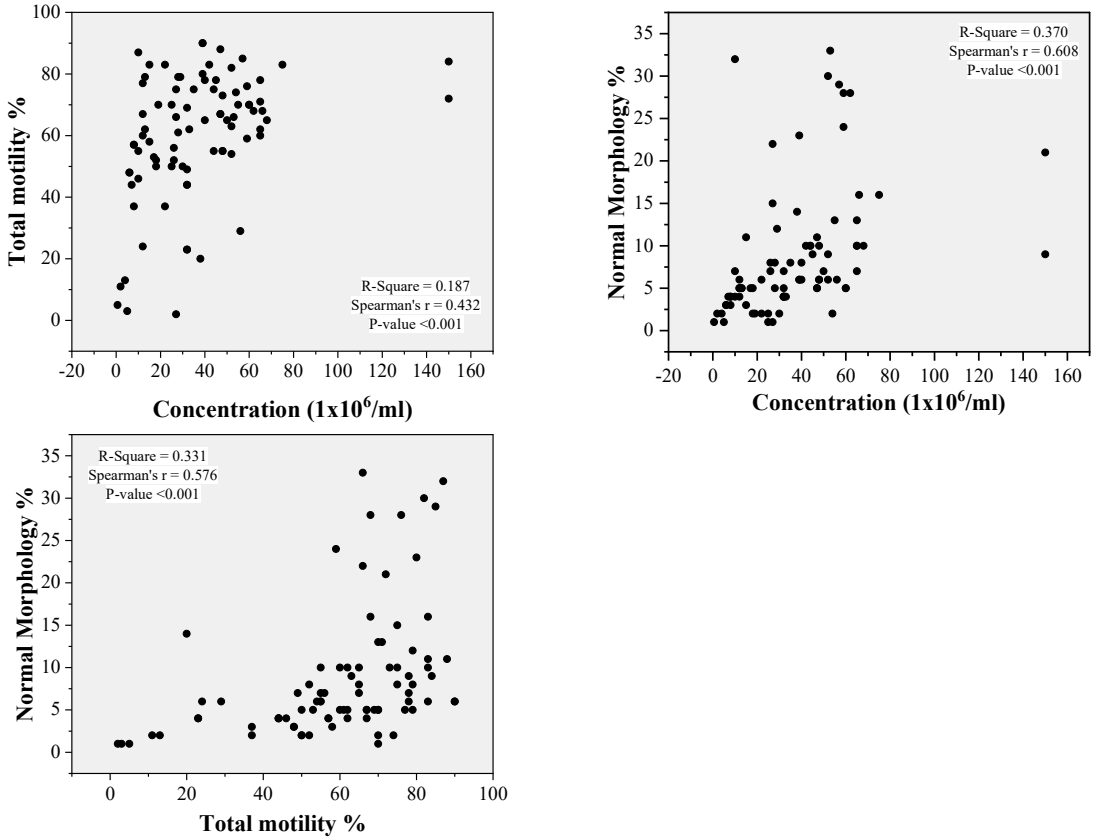

Figure 4.3: Scatter plots of conventional semen parameters correlations including Spearman's correlation coefficient, r^2 and significance level.

4.2.2 Correlations between the assessed sperm functional parameters

Chromomycin A3 staining was significantly positively correlated with acridine orange staining (r=0.449, p<0.001) as shown in Figure 4.4, but it has not been significantly correlated with aniline blue staining (r=0.151, p=0.166). Aniline blue staining was not significantly correlated with acridine orange staining (r=0.195, p=0.072).

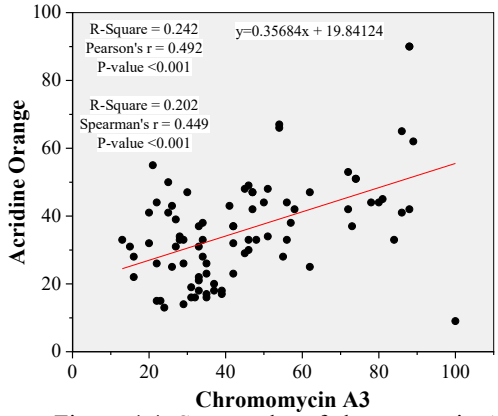

Figure 4.4: Scatter plot of chromomycin A3 and acridine orange correlation showing their Spearman's and Pearson's correlation coefficient, r^2 and significant levels. Regression equation is given and indicated with a red line.

4.2.3 Correlations between the intracytoplasmic sperm injection (ICSI) outcomes

Figure 4.5 shows the correlation between all ICSI outcomes in the studied samples (n=84). These outcomes include fertilization rate, cleavage score, embryo quality score and embryo development score. The fertilization rate was significantly positively correlated with embryo quality score (r=0.271, p=0.013) and embryo development score (r=0.259, p=0.017), but it has not been significantly correlated with cleavage score (r=0.213, p=0.052). The cleavage score was significantly positively correlated with embryo quality score (r=0.592, p<0.001) and embryo development score (r=0.905, p<0.001). The embryo quality score was significantly positively correlated embryo development score (r=0.862, p<0.001).

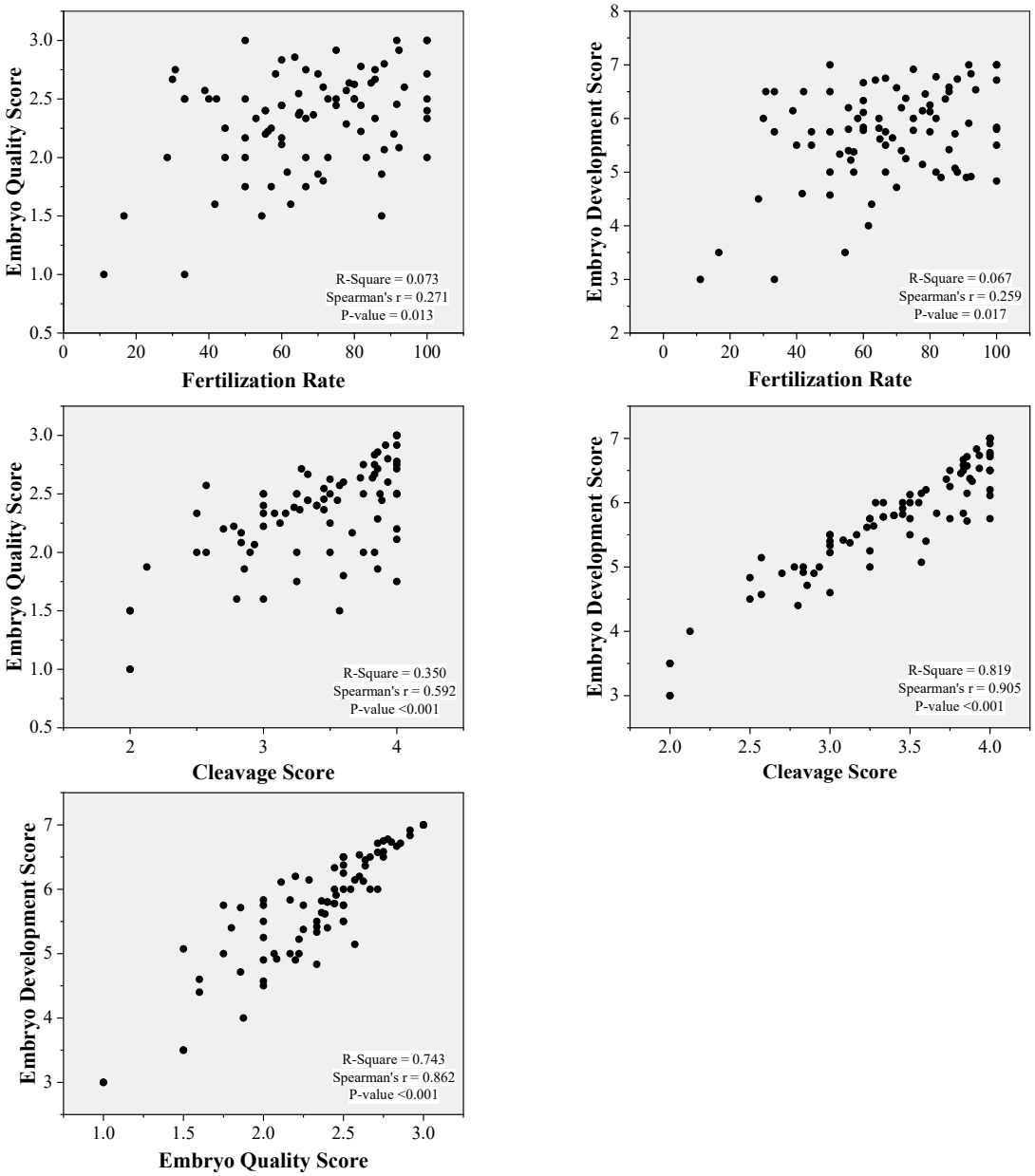

Figure 4.5: Scatter plots of ICSI outcomes correlations including Spearman's correlation coefficient, r^2 and significance levels.

4.2.4 Correlations between the assessed conventional semen parameters and sperm functional parameters

Figure 4.6 shows the correlation between all conventional semen parameters and sperm functional parameters in all studied samples (n=85). These parameters include age, volume, concentration, total motility, morphology, chromomycin A3 staining, acridine orange staining and aniline blue staining. Chromomycin A3 staining was significantly negatively correlated with sperm concentration (r=-0.388,

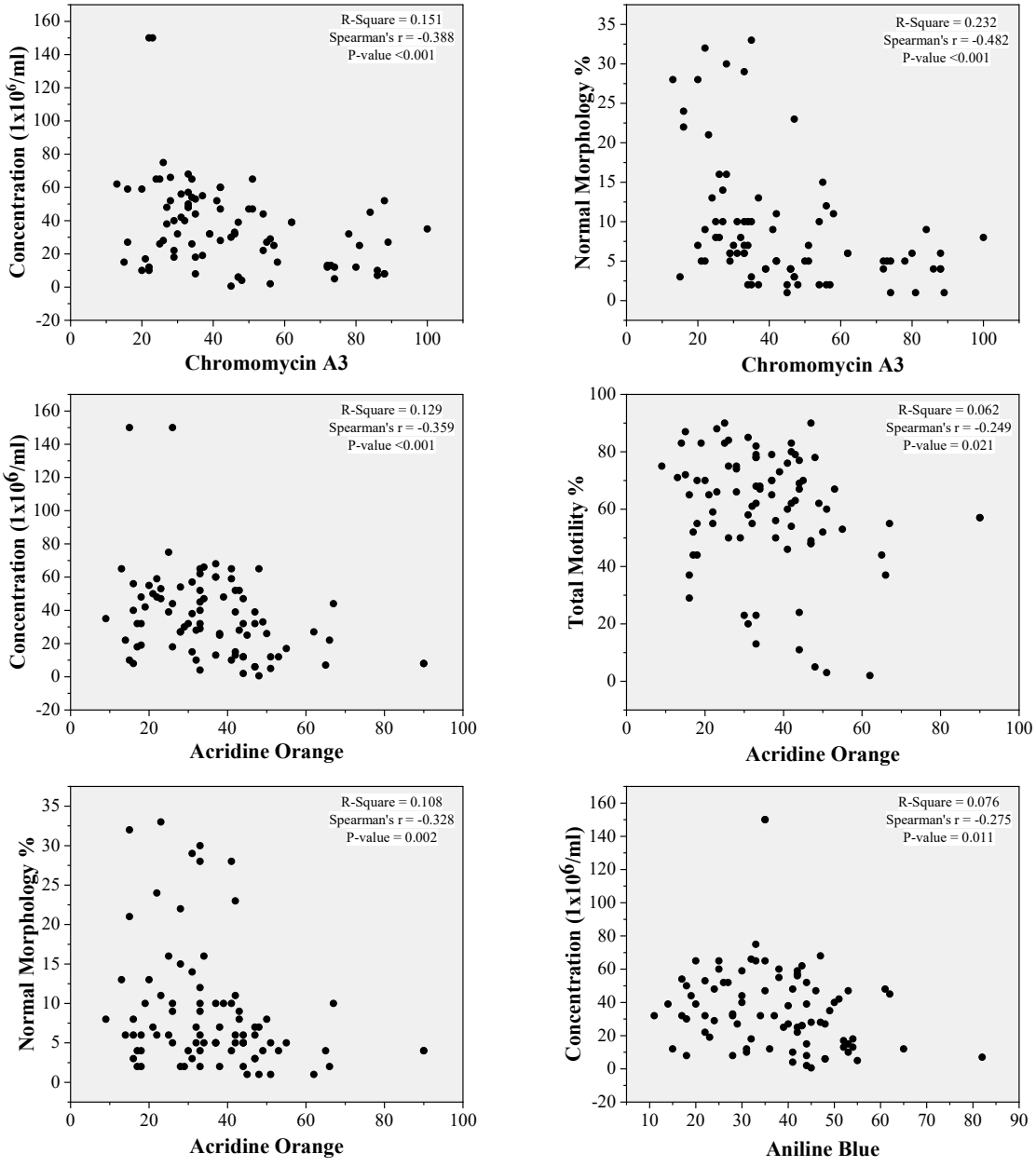

Figure 4.6: Scatter plots of conventional semen parameters and sperm functional parameters correlations indicating their Spearman's correlation coefficients, r^2 and significance levels.

p<0.001) and sperm morphology (r=-0.482, p<0.001), but it has not been significantly correlated with the total sperm motility (r=-0.183, p=0.092), donor age (r=0.092, p=0.398), an d semen volume (r=-0.08, p=0.466). Acridine orange staining was significantly negatively correlated with sperm concentration (r=-0.359, p<0.001), total sperm motility (r=-0.249, p=0.021) and sperm morphology (r=-0.328, p=0.002), but it has not been significantly correlated with donor age (r=0.081, p=0.461), and semen volume (r=-0.128, p=0.242). Aniline blue staining was significantly negatively correlated with sperm concentration (r=-0.275, p=0.011), but it has not been significantly correlated with total sperm motility (r=-0.055, p=0.611), sperm morphology (r=-0.049, p=0.654), donor age (r=-0.185, p=0.089), and semen volume (r=-0.150, p=0.169).

4.2.5 Correlations between the assessed conventional semen parameters and ICSI outcomes

All conventional semen parameters and ICSI outcomes were tested for correlations in all studied samples (n=85 for fertilization rate and n=84 for other outcomes). These parameters include age, volume, concentration, total motility, morphology, fertilization rate, cleavage score, embryo quality score and embryo development score. As illustrated in Figure 4.7 sperm concentration was significantly positively

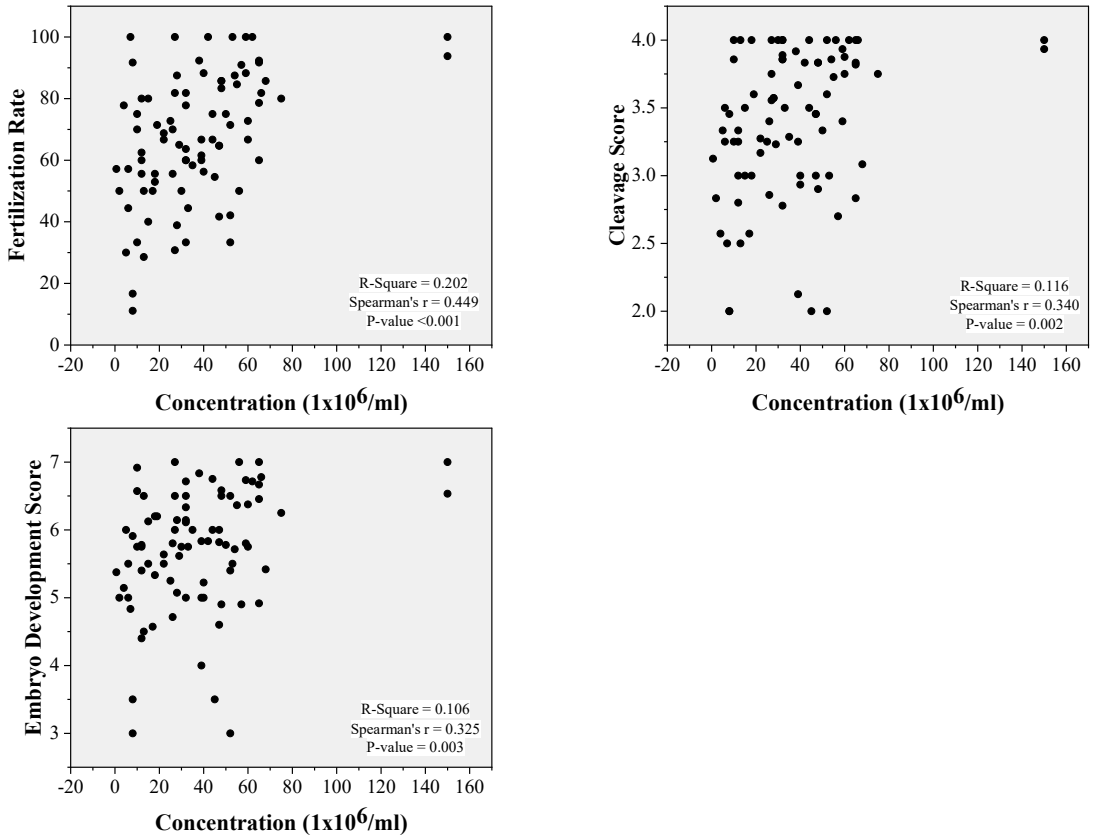

Figure 4.7: Scatter plots of sperm concentration and ICSI outcomes correlations indicating their Spearman's correlation coefficients, r^2 and significance levels.

correlated with the fertilization rate (r=0.449, p<0.001), cleavage score (r=0.34, p=0.002) and embryo development score (r=0.325, p=0.003), but it has not been significantly correlated with embryo quality score (r=0.208, p=0.058). As illustrated in Figure 4.8 sperm morphology was significantly positively correlated with the fertilization rate (r=0.487, p<0.001), cleavage score (r=0.222, p=0.042), embryo quality score (r=0.3, p=0.006) and embryo development score (r=0.299, p=0.006). Total motility was not significantly correlated with the fertilization rate (r=0.208, p=0.056), cleavage score (r=0.042, p=0.701), embryo quality score (r=-0.036, p=0.741) and embryo development score (r=-0.018, p=0.869). Semen volume was not significantly correlated with the fertilization rate (r=0.108, p=0.323), cleavage score (r=0.025, p=0.821), embryo quality score (r=-0.026, p=0.812) and embryo development score (r=0.015, p=0.888). Donor age was not significantly correlated with the fertilization rate (r=-0.171, p=0.117), cleavage score (r=-0.117, p=0.285), embryo quality score (r=-0.155, p=0.157) and embryo development score (r=-0.169, p=0.124).

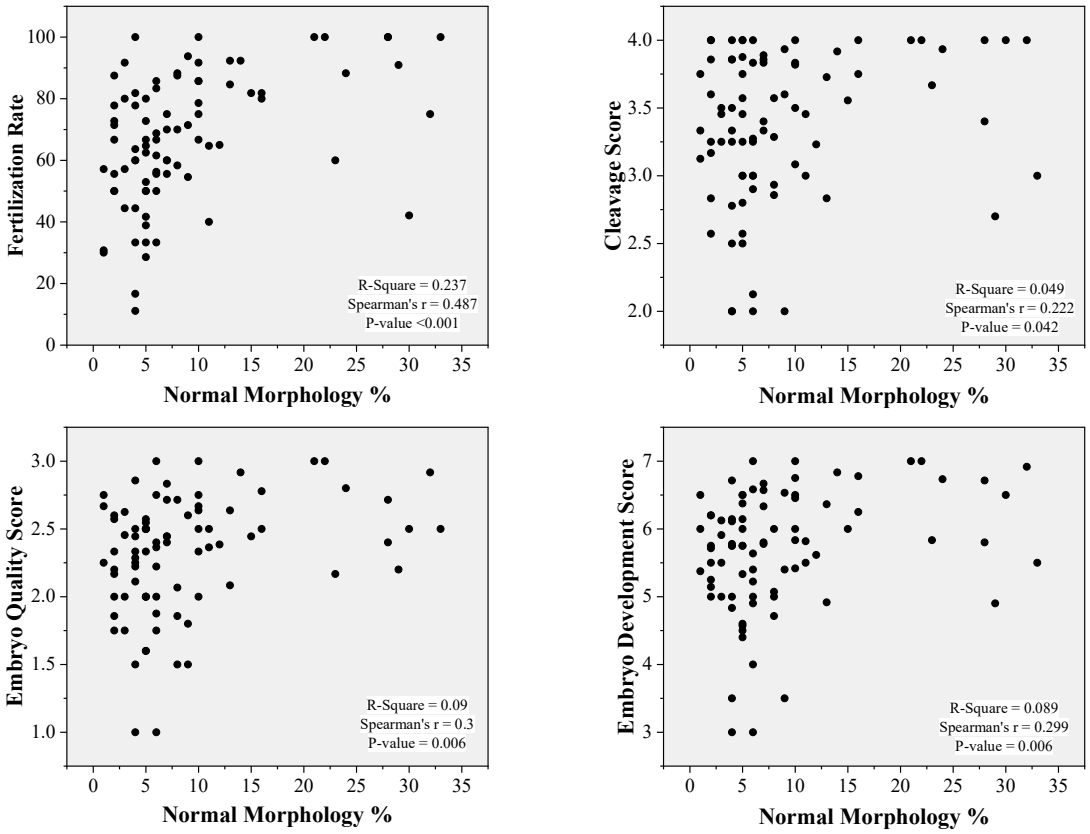

Figure 4.8: Scatter plots of sperm morphology and ICSI outcomes correlations indicating their Spearman's correlation coefficients, r^2 and significance levels.

4.2.6 Correlations between the assessed sperm functional parameters and ICSI outcomes

All sperm functional parameters and ICSI outcomes were tested for correlations in all studied samples (n=85 for fertilization rate and n=84 for other outcomes). These parameters include chromomycin A3 staining, acridine orange staining and aniline blue staining, fertilization rate, cleavage score, embryo quality score and embryo development score. As illustrated in Figure 4.9 chromomycin A3 staining was significantly negatively correlated with the fertilization rate (r=-0.626, p<0.001), cleavage score (r=-0.386, p<0.001), embryo quality score (r=-0.319, p=0.003) and embryo development score (r=-0.388, p<0.001). As illustrated in Figure 4.10 acridine orange staining was significantly negatively correlated with the fertilization rate (r=-0.466, p<0.001), cleavage score (r=-0.238, p=0.029), embryo quality score (r=-0.254, p=0.019) and embryo development score (r=-0.284, p=0.009). Aniline blue staining was not significant correlated with the fertilization rate (r=-0.207, p=0.057), cleavage score (r=-0.181, p=0.098), embryo quality score (r=-0.099, p=0.368) and embryo development score (r=-0.156, p=0.156).

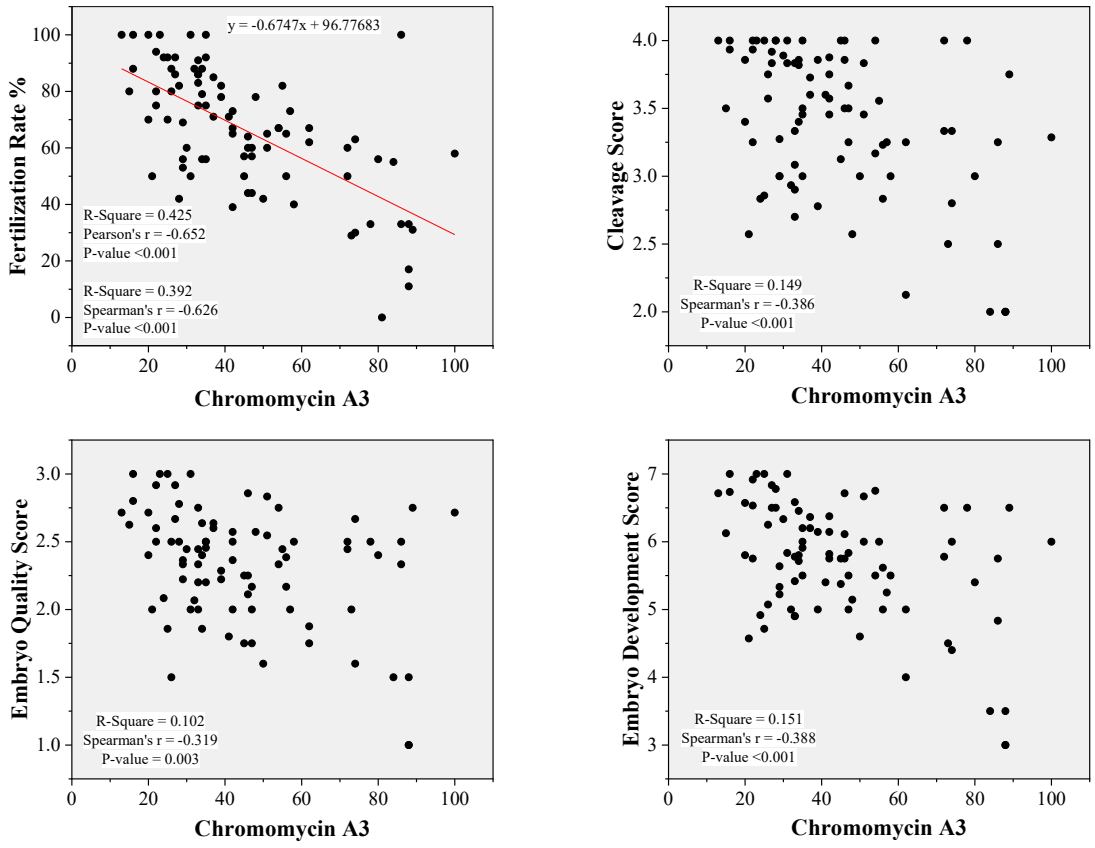

Figure 4.9: Scatter plots of chromomycin A3 and ICSI outcomes correlations indicating their Spearman's correlation coefficients, r^2 and significance levels. Regression equation and Pearson's correlation are given for chromomycin A3 and fertilization rate. Regression equation is given and indicated with a red line.

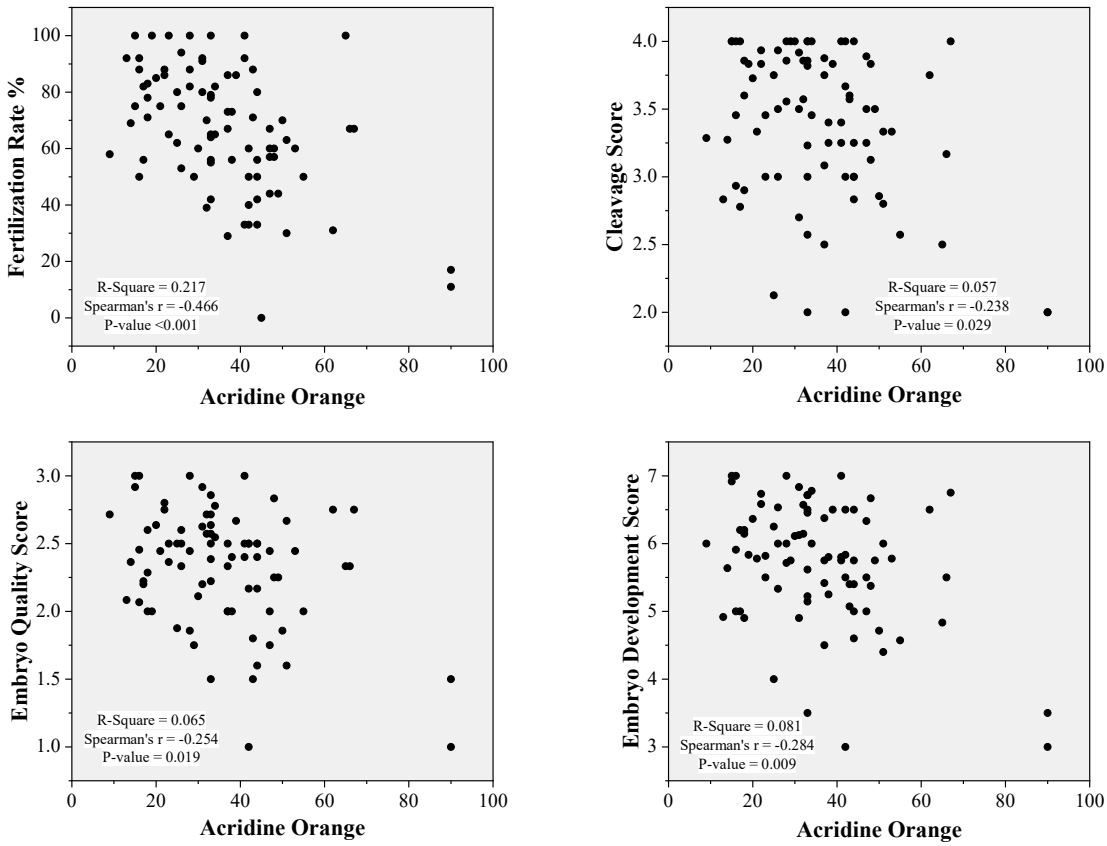

Figure 4.10: Scatter plots of acridine orange and ICSI outcomes correlations indicating their Spearman's correlation coefficients, r^2 and significance levels.

4.3 Sample classification

To investigate the effect of sperm chromatin condensation on the ICSI outcomes, and later to investigate the ability of Raman spectroscopy to detect different levels of sperm chromatin condensation the samples were classified in groups. Samples were classified according to the result of sperm functional test, especially the chromomycin A3 result. Chromomycin A3 test (protamine deficiency test) was selected because its result shows significant correlations with all studied ICSI outcomes. These outcomes include fertilization rate, cleavage score, embryo quality score and embryo development score. Fertilization rate shows the best correlation with chromomycin A3 result and therefore selected to classify the samples. The relationship between the chromomycin A3 and fertilization rate was analyzed by receiver operating characteristics (ROC) curve Figure 4.11 to determine the cutoff value of chromomycin A3 to distinguish between donors with low and high fertilization prognosis. Condensed (yes) or non-condensed (no) was used as discriminator. Different thresholds values were tested to determine a cutoff value of CMA3, and 41%

(positive) was used. Samples were classified into two groups CMA3≤41 (n=44) and CMA3>41 (n=41). The ROC curve result indicates that the area under the curve was 0.8589 with 87.8% specificity and 81.8% sensitivity. That means CMA3 could be an excellent diagnostic test in predicting fertilization rate (figure). Additionally, samples were classified into three groups by calculating two cutoff points around the CMA3 median (39) value (± 0.5 SD of CMA3 positive). Using these two cutoff points samples were classified into the following groups: group A CMA3<28 (n=18), group B 28≤CMA3≤50 (n=40), group C CMA3>50 (n=27).

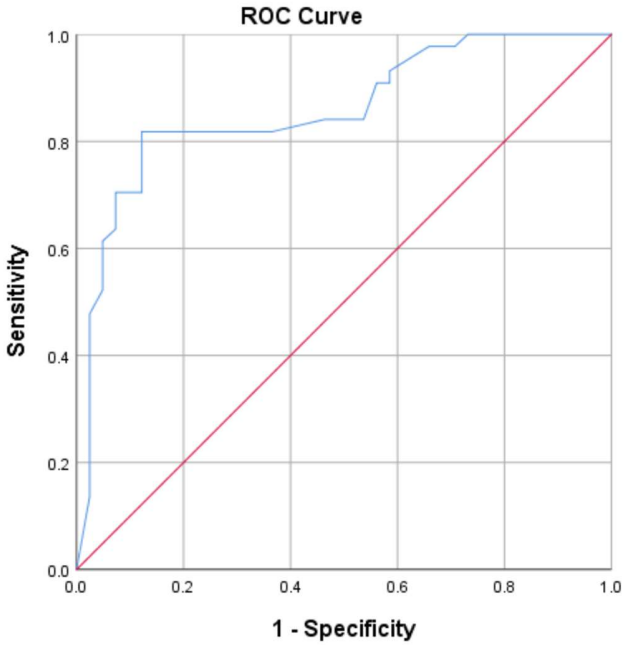

Figure 4.11: Receiver operating characteristic (ROC) curve of chromomycin A3 and fertilization rate with 41% cutoff point, the area under the curve was 0.8589 with 87.8% specificity and 81.8% sensitivity.

4.4 Effect of chromatin condensation

4.4.1 Effect of chromatin condensation based on one cutoff point

Based on the cutoff value of CMA3 determined by the ROC curve, studied samples were categorized into two groups. Group A includes donors with CMA3 positive percentage ≤41and group B donors with CMA3 positive percentage >41.

4.4.1.1 Effect of chromatin condensation on conventional semen parameters

The median of donor's age (CMA3≤41 (32.5±9.95), CMA3>41 (34±7.55), p=0.503), semen volume (CMA3≤41 (3±1.44), CMA3>41 (2.7±1.55), p=0.116) and sperm motility (CMA3≤41 (65.5±15.21), CMA3>41 (61±24.9), p=0.056) did not show a significant difference between the studied groups. The median of sperm morphology (CMA3≤41 (8.5±8.93), CMA3>41 (5±4.23), p<0.001) and sperm

concentration (CMA3≤41 (46±29.58), CMA3>41 (27±17.71), p<0.001) showed a significant difference between the studied groups as illustrated in Figure 4.12.

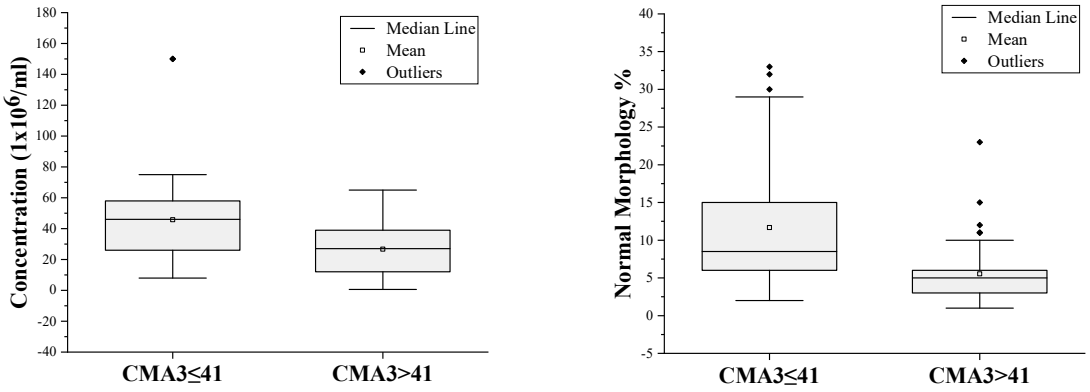

Figure 4.12: Box plots showing the differences of semen parameters that show significant differences between CMA3≤41 (n=44) and CMA3>41 (n=41) groups (Mann-Whitney p-values for the differences in the medians were p<0.001 for concentration and p<0.001 for normal morphology).

4.4.1.2 Effect of chromatin condensation on sperm functional parameters

The median acridine orange (CMA3≤41 (27±10.93), CMA3>41 (42±15.74), p<0.001) show a significant difference between the studied groups as illustrated in Figure 4.13, while the median aniline blue (CMA3≤41 (35±11.66), CMA3>41 (42±14.41), p=0.058) did not show a significant difference between the studied groups.

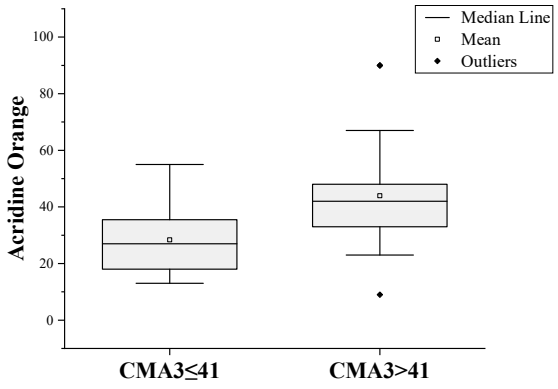

Figure 4.13: Box plot showing the differences of acridine orange between CMA3≤41 (n=44) and CMA3>41 (n=41) groups (Mann-Whitney p-value for the difference in the median was p<0.001).

4.4.1.3 Effect of chromatin condensation on ICSI outcomes

The median fertilization rate (CMA3≤41 (82±15.5), CMA3>41 (57±19.73), p<0.001), cleavage score (CMA3≤41 (3.66±0.44), CMA3>41 (3.25±0.78), p=0.009), embryo quality score (CMA3≤41 (2.47±0.35), CMA3>41 (2.33±0.57), p=0.014) and embryo development score (CMA3≤41 (6.06±0.71), CMA3>41 (5.61±1.28), p=0.006) showed a significant difference between the studied groups as illustrated in Figure 4.14.

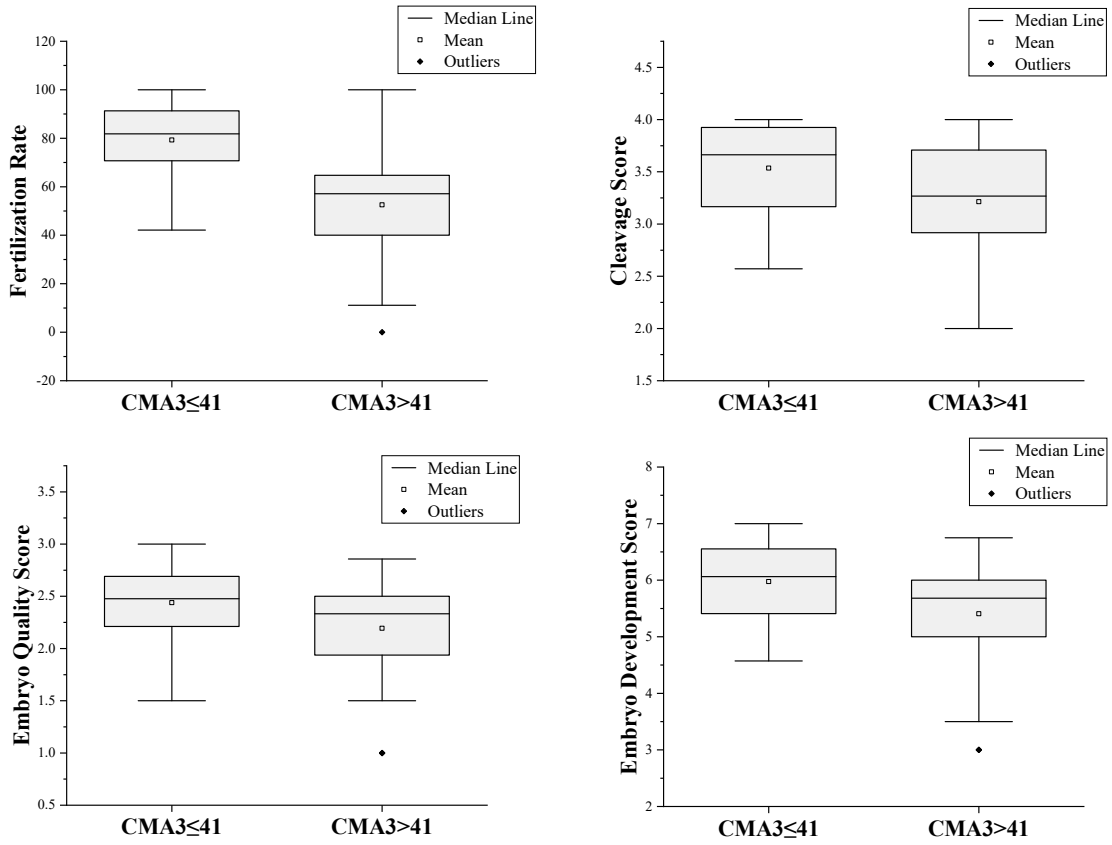

Figure 4.14: Box plots showing the differences of ICSI outcomes between CMA3≤41 (n=44) and CMA3>41 (n=40, n=41 for fertilization rate) groups (Mann-Whitney p-values for the differences in the medians were p<0.001 for fertilization rate, p=0.009 for cleavage score, p=0.014 for embryo quality score and p=0.006 for embryo development score).

4.4.2 Effect of chromatin condensation based on two cutoff points

Based on the two cutoff values of CMA3 that were determined around the CMA3 median value (± 0.5 SD of CMA3 positive), studied samples were categorized into three groups. Group A includes donors with CMA3 positive percentage <28, group B donors with 28≤ CMA3 positive percentage ≤50 and group C includes donors with CMA3 positive percentage >50.

4.4.2.1 Effect of chromatin condensation on conventional semen parameters

The median of donor's age (CMA3<28 (31.5±6.18), 28≤CMA3≤50 (34±8.23), CMA3>50 (34±5.68), p=0.189), semen volume (CMA3<28 (3±1.32), 28≤CMA3≤50 (3±1.74), CMA3>50 (3±1.19), p=0.666) and sperm motility (CMA3<28 (69.5±15.91), 28≤CMA3≤50 (62.5±19.83), CMA3>50 (62±24.63), p=0.340) did not show a significant difference between the studied groups. The median of sperm morphology (CMA3<28 (11.5±9.03), 28≤CMA3≤50 (6±7.74), CMA3>50 (5±3.47), p<0.001) and sperm concentration (CMA3<28 (43±42.05), 28≤CMA3≤50 (40±18.41), CMA3>50 (25±16.52), p=0.007) showed a significant difference between the studied groups. Dunn's Post Hoc test was applied to determine which groups are different, groups that show a significant difference are illustrated in Figure 4.15 with the Bonferroni corrected p-values.

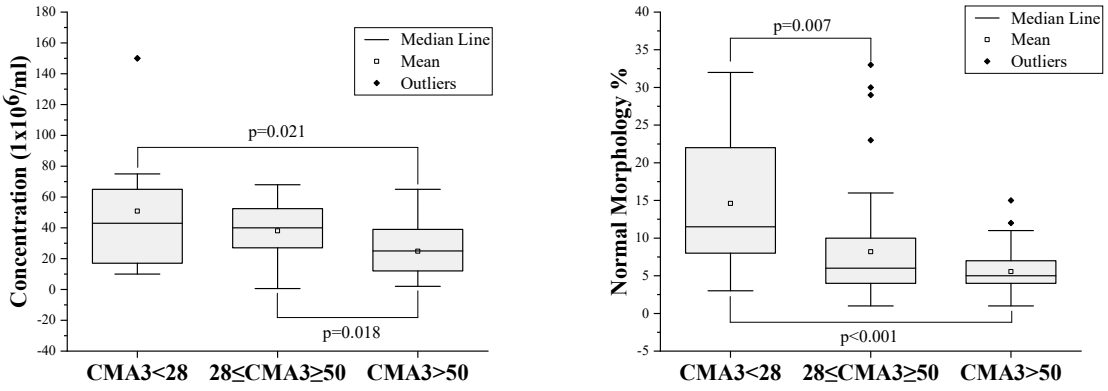

Figure 4.15: Box plots showing the differences of conventional semen parameters that show significant differences between CMA3<28 (n=18), 28≤CMA3≥50 (n=40) and CMA3>50 (n=27) groups (Kruskal-Wallis p-values for the differences in the medians were p=0.007 for concentration and p<0.001 for morphology).

4.4.2.2 Effect of chromatin condensation on sperm functional parameters

The medians of acridine orange (CMA3<28 (31.5±12.05), 28≤CMA3≤50 (30.5±10.68), CMA3>50 (44±17.81), p<0.001) showed a significant difference between the studied groups, while the median aniline blue (CMA3<28 (40±8.12), 28≤CMA3≤50 (33.5±12.58), CMA3>50 (44±16.03), p=0.151) did not show a significant difference between the studied groups. Dunn's Post Hoc test was applied to determine which groups are different, groups that show a significant difference are illustrated in the Figure 4.16 with the Bonferroni corrected p-values.

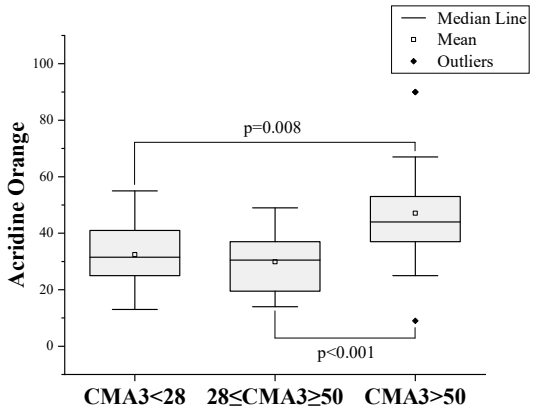

Figure 4.16: Box plot showing the difference of acridine orange between CMA3<28 (n=18), 28≤CMA3≥50 (n=40) and CMA3>50 (n=27) groups (Kruskal-Wallis p-values for the difference in the median was p<0.001).

4.4.2.3 Effect of chromatin condensation on ICSI outcomes

The median fertilization rates (CMA3<28 (88±13.27), 28≤CMA3≤50 (70±16.83), CMA3>50 (56±22.6), p<0.001), cleavage scores (CMA3<28 (3.84±0.46), 28≤CMA3≤50 (3.53±0.41), CMA3>50 (3.24±0.65),

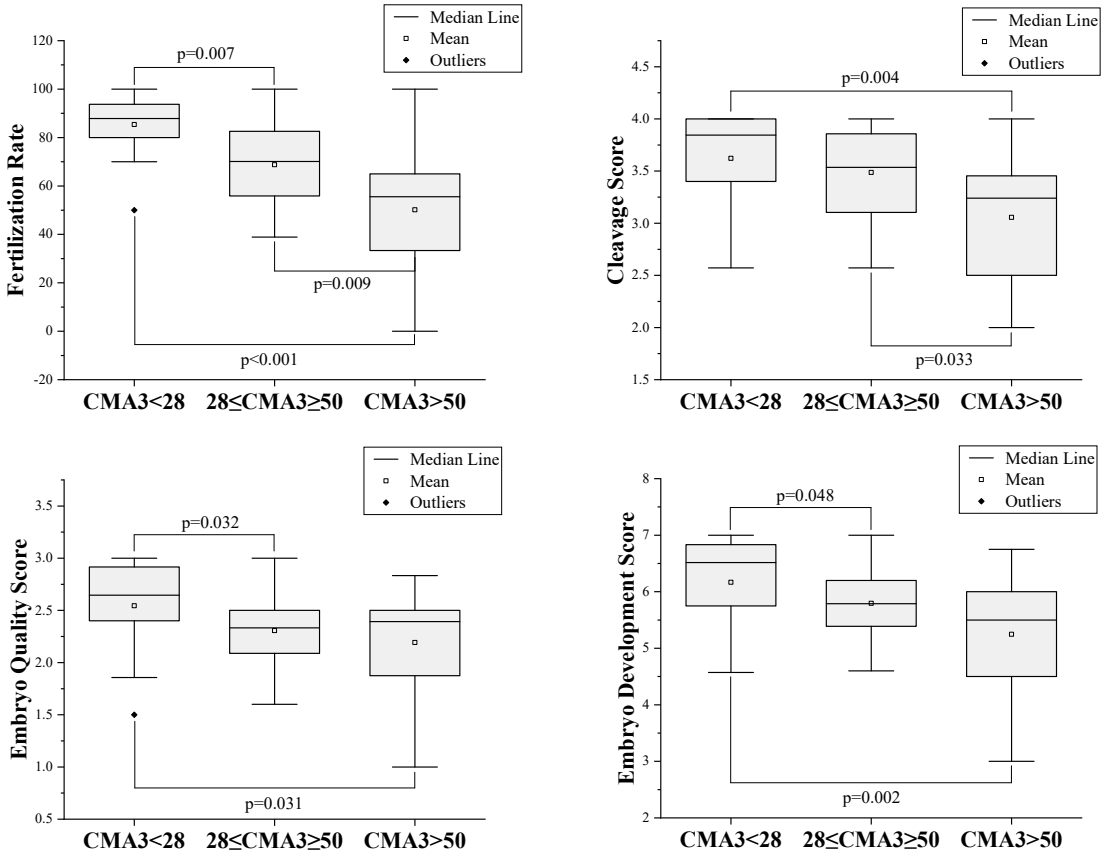

Figure 4.17: Box plots showing the differences of ICSI outcomes between CMA3<28 (n=18), 28≤CMA3≥50 (n=40) and CMA3>50 (n=26, n=27 for fertilization rate) groups (Kruskal-Wallis p-values for the differences in the medians were p<0.001 for fertilization rate, p=0.003 for cleavage score, p=0.018 for embryo quality score and p=0.007 for embryo development score).

p=0.003), embryo quality scores (CMA3<28 (2.64±0.43), 28≤CMA3≤50 (2.33±0.31), CMA3>50 (2.39±0.52), p=0.018) and embryo development scores (CMA3<28 (6.51±0.83), 28≤CMA3≤50 (5.78±0.57), CMA3>50 (5.5±1.12), p=0.007) showed a significant difference between the studied groups. Dunn's Post Hoc test was applied to determine which groups are different, groups that show a significant difference are illustrated in Figure 4.17 with the Bonferroni corrected p-values.

4.5 Effect of (WHO) semen parameters

Samples were classified according to the WHO standard into two groups: fertile (n=53) and subfertile (n=32).

4.5.1 Effect of (WHO) semen parameters on sperm functional parameters

The medians of CMA3 (fertile (34±18.33), subfertile (47.5±23.16), p=0.004) and acridine orange (fertile (33±12.12), subfertile (41.5±18.69), p=0.004) showed a significant difference between the studied groups as illustrated in Figure 4.18. Aniline blue (fertile (35±12.02), subfertile (41±15.05), p=0.257) did not show a significant difference between the studied groups.

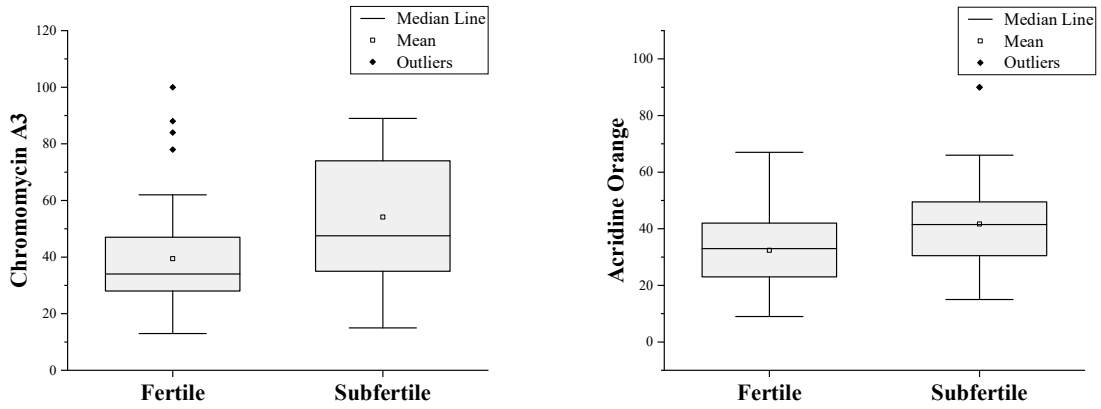

Figure 4.18: Box plots showing the differences of the functional sperm parameters that show significant differences between fertile (n=53) and subfertile (n=32) groups (Mann-Whitney p-values for the differences in the medians were p=0.004 for chromomycin A3 and p=0.004 for acridine orange).

4.5.2 Effect of (WHO) conventional semen parameters on ICSI outcomes

The median fertilization rates (fertile (73±19.02), subfertile (58.5±24.09), p=0.006) showed a significant difference between the studied groups as illustrated in Figure 4.19. Cleavage scores (fertile (3.5±0.53), subfertile (3.33±0.58), p=0.694), embryo quality scores (fertile (2.4±0.41), subfertile (2.4±0.46), p=0.798) and embryo development scores (fertile (5.81±0.87), subfertile (5.75±0.93), p=0.569) did not show a significant difference between the studied groups.

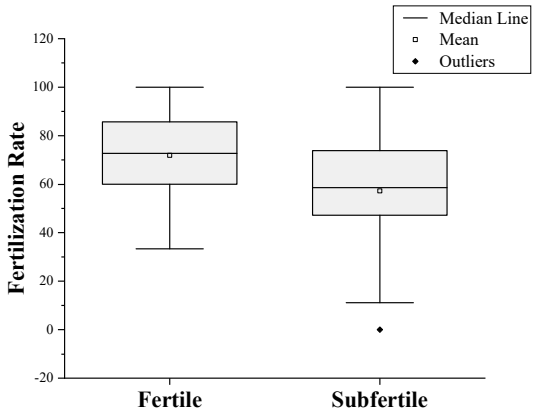

Figure 4.19: Box plot showing the difference of fertilization rate between fertile (n=53) and subfertile (n=32) groups (Mann-Whitney p-values for differences in the medians was p=0.006).

4.6 Raman spectroscopy (system optimization)

4.6.1 Substrate Study

To minimize the effect of background substrate contribution on the Raman spectra of the measured cells, three substrates were investigated. Raman spectra were acquired for the glass, quartz and stainless steel slides using the 660 nm laser and the same acquisition parameters. The Raman spectra of the measured substrates are showed in Figure 4.20. As shown in the figure the glass spectrum yields a very high intensity throughout the measured wavenumber range that can easily mask the Raman spectra of the measured cells. The Quartz spectrum shows relatively high intensities around 600 cm^{-1}, 800 cm^{-1} and 1050 cm^{-1} that may interfere with the Raman spectra of the measured cells. Stainless steel has the lowest intensity among the three investigated substrates. Figure 4.21 shows sperm Raman spectra measured on the three selected substrates. As shown in the figure, using the glass slide as substrate make the Raman peaks of sperm is hardly to be detected. Quartz slide has a notable decreased contribution compared to glass, but its contribution can still be observed in the elevated intensity in the main Raman peak around 785 cm^{-1} and the Raman peak shoulder around 1050 cm^{-1}. These results indicate that the stainless steel substrates have the lowest contribution of substrate background and best represent the true Raman spectra of the measured cells. This minimizes required corrections and is a key factor for quantitative spectral analysis.

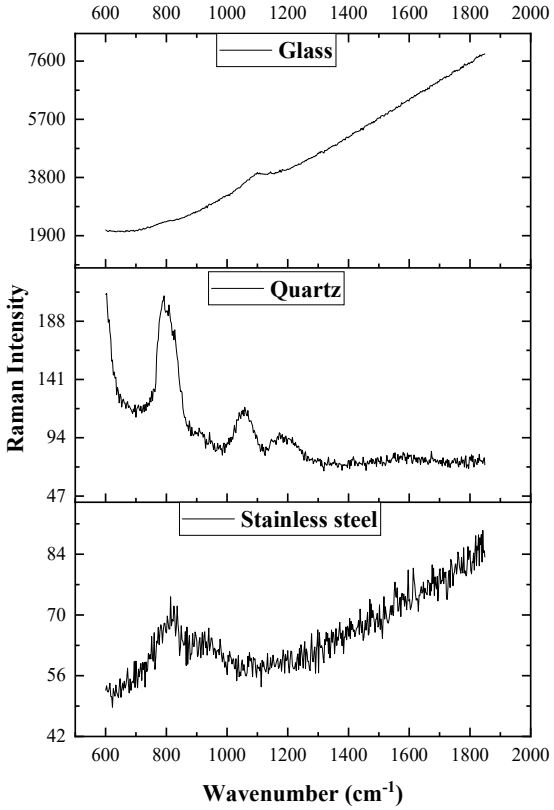

Figure 4.20: Raman spectra of different background substrates.

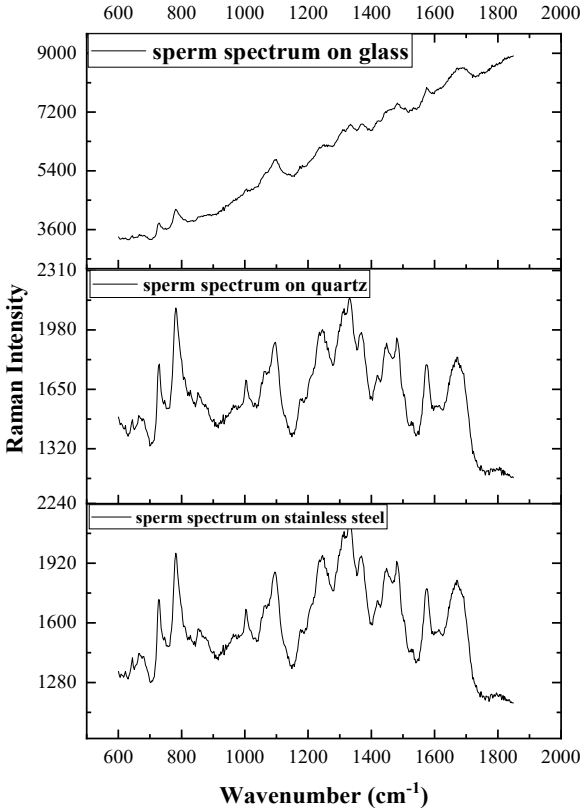

Figure 4.21: Raman spectra of sperm using different background substrates.

4.6.2 Evaluation of the sperm regions and Raman spectroscopy resolution

Raman spectra were obtained from four different parts of the human sperm to investigate the Raman system's resolution. These parts include acrosome, head, midpiece and the tail. As illustrated in Figure 4.22, the Raman spectra of these parts varied greatly in both Raman intensity and in the presence of Raman peaks due to the presence of different biochemical compositions in the investigated parts. The Raman spectra of sperm head were dominated by the Raman peaks of sperm chromatin including DNA and protein, that are not found in the other parts of the human sperm. To investigate the chromatin condensation status, sperm head was used and all Raman spectra in this study were obtained from the postacrosomal region.

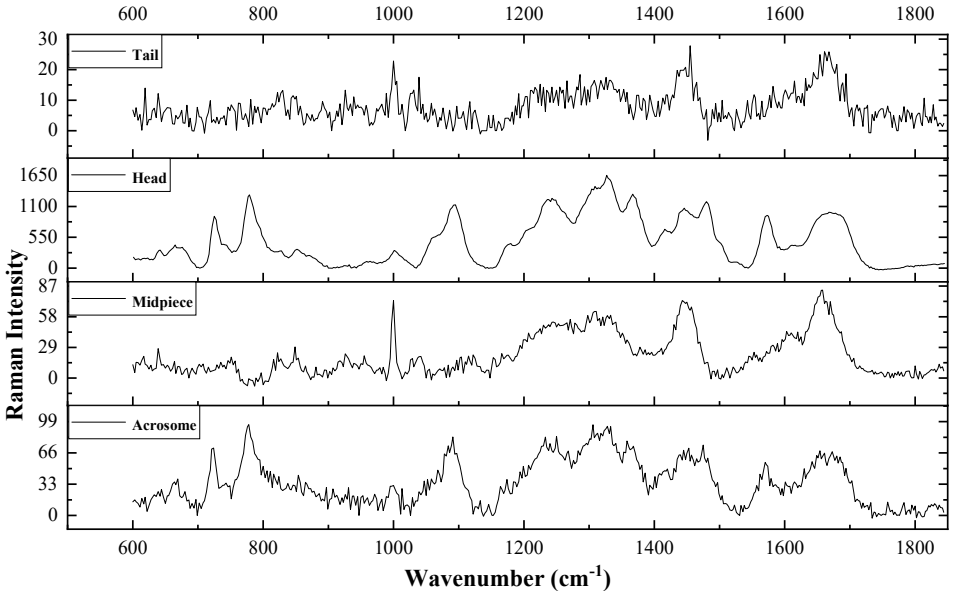

Figure 4.22: Raman spectra of different sperm regions.

4.7 Reproducibility test

The Raman intensities for the measured sperm show variations within the same donor. To minimize the effect of variation within the donors, 50 sperm were measured for each donor. In order to determine if 50 sperm are enough to overcome this variation, three sets of 50 sperm from the same donor were measured separately and yielded virtually identical spectra as illustrated in Figure 4.23. Also, the intensities of the major Raman peaks were extracted and tested for differences and the result indicates no statistical differences in all the extracted Raman peaks.

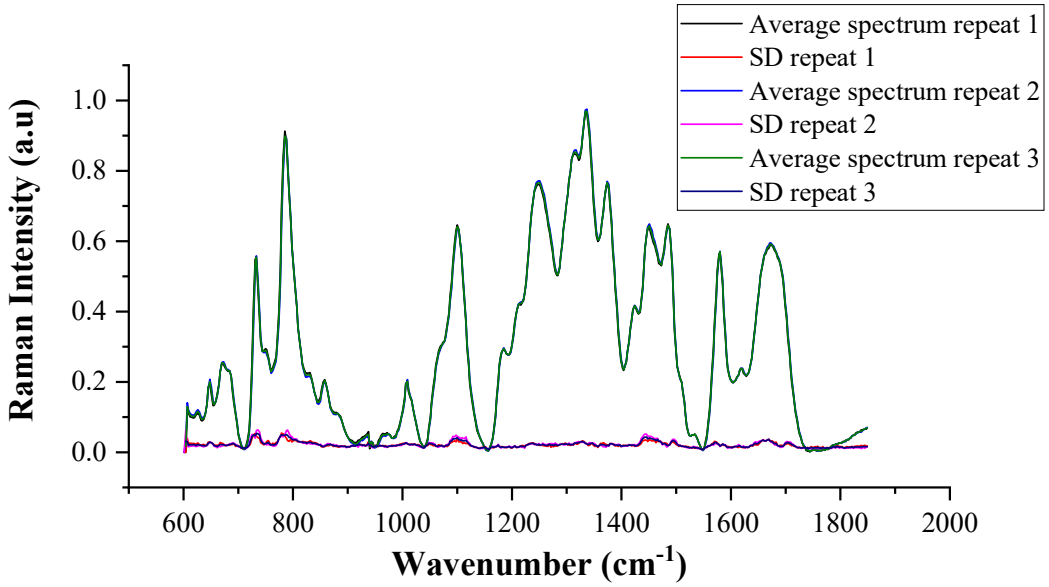

Figure 4.23: Average Raman spectra and their SD of three separately measured 50 cell subsets for the same donor.

4.8 Spectra processing

4.8.1 Baseline correction

To eliminate the spectral background caused by fluorescence of cell components, all acquired Raman spectra were filtered by applying a 5 points model fit subtraction and setting the lowest intensity value to zero. Processing was performed using a home-written program (by Prof. M. Baller) in LabVIEW software. This program subtracts the background from the raw spectra without providing a significant distortion of the Raman peaks of the measured samples resulting in virtually background-free Raman peaks. Figure 4.24 describe the baseline removal process, where the black spectrum represents the raw spectrum, the red trace represents the model fit subtraction and the blue spectrum represents the background-free spectrum.

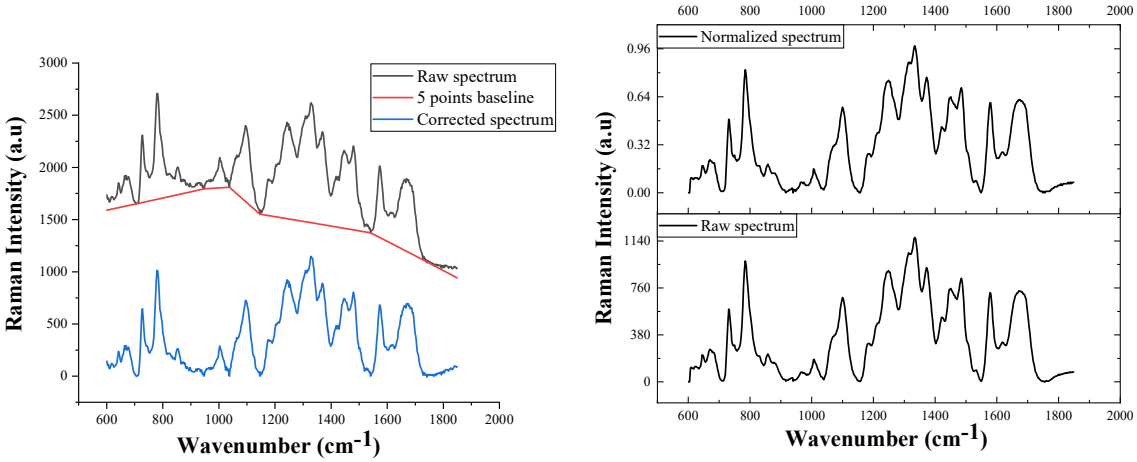

Figure 4.24: Raman spectra processing. Raman spectra of raw versus baseline corrected data (left). Raman spectra of raw (only baseline corrected) versus normalized data (right).

4.8.2 Spectral normalization

For quantitative evaluation, spectral intensities values are rescaled for uniformity by normalization. Spectra normalization was performed by home-written program (by Prof. M. Baller) in LabVIEW software. The program normalizes the spectra by setting the lowest intensity of the spectra to zero, and dividing the whole spectrum by the average intensity value of the whole spectrum. Then, multiplying the resulting value by 3 to arbitrarily set the maximum intensity to around 1. Both raw and normalized spectra are showed in Figure 4.24. The methods of normalization enable quantitative comparisons of individual spectral features within a spectrum as no single wavenumber or peak is normalized to a fixed value, e.g. 1.

4.9 Raman spectral analysis

4.9.1 Average spectrum

Figure 4.25 shows the average Raman spectrum and the standard deviation of all studied samples. Several peaks in the average Raman spectrum show a high variation in their intensities as indicated by the elevated values of standard deviation and show a significant difference among one or more of the studied groups. These peaks were 670 cm^{-1}, 731 cm^{-1}, 785 cm^{-1}, 1062 cm^{-1}, 1098 cm^{-1}, 1185 cm^{-1}, 1334 cm^{-1}, 1372 cm^{-1}, 1424 cm^{-1}, 1450 cm^{-1}, 1532 cm^{-1}, 1618 cm^{-1} and 1673cm^{-1}.

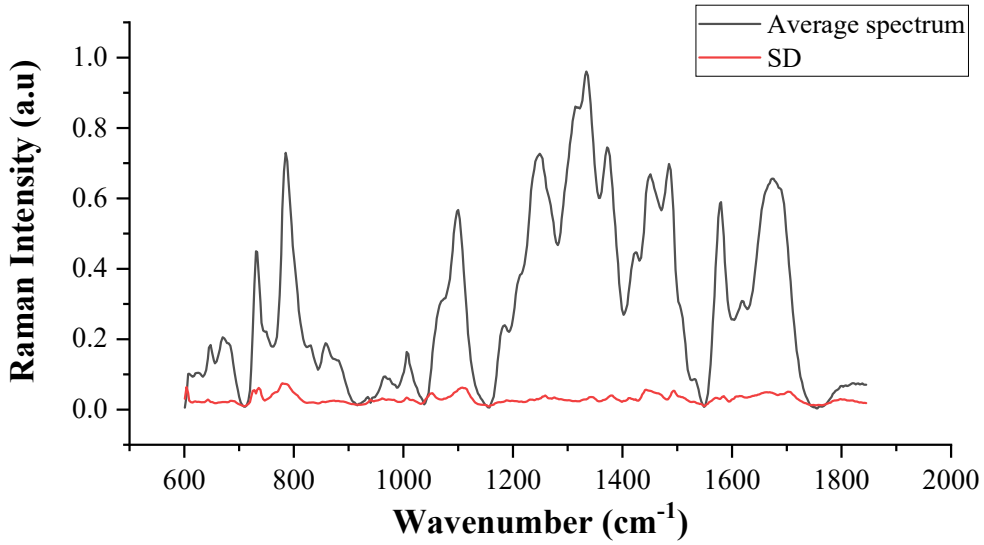

Figure 4.25: Average Raman spectrum and standard deviation spectrum of all studied samples.

4.9.2 Fertile and subfertile groups spectra

Figure 4.26 shows the average Raman spectrum and the standard deviation of fertile versus subfertile groups. 4 Raman peaks (1098 cm^{-1}, 1314 cm^{-1}, 1372 cm^{-1} and 1532 cm^{-1}) show a significant difference between the fertile and subfertile groups in their median peaks intensities and standard deviation. Raman peaks at 1098 cm^{-1} (fertile (0.583±0.034), subfertile (0.557±0.042), p=0.002), 1334 cm^{-1} (fertile (0.973±0.013), subfertile (0.965±0.019), p=0.033) and 1372 cm^{-1} (fertile (0.761±0.013), subfertile (0.747±0.017), p<0.001) showed higher medians intensities in the fertile group, while the Raman peak at 1532 cm^{-1} (fertile (0.0884±0.0149), subfertile (0.1006±0.0142), p=0.008) showed a higher median intensity in the subfertile group as illustrated in Figure 4.28. Generally, the subfertile group shows a higher variation than the fertile group as indicated by the higher standard deviation values throughout their spectra and specifically the following Raman peaks intensity at 1098 cm^{-1}, 1334 cm^{-1}, 1372 cm^{-1} and 1532 cm^{-1} that showed a significant difference in their standard deviation as illustrated in Figure 4.29. Additionally, the

differential spectrum of the averages of fertile group minus the subfertile group shows that the DNA Raman peaks are in the positive range, while the protein Raman peaks are in the negative range as illustrated in Figure 4.27.

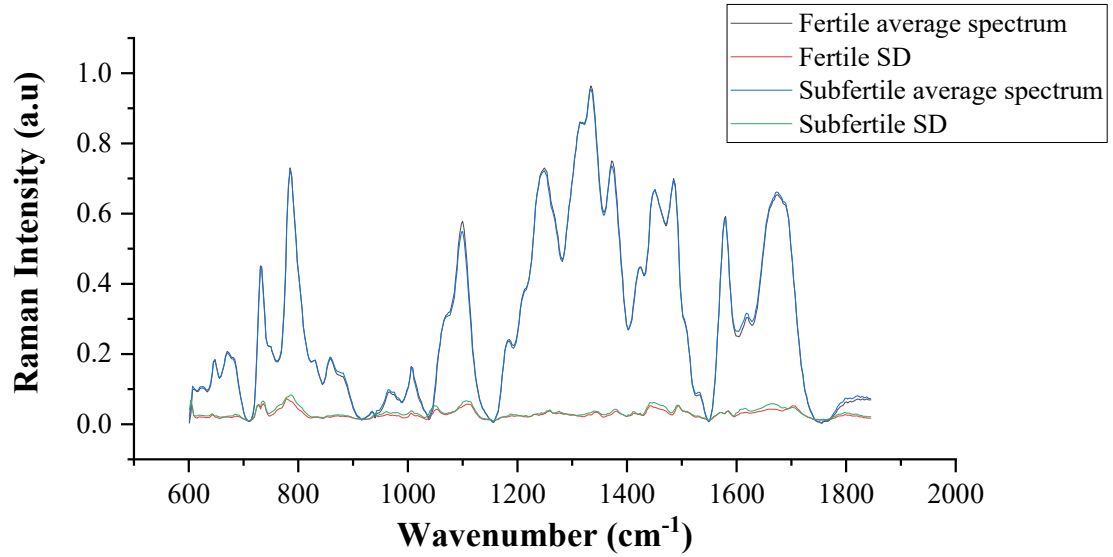

Figure 4.26: Average Raman spectra of fertile versus subfertile groups.

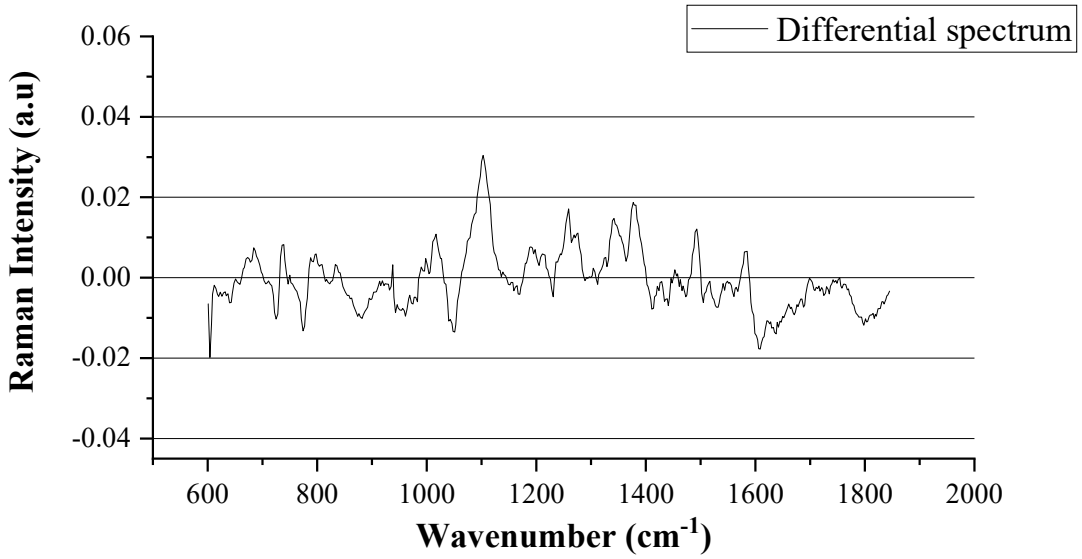

Figure 4.27: Differential spectrum for the averages of fertile group minus subfertile group.

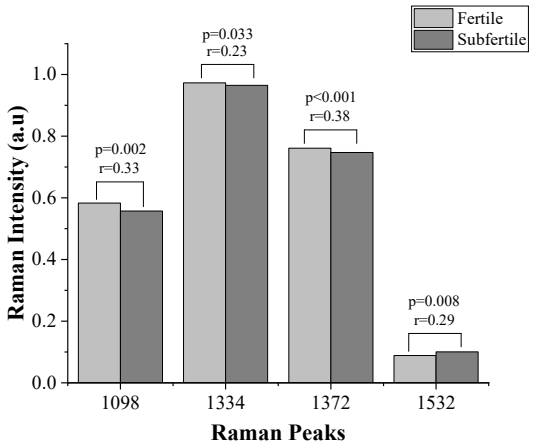

Figure 4.28: Bar plot of the median intensity of the Raman peaks that show a significant difference between the fertile and subfertile groups. The indicated r-values represent the effect size of the corresponding Raman peaks.

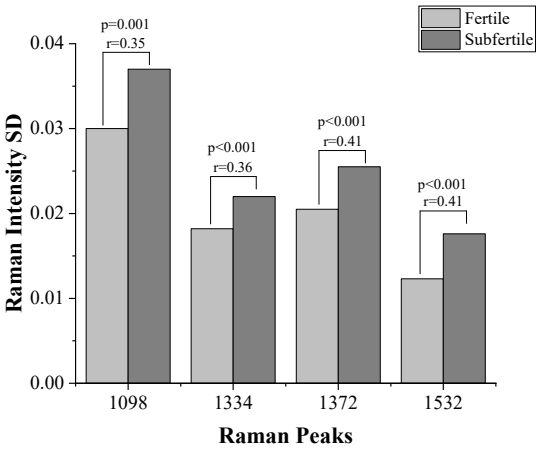

Figure 4.29: Bar plot of the median of the Raman peaks standard deviations that show a significant difference between the fertile and subfertile groups. The indicated r-values represent the effect size of the corresponding Raman peaks SD.

4.9.3 CMA3≤41 and CMA3>41 groups spectra

Figure 4.30 shows the average Raman spectrum and the standard deviation of CMA3≤41 versus CMA3>41 groups. 12 Raman peaks (670 cm^{-1}, 731 cm^{-1}, 785 cm^{-1}, 1062 cm^{-1}, 1098 cm^{-1}, 1185 cm^{-1}, 1372 cm^{-1}, 1424 cm^{-1}, 1450 cm^{-1}, 1532 cm^{-1}, 1618 cm^{-1} and 1673 cm^{-1}) show a significant difference between the CMA3≤41 and CMA3>41groups in their median peaks intensities as illustrated in Figure 4.32. Raman peaks at 670 cm^{-1} (CMA3≤41 (0.223±0.013), CMA3>41 (0.201±0.015), p=0.001), 731 cm^{-1} (CMA3≤41 (0.479±0.029), CMA3>41 (0.462±0.028), p=0.002), 785 cm^{-1} (CMA3≤41 (0.763±0.05), CMA3>41 (0.691±0.064),

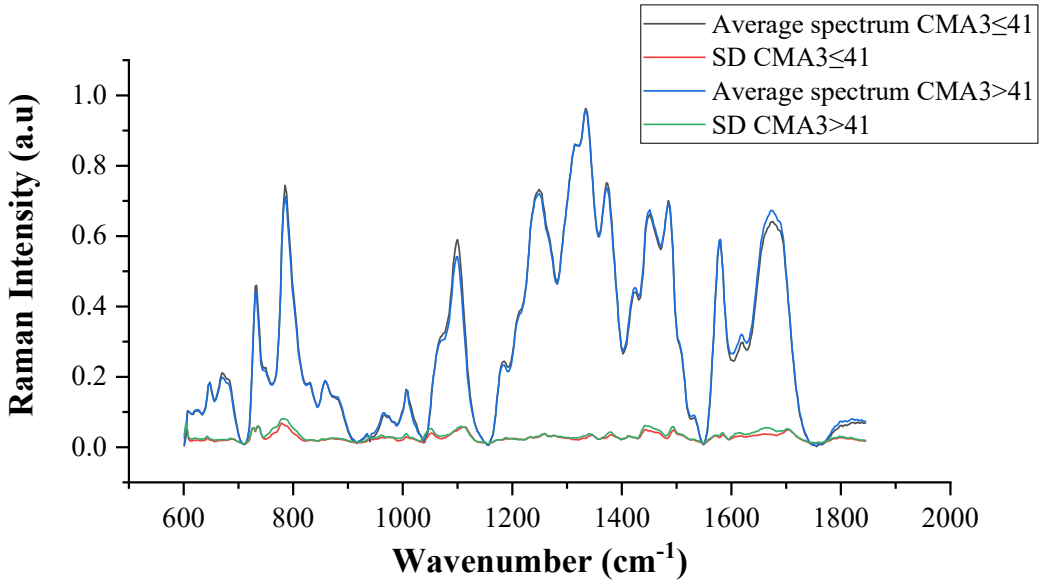

Figure 4.30: Average Raman spectra of CMA3≤41 versus CMA3>41 groups.

p=0.015), 1062 cm^{-1} (CMA3≤41 (0.327±0.018), CMA3>41 (0.314±0.024), p=0.002), 1098 cm^{-1} (CMA3≤41 (0.594±0.031), CMA3>41 (0.553±0.033), p<0.001), 1185 cm^{-1} (CMA3≤41 (0.251±0.015), CMA3>41 (0.238±0.015), p=0.007) and 1372 cm^{-1} (CMA3≤41 (0.763±0.0123), CMA3>41 (0.748±0.0171), p<0.001) showed higher medians intensities in the CMA3≤41 group, while the Raman peaks at 1424 cm^{-1} (CMA3≤41 (0.444±0.019), CMA3>41 (0.462±0.017), p=0.001), 1450 cm^{-1} (CMA3≤41 (0.715±0.0137), CMA3>41 (0.719±0.0213), p=0.028), 1532 cm^{-1} (CMA3≤41 (0.0864±0.0153), CMA3>41 (0.0998±0.0139), p=0.003), 1618 cm^{-1} (CMA3≤41 (0.295±0.025), CMA3>41 (0.332±0.031), p<0.001) and 1673 cm^{-1} (CMA3≤41 (0.643±0.027), CMA3>41 (0.694±0.041), p<0.001) showed higher medians intensities in the CMA3>41 group. Generally, the CMA3>41 group show a higher variation than the CMA3≤41 group as indicated by the higher standard deviation values throughout the spectra and specifically the following Raman peaks intensity at 785 cm^{-1}, 1062 cm^{-1}, 1098 cm^{-1}, 1185 cm^{-1}, 1372 cm^{-1}, 1450 cm^{-1}, 1532 cm^{-1}, 1618 cm^{-1} and 1673 cm^{-1} that showed a significant difference in their standard deviations as illustrated in Figure 4.33. Additionally, the differential spectrum of the averages of CMA3≤41 group minus CMA3>41 group shows that the DNA Raman peaks are in the positive range, while the protein Raman peaks are in the negative range as illustrated in Figure 4.31.

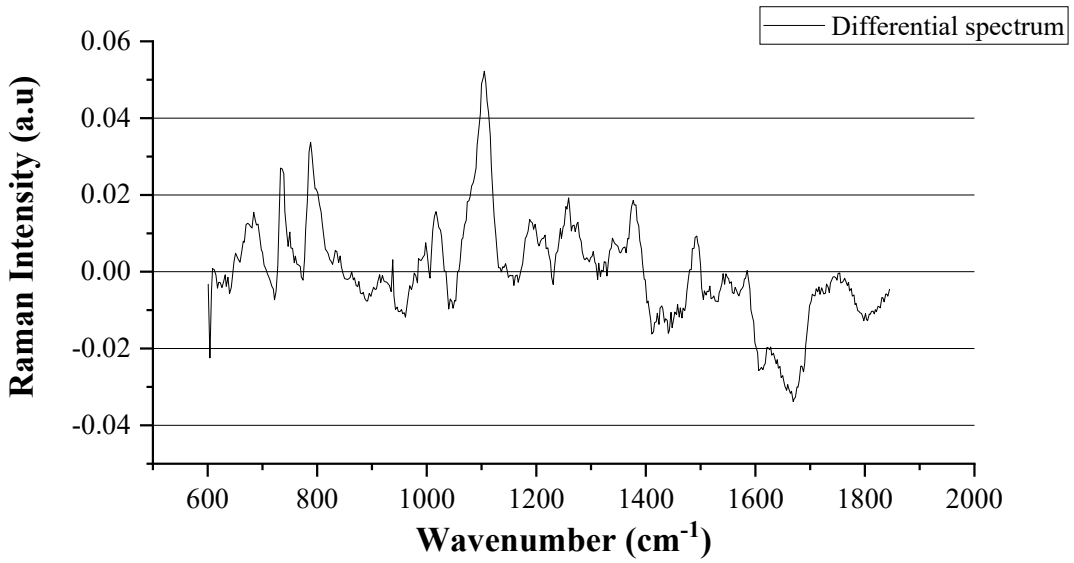

Figure 4.31: Differential spectrum for the averages of CMA3≤41 group minus CMA3>41 group.

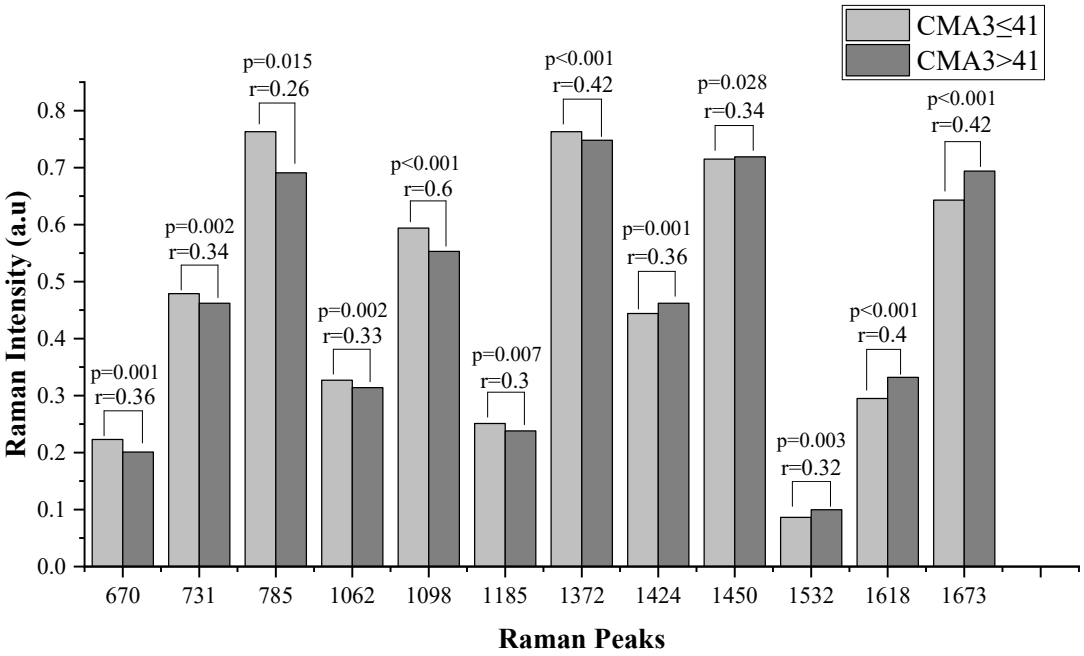

Figure 4.32: Bar plot of the median intensity of the Raman peaks that show a significant difference between the CMA3≤41 and CMA3>41 groups. The indicated r-values represent the effect size of the corresponding Raman peaks.

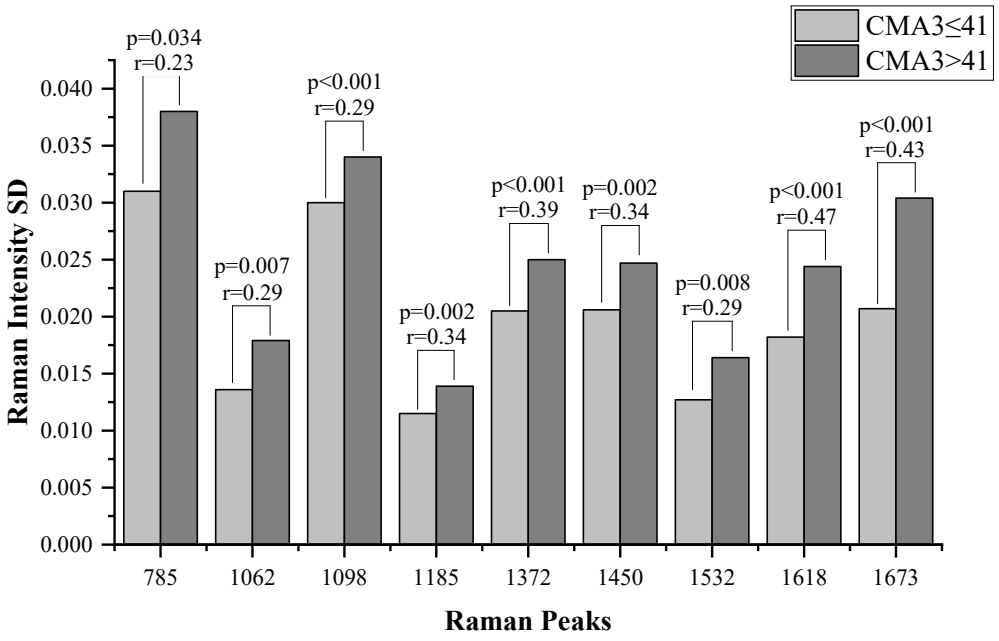

Figure 4.33: Bar plot of the median of the Raman peaks standard deviations that show a significant difference between the CMA3≤41 and CMA3>41 groups. The indicated r-values represent the effect size of the corresponding Raman peaks SD.

4.9.4 CMA3<28, 28≤CMA3≤50 and CMA3>50 groups spectra

Figure 4.34 shows the average Raman spectrum and the standard deviation of CMA3<28, 28≤CMA3≤50 and CMA3>50 groups. 9 Raman peaks (670 cm^{-1}, 731 cm^{-1}, 1062 cm^{-1}, 1098 cm^{-1}, 1185 cm^{-1}, 1372 cm^{-1}, 1424 cm^{-1}, 1618 cm^{-1} and 1673 cm^{-1}) show a significant difference between the CMA3<28, 28≤CMA3≤50 and CMA3>50 groups in their median peak intensities as illustrated in Figure 4.35. Raman peaks at 670 cm^{-1} (CMA3<28 (0.225 ±0.011), 28≤CMA3≤50 (0.207±0.015), CMA3>50 (0.204±0.016), p=0.005), 731 cm^{-1} (CMA3<28 (0.487 ±0.032), 28≤CMA3≤50 (0.468±0.028), CMA3>50 (0.462±0.026), p=0.007), 1062 cm^{-1} (CMA3<28 (0.331 ±0.019), 28≤CMA3≤50 (0.319±0.017), CMA3>50 (0.315±0.026), p=0.001), 1098 cm^{-1} (CMA3<28 (0.597±0.033), 28≤CMA3≤50 (0.582±0.037), CMA3>50 (0.547±0.023), p<0.001), 1185 cm^{-1} (CMA3<28 (0.262±0.015), 28≤CMA3≤50 (0.243±0.014), CMA3>50 (0.240±0.016), p=0.026) and 1372 cm^{-1} (CMA3<28 (0.759±0.012), 28≤CMA3≤50 (0.757±0.014), CMA3>50 (0.748±0.018), p=0.019) showed a higher medians intensities in the CMA3<28 group, followed by 28≤CMA3≤50 group and the lowest Raman intensity was in CMA3>50 group. While the Raman peaks at 1424 cm^{-1} (CMA3<28 (0.437±0.019), 28≤CMA3≤50 (0.454±0.019), CMA3>50 (0.462±0.014), p<0.001), 1618 cm^{-1} (CMA3<28 (0.291±0.023), 28≤CMA3≤50 (0.317±0.031), CMA3>50 (0.330±0.029), p=0.002) and 1673 cm^{-1} (CMA3<28 (0.634±0.023), 28≤CMA3≤50 (0.671±0.032), CMA3>50 (0.679±0.045), p=0.001) showed higher medians intensities in the CMA3>50 group, followed by the 28≤CMA3≤50 group. The lowest Raman intensity was observed in CMA3<28 group. Generally, the variation was the lowest in CMA3<28 group followed by the 28≤CMA3≤50 group. The highest variation was observed in the CMA3>50 group as indicated by the standard deviation values throughout the spectra. More specifically, the Raman peaks intensities at 1062 cm^{-1}, 1098 cm^{-1}, 1185 cm^{-1}, 1372 cm^{-1}, 1618 cm^{-1} and 1673 cm^{-1} showed a significant difference in their standard deviation as illustrated in Figure 4.36.

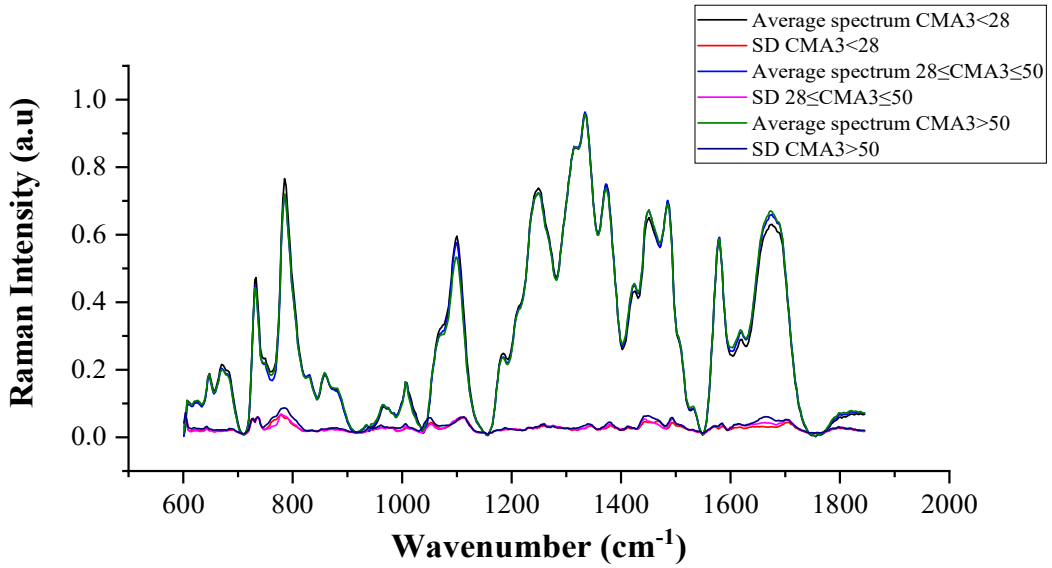

Figure 4.34: Average Raman spectra of CMA3<28, 28≤CMA3≤50 and CMA3>50 groups.

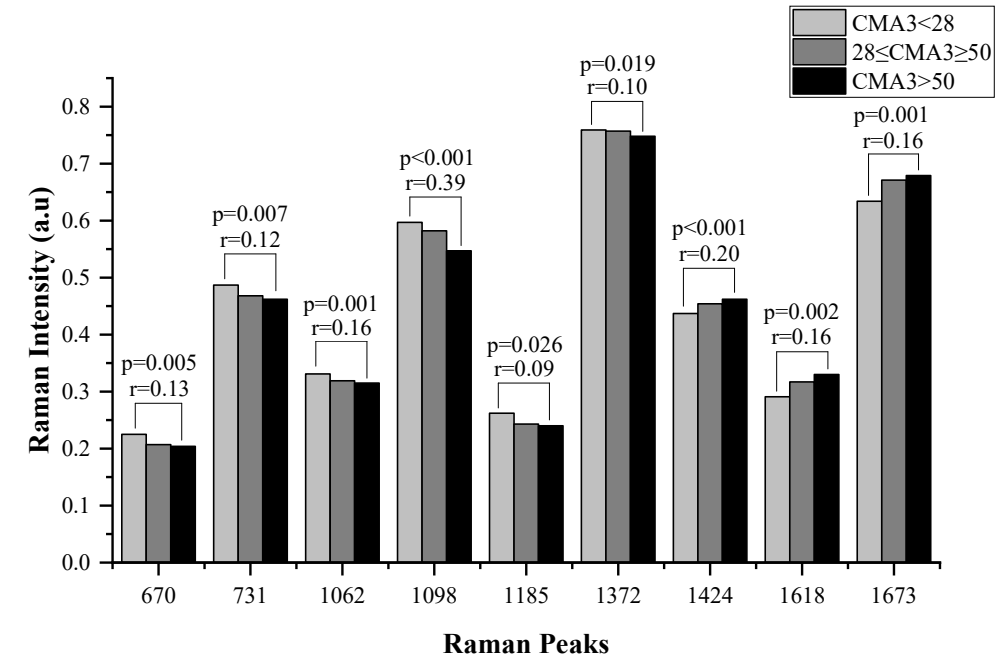

Figure 4.35: Bar plot of the median intensity of the Raman peaks that show a significant difference between CMA3<28, 28≤CMA3≤50 and CMA3>50 groups. The indicated r-values represent the effect size of the corresponding Raman peaks. By applying Dunn's Post Hoc test the Raman peaks at 670 cm^{-1}, 731 cm^{-1}, 1062 cm^{-1}, 1185 cm^{-1}, 1424 cm^{-1}, 1618 cm^{-1} and 1673 cm^{-1} didn't show a significant difference between the 28≤CMA3≤50 and CMA3>50 groups, while the Raman peaks at 1098 cm^{-1} and 1372 cm^{-1} didn't show a significant difference between the CMA3<28 and 28≤CMA3≤50 groups.

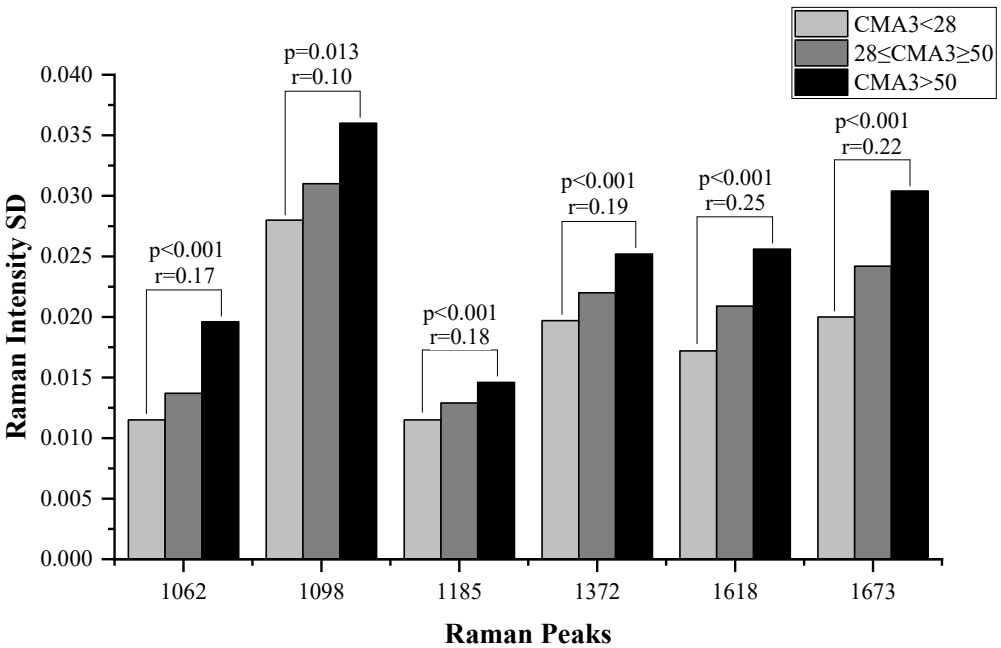

Figure 4.36: Bar plot of the median of the Raman peaks standard deviations that show a significant difference between CMA3<28, 28≤CMA3≤50 and CMA3>50 groups. The indicated r-values represent the effect size of the corresponding Raman peaks. By applying Dunn's Post Hoc test the SD of Raman peaks at 1062 cm^{-1}, 1098 cm^{-1}, 1185 cm^{-1}, 1372 cm^{-1}, and 1673 cm^{-1} didn't show a significant difference between the CMA3<28 and 28≤CMA3≤50 groups.

4.9.5 Correlation between sperm functional parameters and Raman peaks intensities

Table 4.4 shows the correlations between the Raman peaks intensities that were significantly correlated with at least one of the functional sperm parameters in all studied samples (n=85). These parameters include chromomycin A3 staining, acridine orange staining and aniline blue staining. Chromomycin A3 staining was significantly negatively correlated with the DNA related Raman peak intensities around 670 cm^{-1} (r=-0.313, p=0.003), 731 cm^{-1} (r=-0.293, p=0.006), 785 cm^{-1} (r=-0.234, p=0.030), 1062 cm^{-1} (r=-0.295, p=0.007), 1098 cm^{-1} (r=-0.610, p<0.001), 1185 cm^{-1} (r=-0.250, p=0.021) and 1372 cm^{-1} (r=-0.442, p<0.001). It was significantly positively correlated with the protein related Raman peak intensities around 858 cm^{-1} (r=0.334, p=0.002), 1424 cm^{-1} (r=0.368, p=<0.001), 1450 cm^{-1} (r=0.262, p=0.015), 1532 cm^{-1} (r=0.293, p=0.006), 1618 cm^{-1} (r=0.356, p=0.001) and 1673 cm^{-1} (r=0.398, p<0.001).

Table 4.4: Correlations of the three examined sperm functional parameters (Chromomycin A3, Acridine Orange, Aniline Blue) with Raman peak intensities. (* significant p<0.05, ** highly significant p<0 .005)

Peak		Chromomycin A3 (positive %)	Aniline blue (positive %)	Acridine Orange (positive %)
670	R	-0.313	0.003	-0.086
	P	**0.003****	0.976	0.433
731	R	-0.293	-0.125	-0.233
	P	**0.006***	0.253	**0.032***
785	R	-0.234	0.087	-0.066
	P	**0.030***	0.422	0.545
858	R	0.334	0.191	0.221
	P	**0.002****	0.079	**0.042***
1062	R	-0.295	0.124	-0.060
	P	**0.007***	0.256	0.5840
1098	R	-0.610	-0.288	-0.308
	P	**<0.001****	**0.008***	**0.004****
1185	R	-0.250	-0.068	-0.112
	P	**0.021***	0.533	0.307
1372	R	-0.442	-0.264	-0.461
	P	**<0.001****	**0.014***	**<0.001****
1424	R	0.368	0.093	0.220
	P	**<0.001****	0.396	**0.043***
1450	R	0.262	0.012	0.315
	P	**0.015***	0.906	**0.003****
1532	R	0.293	0.132	-0.024
	P	**0.006***	0.226	0.822
1618	R	0.356	0.002	0.183
	P	**0.001****	0.979	0.092
1673	R	0.398	0.0104	0.212
	P	**<0.001****	0.928	0.051
1050/1098	R	0.273	0.364	0.227
	P	**0.011***	**<0.001****	**0.036***

Aniline blue staining was significantly negatively correlated with the DNA related Raman peak intensity around 1098 cm^{-1} (r=-0.288, p=0.008) and 1372 cm^{-1} (r=-0.264, p=0.014). Acridine orange staining was significantly negatively correlated with the DNA related Raman peak intensities around 731 cm^{-1} (r=-0.233, p=0.032), 1098 cm^{-1} (r=-0.308, p=0.004), 1372 cm^{-1} (r=-0.461, p<0.001) and 1424 cm^{-1} (r=-0.220, p=0.043), while it was significantly positively correlated with the protein related Raman peak intensity around 858 cm^{-1} (r=0.221, p=0.042) and 1450 cm^{-1} (r=0.315, p=0.003). Finally, the Raman peak intensities ratio (1050 cm^{-1}/1098 cm^{-1}) was significantly positively correlated with the percentage of the chromomycin A3 positive (r=0.273, p=0.011), aniline blue staining (r=0.364, p<0.001) and acridine orange (r=0.227, p=0.036).

4.10 Spectral fitting model

To estimate the relative amount of DNA and protein, a fitting model program in LabVIEW software was used to extract a separated Raman peaks from the pre-processed Raman spectra. This estimation is based on the area under the Raman peaks associated to either protein or DNA. 62 peaks were extracted and 43 peaks were assigned for DNA or protein based on two factors as illustrated in Table 4.5. The first one was the assignment of the selected peaks in the literature. The second factor was a confirming factor by testing the correlation of each peak with a protein or DNA separated peaks. Figure 4.37 illustrated an example of the original spectrum versus the model fit spectrum. The black spectrum represents the original spectrum and the red spectrum represents the model fit spectrum. The residual of the model fit is mostly noise represented by the blue spectrum, indicating that the Raman peaks of sperm is represented well by the model fit spectrum. Figure 4.38 shows all the selected Raman peaks that are assigned to DNA or to protein and were included in the next quantitative analysis. The red spectrum represents the sum of all assigned DNA peaks, and the blue spectrum represents the sum of all assigned protein peaks.

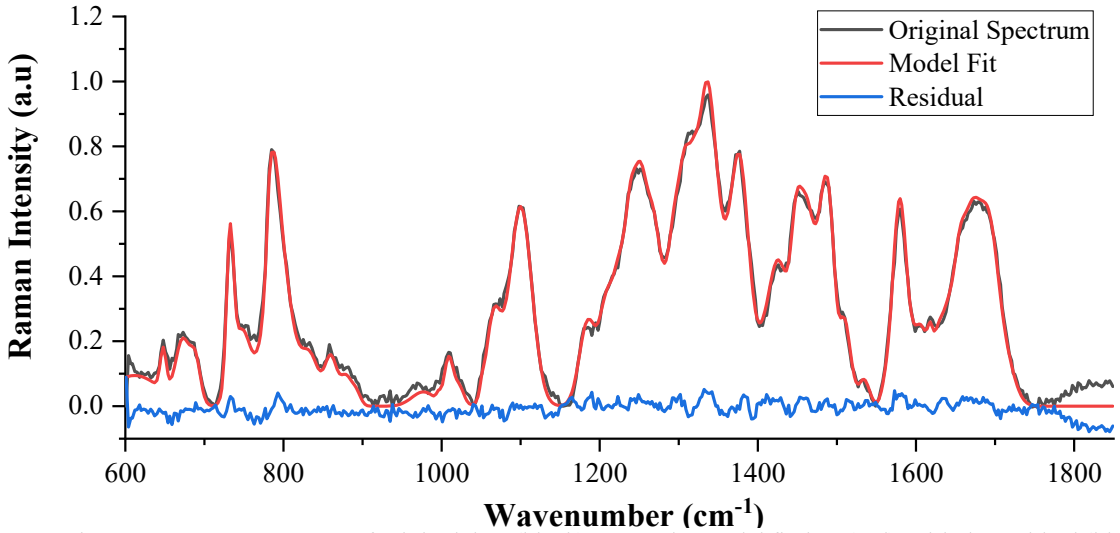

Figure 4.37: Raman spectra of original data (black) versus the model fit data (red), with the residual (blue).

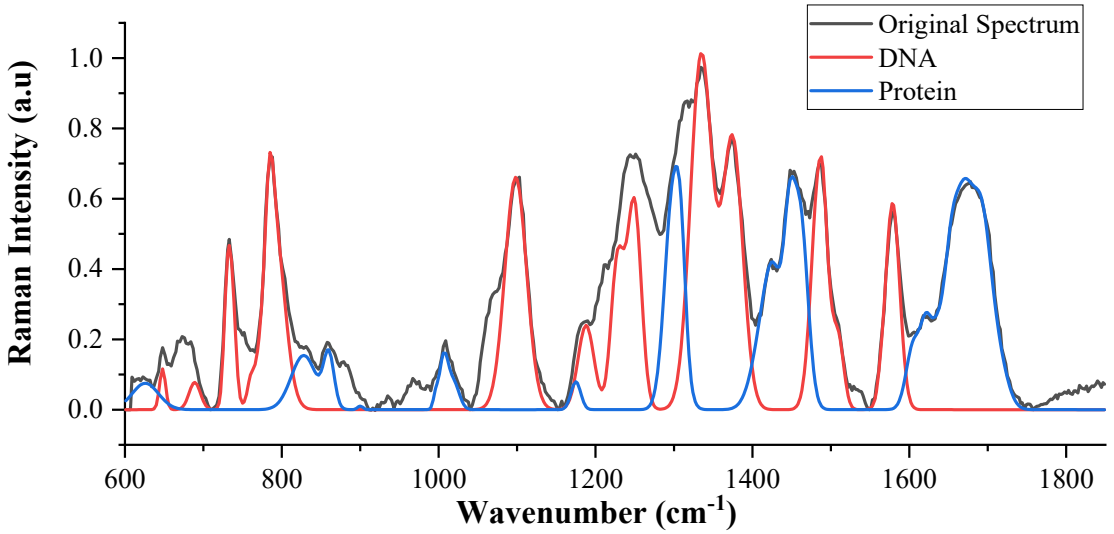

Figure 4.38: Raman spectra of original data (black) versus the sum of all assigned DNA (red) and protein (blue) peaks that extracted from the model fit data.

Table 4.5: Raman peaks assignment.

Peak (cm^{-1})	Assignment	Literature assignment	References
624	Protein	Phenylalanine (621)	Talari *et al.*, 2014
		Phenylalanine (622)	Peticolas *et al.*, 1996
		Phenylalanine (626)	De Mul *et al.*, 1984
649	DNA	DNA base C (638)	Angelis *et al.*, 2017
		DNA base T (665)	Angelis *et al.*, 2017
		DNA base C (642), T (670)	Huser *et al.*, 2009
682	DNA	DNA bases (678)	Angelis *et al.*, 2019
		DNA base G (681)	Angelis *et al.*, 2017
		DNA base G (678)	Talari *et al.*, 2014
		DNA base G (681)	Huser *et al.*, 2009
		DNA base G (681)	Thomas, 1999
		DNA base G (681)	Peticolas *et al.*, 1996
		DNA base G (682)	De Mul *et al.*, 1984
729-735 (two peaks)	DNA	DNA base A (726)	Angelis *et al.*, 2017
		DNA base A (726)	Ferrara *et al.*, 2015
		DNA base A (729)	Talari *et al.*, 2014
		DNA base A (728)	Huser *et al.*, 2009
		DNA base A (729)	Peticolas *et al.*, 1996
		DNA base A (730)	De Mul *et al.*, 1984
755	DNA	DNA, RNA bases C, U (748)	Nazarenko *et al.*, 2018
		DNA, RNA bases C, U (751)	Ferrara *et al.*, 2015
		DNA, RNA bases C, U (751)	De Luca *et al.*, 2014
		DNA base T (747)	Peticolas *et al.*, 1996
		DNA base T (754)	De Mul *et al.*, 1984
774	DNA	DNA backbone (769)	Peticolas *et al.*, 1996

Table 4.5 continued.

784-787 (two peaks)	DNA	DNA (784)	Angelis *et al*., 2019
		DNA bases T, C (782)	Nazarenko *et al*., 2018
		DNA bases T, C, DNA backbone (785)	Angelis *et al*., 2017
		DNA bases T, C, DNA backbone (785)	Ferrara *et al*., 2015
		DNA, RNA bases U, T, C (782) Backbone (785)	Talari *et al*., 2014
		DNA bases T, C, DNA backbone (785)	De Luca *et al*., 2014
		DNA bases T, C	Thomas, 1999
		DNA bases T, C, DNA backbone (785)	Huser *et al*., 2009
		DNA base C, DNA backbone (784)	Peticolas *et al*., 1996
		DNA bases T, C, DNA backbone (787)	De Mul *et al*., 1984
797	DNA	Deoxyribomononucleotides (800)	Peticolas *et al*., 1996
829	Protein	Tyrosine (830)	Angelis *et al*., 2019
		Tyrosine, Proline, hydroxyproline (827)	Amaral *et al*., 2018
		Tyrosine (831)	Ferrara *et al*., 2015
		Tyrosine (828)	Talari *et al*., 2014
		Tyrosine (831)	De Luca *et al*., 2014
854	Protein	Tyrosine (850)	Angelis *et al*., 2019
		Valine, Proline, hydroxyproline, Tyrosine (850)	Amaral *et al*., 2018
		Tyrosine (859)	Talari *et al*., 2014
		Tryptophan (878)	Thomas, 1999
		Tyrosine (855)	Peticolas *et al*., 1996
		Tyrosine (854)	De Mul *et al*., 1984
898	Protein	Gylcoprotein (890)	Angelis *et al*., 2019
		Protein bands (890)	Talari *et al*., 2014
945	Protein	C-C back bone (933)	De Luca *et al*., 2014
		Protein side chains (943)	Thomas, 1999
		C-C skeletal mode (random coil) (949)	Peticolas *et al*., 1996
997-1003 (two peaks)	Protein	Phenylalanine (1004)	Angelis *et al*., 2019
		Phenylalanine (1002)	Nazarenko *et al*., 2018
		Phenylalanine (1005)	De Luca *et al*., 2014
		Phenylalanine (1003)	Thomas, 1999
		Phenylalanine (1005)	Peticolas *et al*., 1996
		Phenylalanine (1004)	De Mul *et al*., 1984
1020	Protein	Phenylalanine, Proline (1033)	Amaral *et al*., 2018
		Protein (1022)	Talari *et al*., 2014
		Phenylalanine (1033)	De Mul *et al*., 1984
1097	DNA	Phosphate backbone (1095)	Angelis *et al*., 2019
		Phosphate backbone (1092)	Nazarenko *et al*., 2018
		Phosphate backbone (1094)	Amaral *et al*., 2018
		Phosphate backbone (1095)	Ferrara *et al*., 2015
		Phosphate backbone (1095)	De Luca *et al*., 2014
		Phosphate backbone (1093)	Talari *et al*., 2014
		Phosphate backbone (1092)	Huser *et al*., 2009
		Phosphate backbone (1093)	Thomas, 1999
		Phosphate backbone (1095)	Peticolas *et al*., 1996
		Phosphate backbone (1096)	De Mul *et al*., 1984

Table 4.5: continued.

1177	Protein	Tyrosine (1175)	Angelis *et al*., 2019
		Tyrosine, phenylalanine (1180)	Amaral *et al*., 2018
		Tyrosine, phenylalanine (1174)	Talari *et al*., 2014
		Tyrosine, phenylalanine (1178)	Peticolas *et al*., 1996
		C-N (1180)	De Mul *et al*., 1984
1186	DNA	DNA bases A, C, G, T (1180)	Amaral *et al*., 2018
		DNA bases C, G, A (1184)	Talari *et al*., 2014
1228	DNA	DNA bases A, C, T, phosphate (1232)	Amaral *et al*., 2018
		Phosphate (1230)	Talari *et al*., 2014
		DNA bases T, C (1237),(1213)	Huser *et al*., 2009
1250	DNA	DNA bases A, C (1251)	Nazarenko *et al*., 2018
		DNA bases A, T (1255)	De Luca *et al*., 2014
		DNA bases G, C (1250)	Talari *et al*., 2014
		DNA bases A, C (1255)	Huser *et al*., 2009
		DNA base A (1240, 1254)	Peticolas *et al*., 1996
		DNA bases C, A (1254)	De Mul *et al*., 1984
1295	Protein	Amide III (1288)	Amaral *et al*., 2018
		Amide III (1290)	Ferrara *et al*., 2015
		Amide III (1290)	De Luca *et al*., 2014
		Amide III (1295)	Peticolas *et al*., 1996
1309	Protein	CH2 (1310)	Angelis *et al*., 2019
		N-H, C-H, Amide III (1307)	Nazarenko *et al*., 2018
		C-N, Aromatic amines (1308)	Talari *et al*., 2014
1334	DNA	DNA bases A, G (1335)	Amaral *et al*., 2018
		DNA base G (1341)	Nazarenko *et al*., 2018
		DNA base A (1335)	Angelis *et al*., 2017
		DNA base G (1335)	De Luca *et al*., 2014
		DNA bases A, G (1335)	Huser *et al*., 2009
		DNA base A (1335)	Thomas, 1999
		DNA base A (1340)	Peticolas *et al*., 1996
		DNA base A (1342)	De Mul *et al*., 1984
1375	DNA	DNA base G (1374)	Nazarenko *et al*., 2018
		DNA bases T, A, G (1375)	Angelis *et al*., 2017
		DNA bases A, G (1374)	De Luca *et al*., 2014
		DNA bases T, A, G (1373)	Talari *et al*., 2014
		DNA bases T, A, C (1374)	Huser *et al*., 2009
		DNA bases A, T, G (1370)	Thomas, 1999
		DNA base A (1377)	Peticolas *et al*., 1996
		DNA bases T, A (1377)	De Mul *et al*., 1984
1418	Protein	Protein (1420)	Angelis *et al*., 2019
		CH_2 of proteins (1420)	Amaral *et al*., 2018
1430	Protein	Valine (1427) Glutamate (1434) Arginine (1436) Histidine (1436) Proline (1434)	Gelder *et al*., 2007

Table 4.5: continued.

1445-1458 (two peaks)	Protein	Protein (1445)	Angelis *et al*., 2019
		Methylene deformation (1445)	Nazarenko *et al*., 2018
		Methylene deformation, C-H (1450)	De Luca *et al*., 2014
		Methylene deformation (1442)	Huser *et al*., 2009
		Methylene deformation (1452)	De Mul *et al*., 1984
1486	DNA	DNA bases G, A (1486)	Nazarenko *et al*., 2018
		DNA bases G, A (1480)	De Luca *et al*., 2014
		DNA base G (1487)	Talari *et al*., 2014
		DNA bases G, A (1484)	Huser *et al*., 2009
1490	DNA	DNA bases A, G (1490)	Thomas, 1999
		DNA base G (1494)	Peticolas *et al*., 1996
		DNA bases G, A (1490)	De Mul *et al*., 1984
1511	DNA	DNA base A (1510)	Talari *et al*., 2014
		DNA bases A, T (1518)	Peticolas *et al*., 1996
		DNA base A (1512)	De Mul *et al*., 1984
1566-1576 (two peaks)	DNA	DNA (1573)	Angelis *et al*., 2019
		DNA bases G, A (1576)	Amaral *et al*., 2018
		DNA bases G, A (1576)	Nazarenko *et al*., 2018
		DNA bases G, A (1575)	Ferrara *et al*., 2015
		DNA bases G, A (1575)	Talari *et al*., 2014
		DNA bases G, A (1575)(1581)	De Luca *et al*., 2014
		DNA bases G, A (1575)	Huser *et al*., 2009
		DNA bases G, A (1579)	Thomas, 1999
		DNA bases G, A (1580)	De Mul *et al*., 1984
1602	Protein	Amide I (1600)	Angelis *et al*., 2019
		Phenylalanine (1583)	Amaral *et al*., 2018
		Tyrosine, Phenylalanine (1607)	De Luca *et al*., 2014
		Tyrosine, Phenylalanine (1608)	De Mul *et al*., 1984
1620	Protein	Tryptophan (1625)	Angelis *et al*., 2019
		Tyrosine, Phenylalanine, Amide I, Tryptophan (1607) (1612)	Amaral *et al*., 2018
		Tyrosine, Tryptophan (1620)	De Luca *et al*., 2014
		Tryptophan (1618)	Talari *et al*., 2014
		Tyrosine, Tryptophan (1618)	Thomas, 1999
1633-1714 (13 peaks)	Protein	Amide I (1634)	Talari *et al*., 2014
		Amide I (1638)	Talari *et al*., 2014
		Amide I (1650)	Talari *et al*., 2014
		Amide I (1664)	De Mul *et al*., 1984
		Amide I (1680)	De Luca *et al*., 2014
		Amide I (1670)	Angelis *et al*., 2019
		Amide I (1663)	Nazarenko *et al*., 2018
		Amide I (1666)	Thomas, 1999
		Amide I (1665)	Talari *et al*., 2014
		Amide I (1690)	Angelis *et al*., 2019
		Amide I, Turns (1697)	Talari *et al*., 2014
		Arginine (1713)	Gelder *et al*., 2007

4.11 Raman quantitative parameters

Several quantitative parameters were obtained from the Raman spectra for all studied samples (n=85). These parameters include protein content, DNA content, DNA/protein ratio, protein content standard deviation, DNA content standard deviation and DNA/protein ratio standard deviation. Table 4.6 showed the means ± standard deviations data of all studied quantitative parameters for all donors (n=85). Protein content ranged from 49.47 to 57.19 (51.84 ± 1.43), DNA content ranged from 57.2 to 65.93 (63.04 ± 1.68), DNA/protein ratio ranged from 1.02 to 1.3 (1.21 ± 0.06). Protein standard deviation ranged from 1.3 to 5.06 (2.44 ± 0.7), DNA standard deviation ranged from 2.88 to 6.9 (3.93 ± 0.77) and the DNA/protein ratio standard deviation ranged from 0.069 to 0.207 (0.109 ± 0.024).

Table 4.6: Raman quantitative parameters.

Parameters	Mean ± SD	Median	Minimum	Maximum
Protein content	51.84 ± 1.43	51.62	49.47	57.19
DNA content	63.04 ± 1.68	63.22	57.2	65.93
DNA/Protein	1.21 ± 0.06	1.23	1.02	1.3
Protein content SD	2.44 ± 0.7	2.24	1.3	5.06
DNA content SD	3.93 ± 0.77	3.81	2.88	6.9
DNA/Protein SD	0.109 ± 0.024	0.106	0.069	0.207

4.11.1 Correlations between the Raman quantitative parameters and sperm functional parameters

All Raman quantitative parameters and sperm functional parameters were tested for correlations in all studied samples (n=85). These parameters include protein content, DNA content, DNA/protein ratio, protein content standard deviation, DNA content standard deviation and DNA/protein ratio standard deviation, chromomycin A3 staining, acridine orange staining and aniline blue staining. As illustrated in Figure 4.39 chromomycin A3 was significantly positively correlated with protein content ($r=0.444$, $p<0.001$) and protein content standard deviation ($r=0.386$, $p<0.001$). Chromomycin A3 was significantly negatively correlated with DNA content ($r=-0.485$, $p<0.001$) and DNA/protein ratio ($r=-0.469$, $p<0.001$), while no but it has not been significantly correlated with DNA content standard deviation ($r=0.201$, $p=0.065$) or with DNA/protein ratio standard deviation ($r= 0.177$, $p=0.105$). As illustrated in Figure 4.40 aniline blue was significantly positively correlated with protein content ($r=0.231$, $p=0.033$), protein content

standard deviation (r=0.356, p<0.001), DNA content standard deviation (r=0.252, p=0.019) and DNA/protein ratio standard deviation (r=0.256, p=0.018). Aniline blue was significantly negatively correlated with DNA content (r=-0.380, p<0.001) and DNA/protein ratio (r=-0.313, p=0.003). As illustrated in Figure 4.41 acridine orange was significantly positively correlated with protein content (r=0.469, p<0.001), protein content standard deviation (r=0.448, p<0.001), DNA content standard deviation (r=0.379, p<0.001) and DNA/protein ratio standard deviation (r=0.338, p=0.002). Acridine orange was significantly negatively correlated with DNA content (r=-0.330, p=0.002) and DNA/protein ratio (r=-0.425, p<0.001).

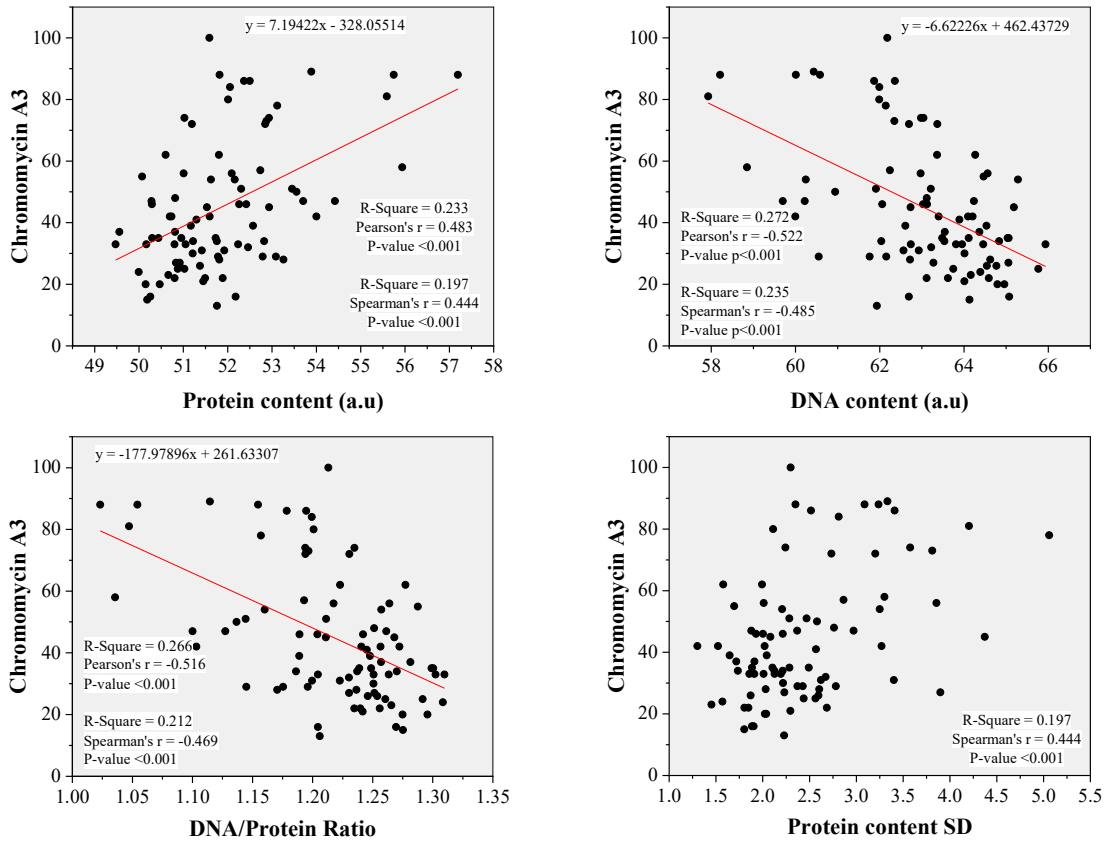

Figure 4.39: Scatter plots of chromomycin A3 and Raman quantitative parameters that show significant correlations. The numbers indicate the corresponding Spearman's correlation and Pearson's correlation coefficients, the significant level and r^2. Regression equations and the corresponding graph (red lines) also are indicated.

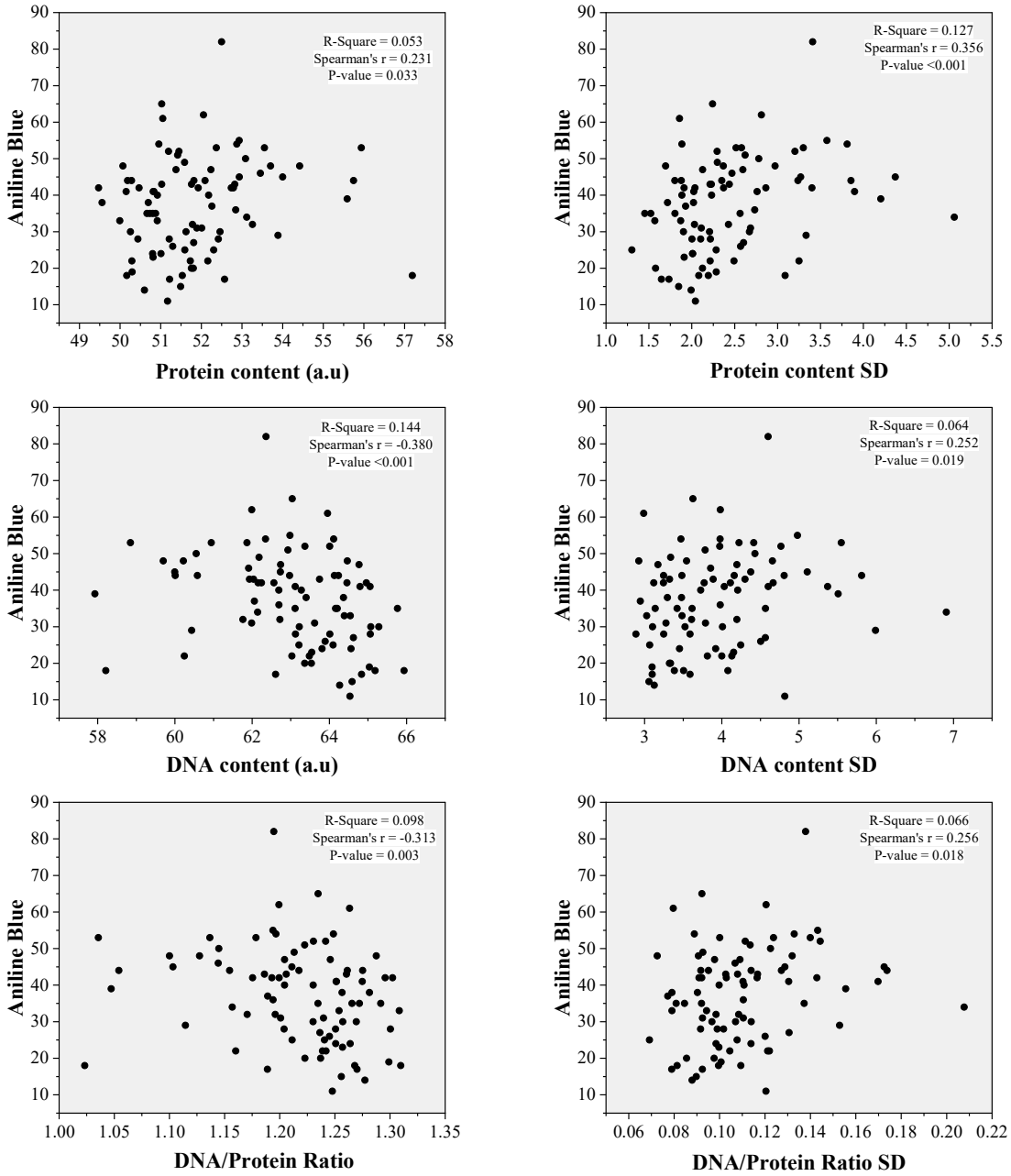

Figure 4.40: Scatter plots of aniline blue and Raman quantitative parameters correlations showing their Spearman's correlation coefficients, r^2 and significance levels.

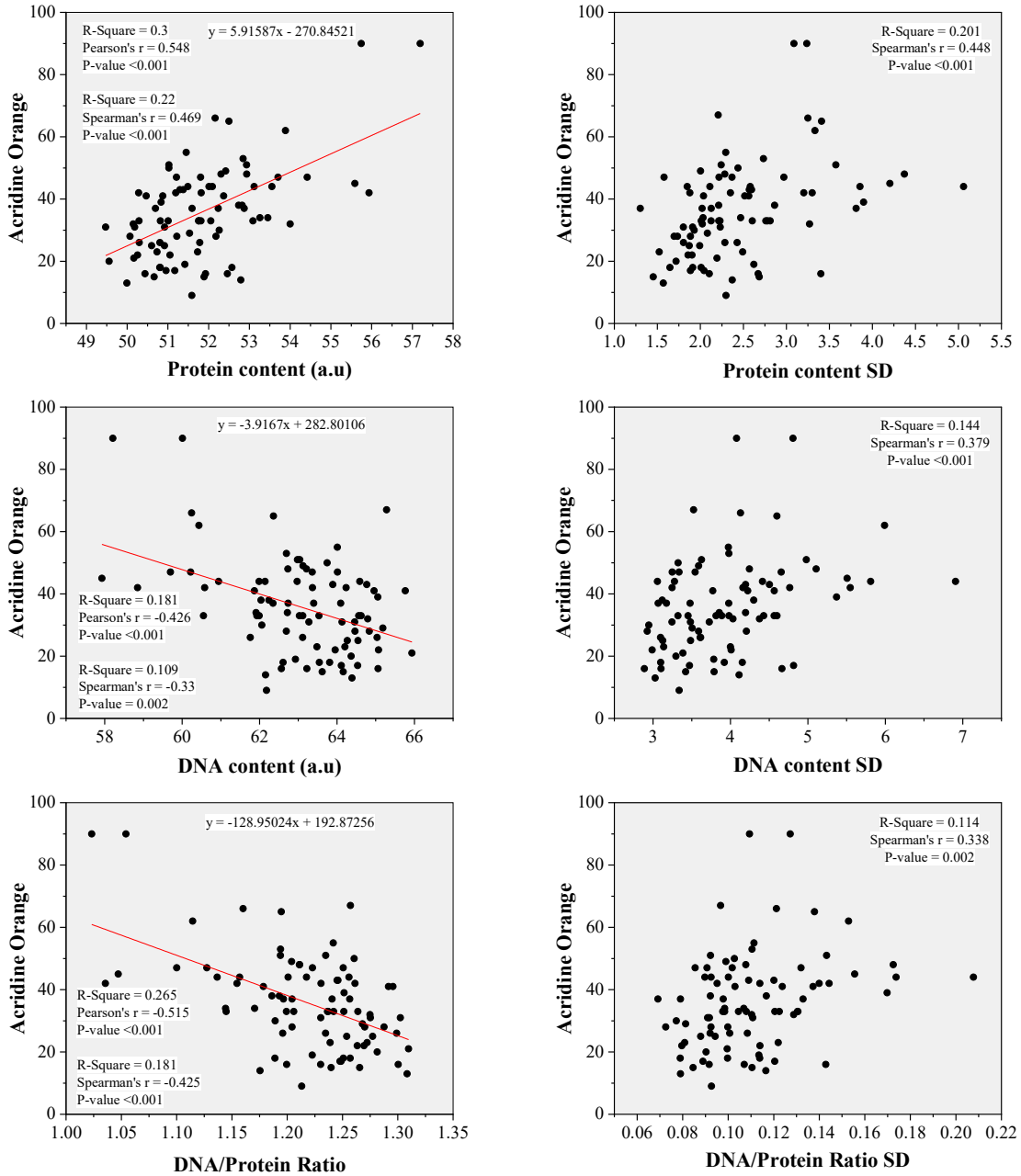

Figure 4.41: Scatter plots of acridine orange and Raman quantitative parameters correlations showing their Spearman's and Pearson's correlation coefficients with the corresponding significance levels and r^2 values. Regression equations and the corresponding graph (red lines) also are indicated.

4.11.2 Correlations between the Raman quantitative parameters and ICSI outcomes

Raman quantitative parameters and ICSI outcomes were tested for correlations in all studied samples (n=85 for fertilization rate and n=84 for other outcomes). These parameters include protein content, DNA content, DNA/protein ratio, protein content standard deviation, DNA content standard deviation and DNA/protein ratio standard deviation, fertilization rate, cleavage score, embryo quality score and embryo development score. As illustrated in Figure 4.42 fertilization rate was significantly positively correlated with DNA

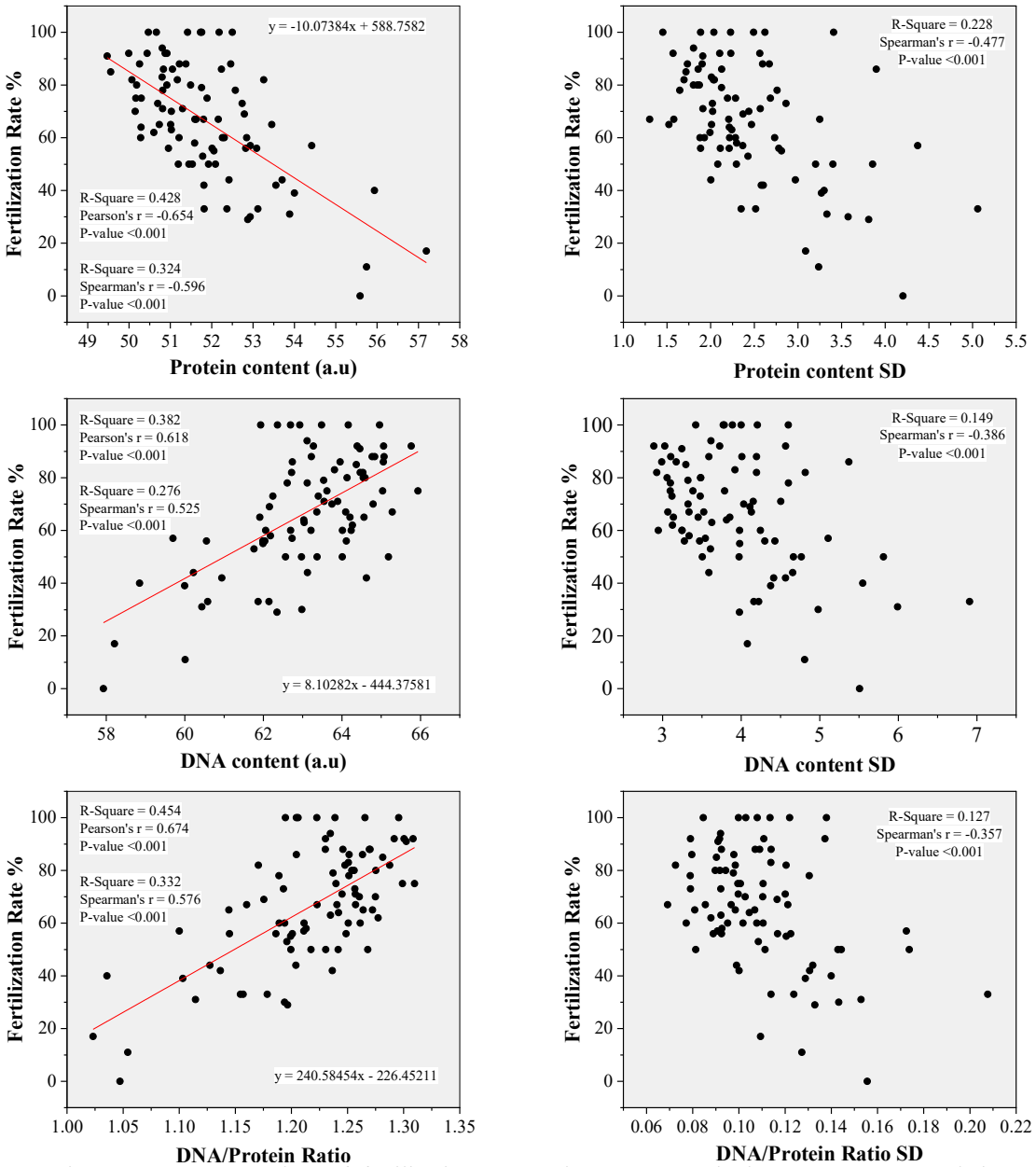

Figure 4.42: Scatter plots of fertilization rate and Raman quantitative parameters correlations showing their Spearman's and Pearson's correlation coefficients with the corresponding significance levels and r^2 values. Regression equations and the corresponding graph (red lines) also are indicated.

content (r=0.525, p<0.001), DNA/protein ratio (r=0.576, p<0.001). Fertilization rate was significantly negatively correlated with protein content (r=-0.569, p<0.001), protein content standard deviation (r=-0.477, p<0.001), DNA content standard deviation (r=-0.386, p<0.001) and DNA/protein ratio standard deviation (r=-0.357, p<0.001). As illustrated in Figure 4.43 cleavage score was significantly positively correlated with DNA content (r=0.295, p=0.006) and significantly negatively correlated with protein content standard deviation (r=-0.247, p=0.023). It was not significantly correlated with protein content (r=-0.176, p=0.108), DNA/protein ratio (r=0.188, p=0.086), DNA content standard deviation (r=-0.032, p=0.768) or with DNA/protein ratio standard deviation (r=-0.154, p=0.161).

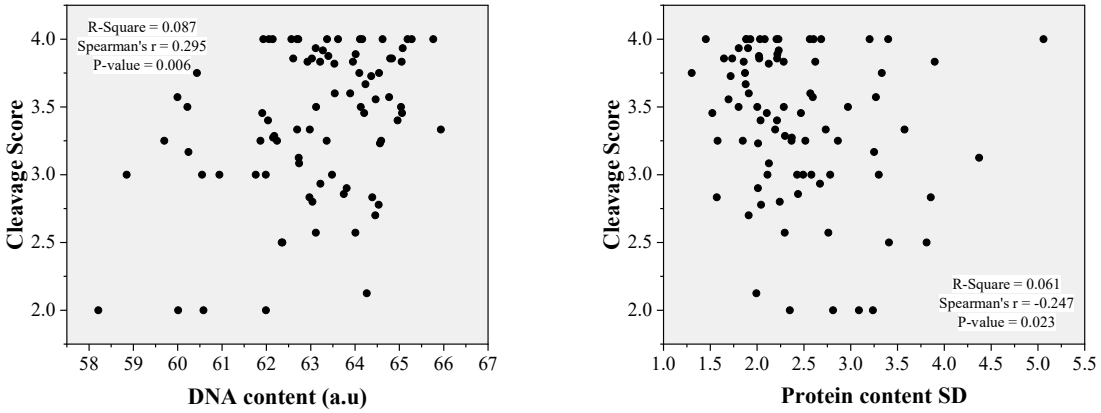

Figure 4.43: Scatter plots of cleavage score and DNA content, protein content SD correlations showing their Spearman's correlation coefficients, r^2 and significance levels.

Embryo quality score was not significantly correlated with protein content (r=-0.189, p=0.083), DNA content (r=0.165, p=0.133), DNA/protein ratio (r=0.167, p=0.126), protein content standard deviation (r=-0.070, p=0.522), DNA content standard deviation (r=0.123, p=0.264) or DNA/protein ratio standard deviation (r=0.110, p=0.319). As illustrated in Figure 4.44 embryo development score was significantly

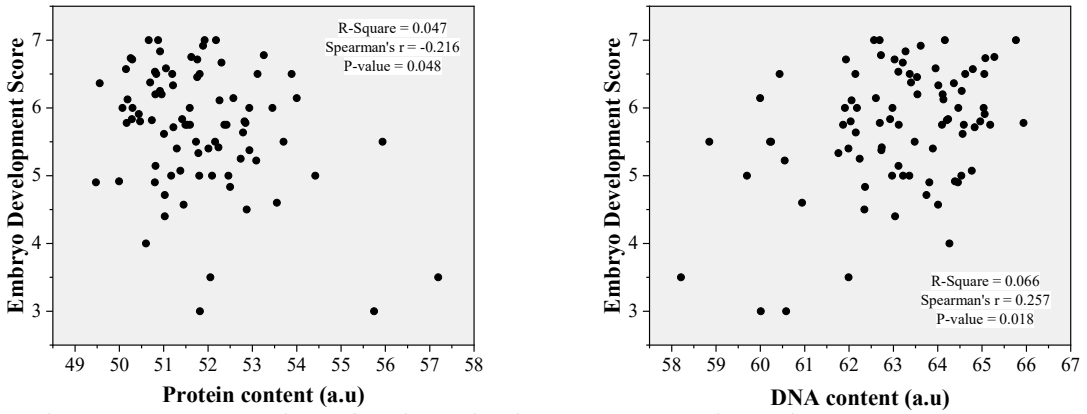

Figure 4.44: Scatter plots of embryo development score and protein content, DNA content correlations showing their Spearman's correlation coefficients, r^2 and significance levels

negatively correlated with protein content (r=-0.216, p=0.048) and significantly positively correlated with DNA content (r=0.257, p=0.018). Embryo development score was not significantly correlated with DNA/protein ratio (r=0.199, p=0.069), protein content standard deviation (r=-0.211, p=0.053), DNA content standard deviation (r=0.007, p=0.943) or DNA/protein ratio standard deviation (r=-0.062, p=0.575).

4.11.3 Correlations between the Raman quantitative parameters

Table 4.7 shows the correlation between all Raman quantitative parameters in all studied samples (n=85). These parameters include protein content, DNA content, DNA/protein ratio, protein content standard deviation, DNA content standard deviation and DNA/protein ratio standard deviation. Protein content was significantly negatively correlated with DNA content (r=-0.796, p<0.001), DNA/protein ratio (r=-0.924, p<0.001). Protein content was significantly positively correlated with protein content standard deviation (r=0.611, p<0.001), DNA content standard deviation (r=0.473, p<0.001) and DNA/protein ratio standard deviation (r=0.438, p<0.001). DNA content was significantly positively correlated with DNA/protein ratio (r=0.926, p<0.001) and significantly negatively correlated with protein content standard deviation (r=-0.522, p<0.001), DNA content standard deviation (r=-0.392, p<0.001) and DNA/protein ratio standard deviation (r=-0.361, p<0.001). DNA/protein ratio was significantly negatively correlated with protein content standard deviation (r=-0.594, p<0.001), DNA content standard deviation (r=-0.504, p<0.001) and DNA/protein ratio standard deviation (r=-0.455, p<0.001). Protein content standard deviation was significantly positively correlated with DNA content standard deviation (r=0.707, p<0.001) and DNA/protein ratio standard deviation (r=0.845, p<0.001). DNA content standard deviation was significantly positively correlated with DNA/protein ratio standard deviation (r=0.879, p<0.001).

Table 4.7: Correlations of all Raman quantitative parameters.

Parameters		Protein	DNA	DNA/Protein	Protein SD	DNA SD
Protein	R					
	P					
DNA	R	-0.796				
	P	**<0.001**				
DNA/Protein	R	-0.924	0.926			
	P	**<0.001**	**<0.001**			
Protein SD	R	0.611	-0.522	-0.594		
	P	**<0.001**	**<0.001**	**<0.001**		
DNA SD	R	0.473	-0.392	-0.504	0.707	
	P	**<0.001**	**<0.001**	**<0.001**	**<0.001**	
DNA/Protein SD	R	0.438	-0.361	-0.455	0.845	0.879
	P	**<0.001**	**<0.001**	**<0.001**	**<0.001**	**<0.001**

4.12 Effect of chromatin condensation on Raman quantitative parameters

4.12.1 Effect of chromatin condensation on Raman quantitative parameters based on one cutoff point

The median of protein content (CMA3≤41 (51.18±0.9), CMA3>41 (52.25±1.62), p<0.001), DNA content (CMA3≤41 (63.98±1.13), CMA3>41 (62.36±1.81), p<0.001), DNA/protein ratio (CMA3≤41 (1.24±0.039), CMA3>41 (1.19±0.068), p<0.001) and protein content standard deviation (CMA3≤41 (2.12±0.46), CMA3>41 (2.51±0.83), p=0.002) showed a significant difference between the studied groups as illustrated in Figure 4.45. DNA content standard deviation (CMA3≤41 (3.74±0.57), CMA3>41 (3.97±0.84), p=0.105) and DNA/protein ratio standard deviation (CMA3≤41 (0.102±0.017), CMA3>41 (0.107±0.03), p=0.349) did not show a significant difference between the studied groups.

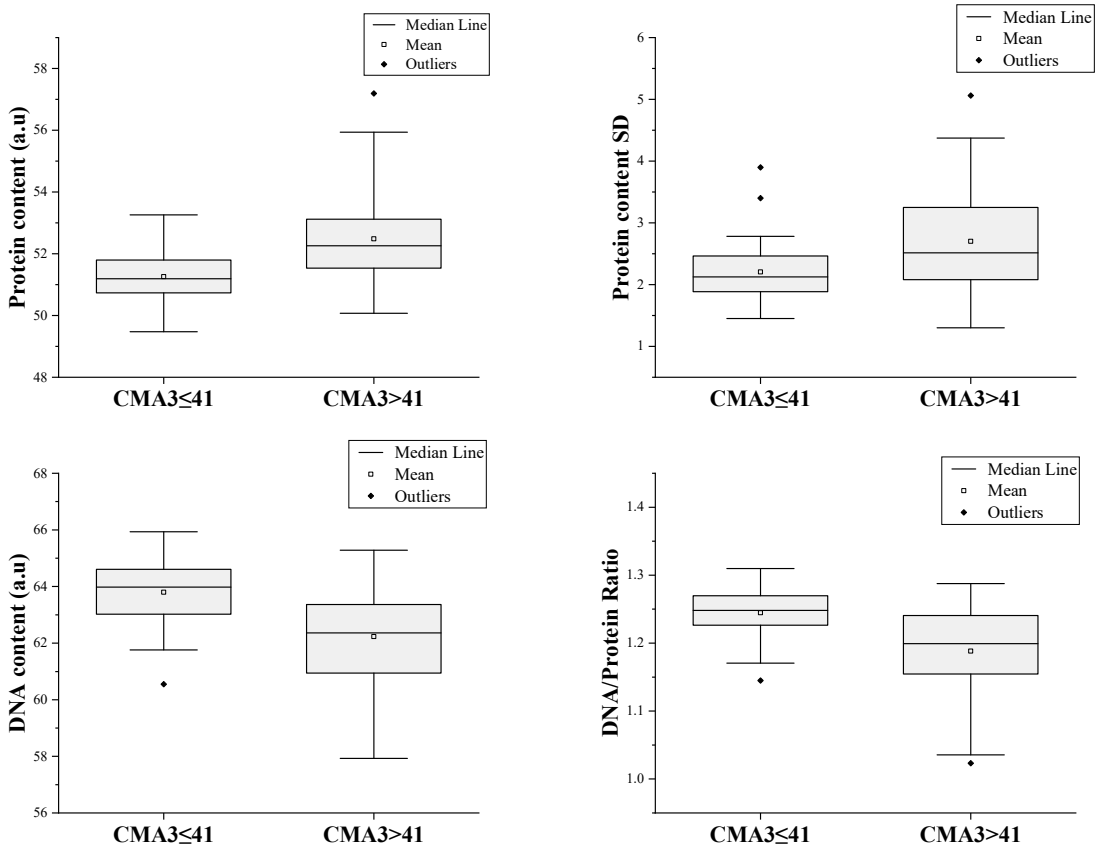

Figure 4.45: Box plots showing the differences of Raman quantitative parameters between CMA3≤41 (n=44) and CMA3>41 (n=41) groups (Mann-Whitney p-values for the differences in the medians were p<0.001 for protein content, p<0.001 for DNA content, p<0.001 for DNA/protein ratio and p=0.002 for protein standard deviation). The effect size was r=0.41 for protein content, r=0.45 for DNA content, r=0.43 for DNA/protein ratio and r=0.32 for protein content SD.

4.12.2 Effect of chromatin condensation on Raman quantitative parameters based on two cutoff points

The median of protein content (CMA3<28 (50.89±0.63), 28≤CMA3≤50 (51.56±1.2), CMA3>50 (52.3±1.7), p<0.001), DNA content (CMA3<28 (64.27±0.95), 28≤CMA3≤50 (63.44±1.47), CMA3>50 (62.24±), p=<0.001), DNA/protein ratio (CMA3<28 (1.25±0.028), 28≤CMA3≤50 (1.23±0.052), CMA3>50 (1.19±0.071), p<0.001) and protein content standard deviation (CMA3<28 (2.03±0.55), 28≤CMA3≤50 (2.15±0.55), CMA3>50 (2.81±0.81), p=0.001) showed a significant difference between the studied groups. Dunn's Post Hoc test was applied to identify which groups are different, the groups that show a significant difference are illustrated in Figure 4.46 with the Bonferroni corrected p-values. DNA content standard deviation (CMA3<28 (3.78±0.55), 28≤CMA3≤50 (3.58±0.61), CMA3>50 (4.07±0.99), p=0.102) and DNA/protein ratio standard deviation (CMA3<28 (0.105±0.02), 28≤CMA3≤50 (0.099±0.02), CMA3>50 (0.113±0.03), p=0.085) did not show a significant difference between the studied groups.

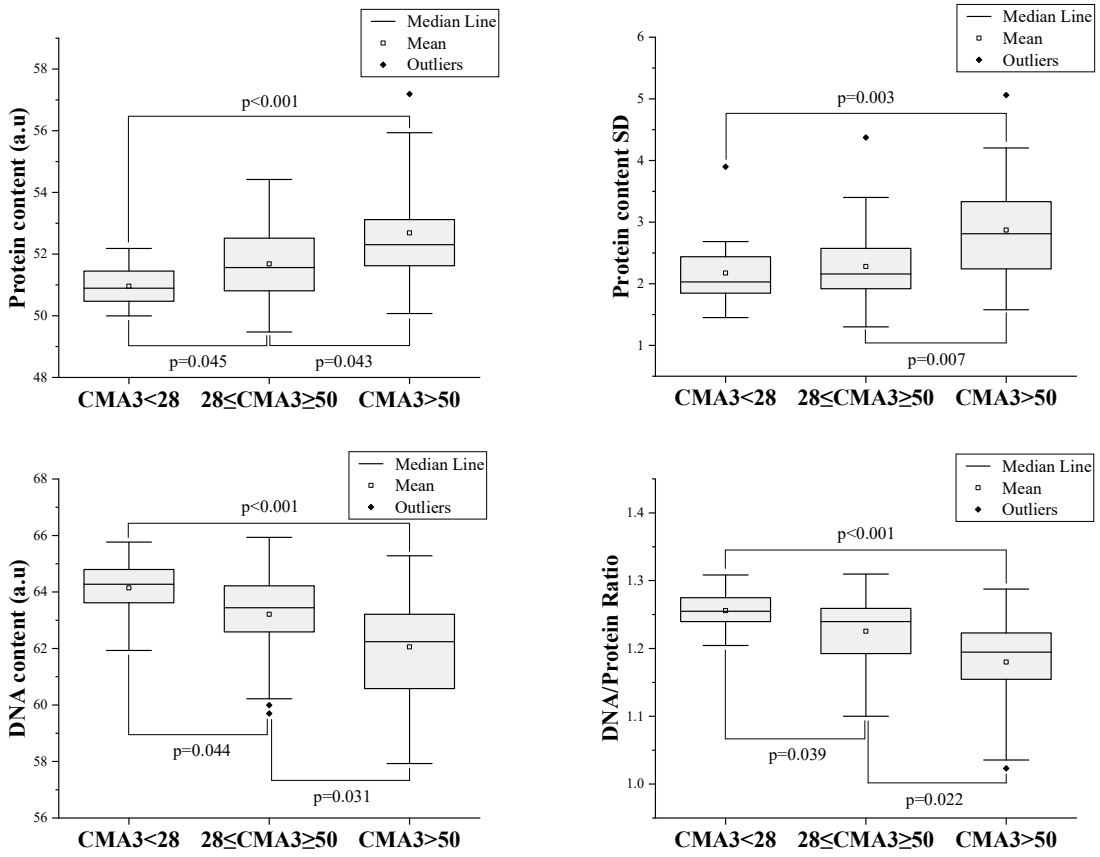

Figure 4.46: Box plots showing the differences of Raman quantitative parameters that show a significant difference between CMA3<28 (n=18), 28≤CMA3≥50 (n=40) and CMA3>50 (n=27) groups (Kruskal-Wallis p-values for the differences in the medians were p<0.001 for protein content, p<0.001 for DNA content, p<0.001 for DNA/protein ratio and p=0.001 for protein content standard deviation). The effect sizes were r=0.21 for protein content, DNA content and DNA/protein ratio, while r=0.16 for the protein content SD.

4.13 Effect of (WHO) semen parameters on Raman quantitative parameters

The median of DNA content (fertile (63.74±1.48), subfertile (62.85±1.86), p=0.028), DNA/protein ratio (fertile (1.24±0.054), subfertile (1.2±0.069), p=0.046) and protein content standard deviation (fertile (2.2±0.61), subfertile (2.7±0.75), p=0.004) showed a significant difference between the fertile and subfertile groups as illustrated in Figure 4.47. Protein content (fertile (51.45±1.2), subfertile (52.05±1.68), p=0.056), DNA content standard deviation (fertile (3.61±0.74), subfertile (3.51±0.8), p=0.065) and DNA/protein ratio standard deviation (fertile (0.101±0.023), subfertile (0.11±0.026), p=0.087) did not show a significant difference between the fertile and subfertile groups.

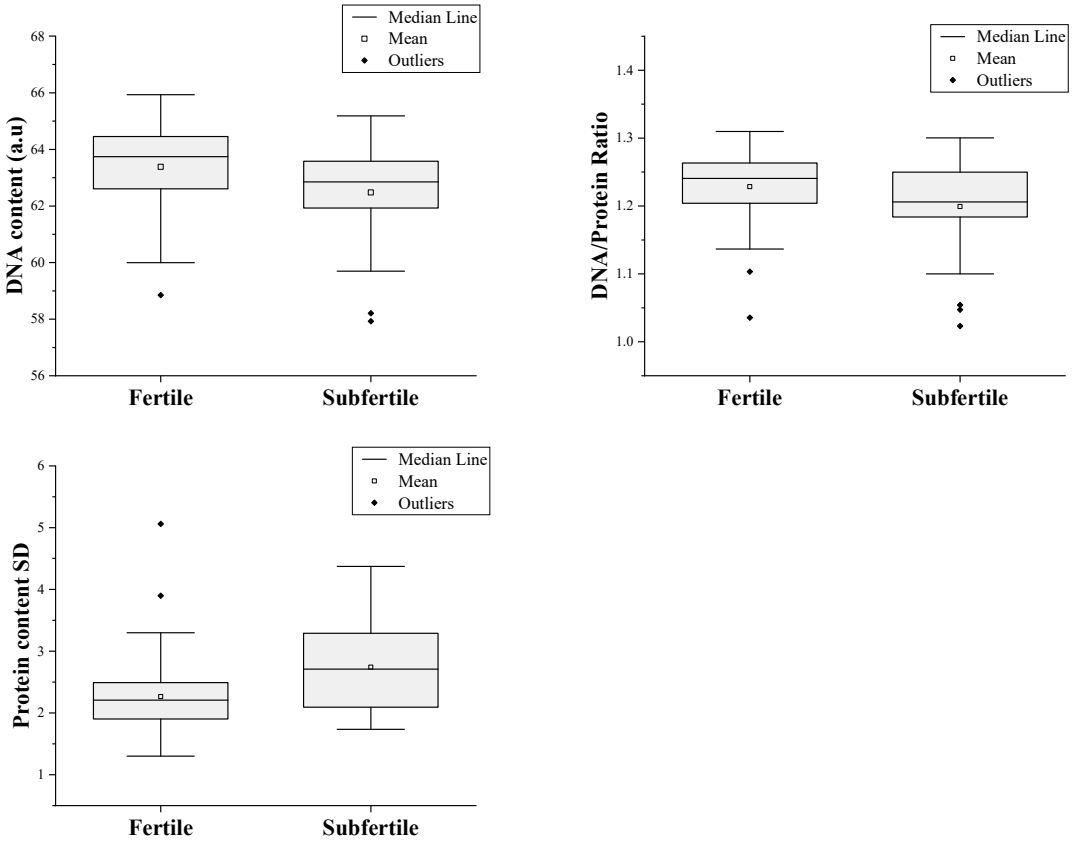

Figure 4.47: Box plots showing the differences of Raman quantitative parameters between fertile (n=53) and subfertile (n=32) groups (Mann-Whitney p-values for the differences in the medians were p=0.028 for DNA content, p=0.046 for DNA/protein ratio and p=0.004 for protein content standard deviation). The effect size was r=0.24 for DNA content, r=0.21 for DNA/protein ratio and r=0.31 for protein content SD.

4.13.1 Effect of sperm concentration on Raman quantitative parameters

The median of protein content (normal (51.49±1.26), oligospermia (52.36±1.77), p=0.021), protein content standard deviation (normal (2.21±0.65), oligospermia (2.76±0.7), p=0.001) DNA content standard deviation (normal (3.67±0.76), oligospermia (4.07±0.56), p=0.041) and DNA/protein ratio standard deviation (normal (0.101±0.026), oligospermia (0.123±0.025), p=0.016) showed a significant difference between normal and oligospermia groups as illustrated in Figure 4.48. DNA content (normal (63.5±1.62), oligospermia (62.73±1.78), p=0.057) and DNA/protein ratio (normal (1.23±0.057), oligospermia (1.2±0.071), p=0.063) did not show a significant difference between normal and oligospermia groups.

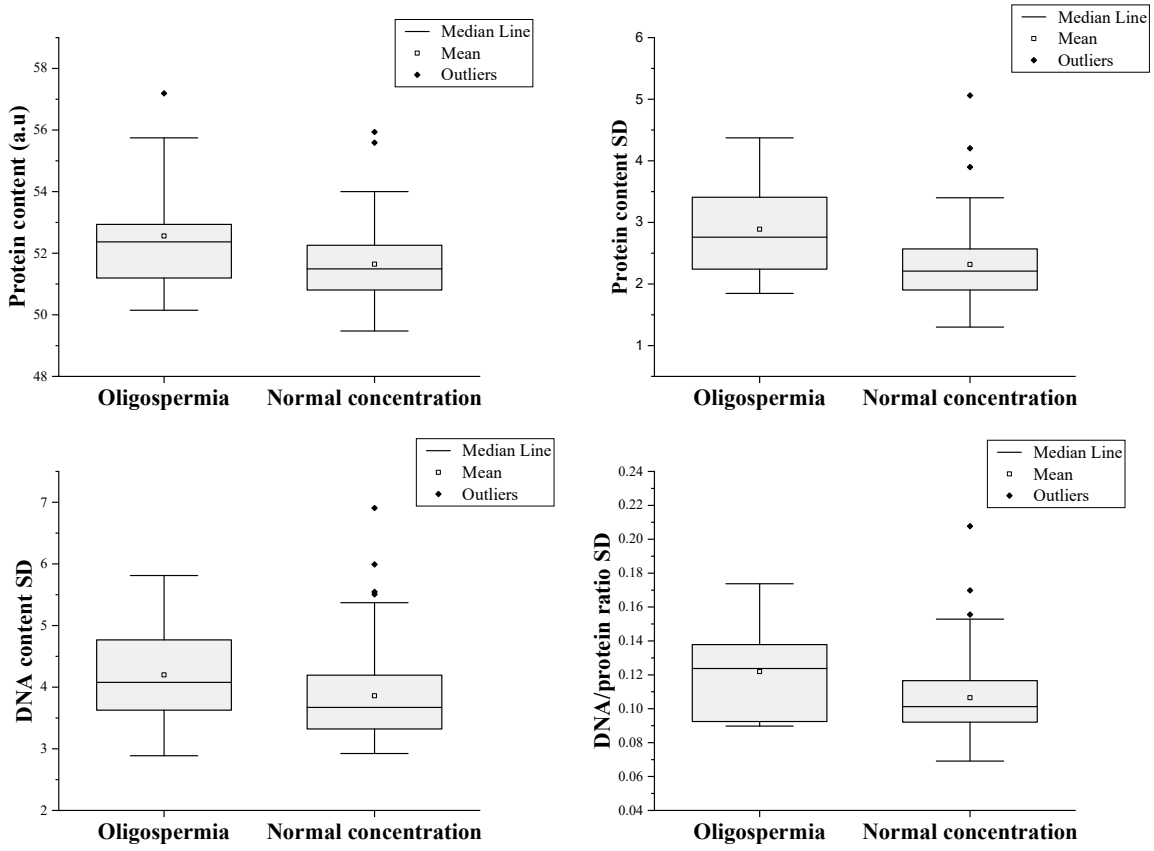

Figure 4.48: Box plots showing the differences of Raman quantitative parameters between normal concentration (n=66) and oligospermia (n=19) groups (Mann-Whitney p-values for the differences in the medians were p=0.021 for protein content, p=0.001 for protein content standard deviation, p=0.041 for DNA content standard deviation and p=0.016 for DNA/protein ratio standard deviation). The effect size was r=0.24 for protein content, r=0.35 for protein content SD, r=0.22 for DNA content SD and r=0.26 for DNA/protein ratio SD.

4.13.2 Effect of sperm motility on Raman quantitative parameters

The median of protein content standard deviation (normal (2.22±0.66), asthenospermia (3.0±0.81), p=0.019) and DNA/protein ratio standard deviation (normal (0.102±0.022), asthenospermia (0.125±0.031), p=0.040) showed a significant difference between normal and asthenospermia groups as illustrated in Figure 4.49. Protein content (normal (51.58±1.49), asthenospermia (52.05±0.09), p=0.540), DNA content (normal (63.48±1.73), asthenospermia (62.85±1.28), p=0.098), DNA/protein ratio (normal (1.23±0.064), asthenospermia (1.2±0.046), p=0.242) and DNA content standard deviation (normal (3.78±0.71), asthenospermia (4.36±1.04), p=0.153) did not show a significant difference between normal and asthenospermia groups.

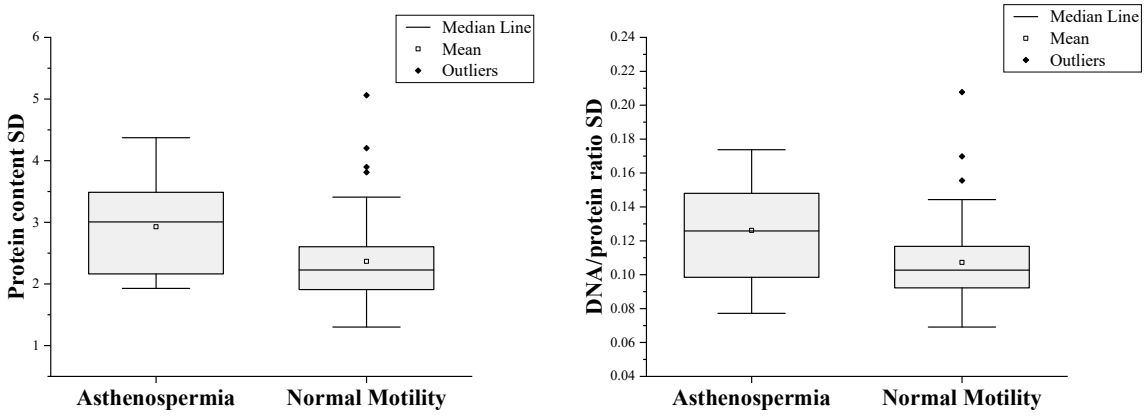

Figure 4.49: Box plots showing the differences of Raman quantitative parameters between normal motility (n=73) and asthenospermia (n=12) groups (Mann-Whitney p-values for the differences in the medians were p=0.019 for protein content standard deviation and p=0.040 for DNA/protein ratio standard deviation). The effect size was r=0.25 for protein content SD and r=0.22 for DNA/protein ratio SD.

4.13.3 Effect of sperm morphology on Raman quantitative parameters

The median of protein content (normal (51.59±1.39), teratospermia (52.12±1.56), p=0.208), DNA content (normal (63.36±1.54), teratospermia (62.97±2.15), p=0.339), DNA/protein ratio (normal (1.23±0.058), teratospermia (1.21±0.073), p=0.486), protein content standard deviation (normal (2.22±0.63), teratospermia (2.81±0.88), p=0.076), DNA content standard deviation (normal (3.78±0.7), teratospermia (4.14±0.98), p=0.113) and DNA/protein ratio standard deviation (normal (0.106±0.022), teratospermia (0.110±0.032), p=0.381) did not show a significant difference between normal and teratospermia groups.

5 Discussion

The evaluation of male infertility has become more important and revealing with the availability of new diagnostic and treatment methods (Kao *et al*., 2008). Sperm chromatin condensation is a primary factor that affecting male fertility, and its association with ICSI outcomes remains a contradictory and debatable issue. It is evident that the typical composition of sperm chromatin is a fundamental factor in maintaining DNA integrity (Cho *et al*., 2003). Any defect in sperm chromatin will probably have a severe effect on sperm DNA integrity and its ability to participate in the fertilization process. Fertilization with sperm that possess improper DNA packaging may have a negative result on early embryonic growth or lead to the development of the genetic disease.

The ICSI procedure is now accepted and used worldwide to solve the male infertility problems, especially in severe oligozoospermic and asthenozoospermic cases, that are difficult to achieve pregnancy in the conventional IVF procedure. ICSI procedure bypasses all the physiological barriers by injecting the sperm inside the mature egg (Palermo *et al*., 1992). In ICSI procedure, after eliminating the female factors the most challenging issue is sperm selection. Generally, sperm selection is based on sperm motility and morphology. It is reported that in several studies that sperm morphology is correlated to the ICSI outcomes (Hammadeh *et al*., 1998; Nasr-Esfahani *et al*., 2001). However, regardless of its success in treating a wide range of male infertility cases, the quality of the selected sperm remains the main challenge of this technique and largely depends on chance (Mallidis *et al*., 2011). But, there is evidence and developing consideration that sperm with normal shape is not necessary completely functional. It may still have abnormal chromatin condensation that consequently affects its DNA integrity (Hofmann and Hilscher, 1991; Schlicker *et al*., 1994; Angelopoulos *et al*., 1998). It is now accepted that proper chromatin condensation is fundamental for sperm to fertilize the oocytes and consequent achievement of normal embryo implantation and development during assisted reproduction technology procedures (Lolis *et al*., 1996; Nasr-Esfahani *et al*., 2001, 2005, 2008; Razavi *et al*., 2003; Bakos *et al*., 2008). In spite of the presence of several techniques that can reveal the sperm chromatin condensation abnormalities such as chromomycin A3 stains and aniline blue stains, none of these have a direct therapeutic use as they render the assessed sample inappropriate for assisted reproductive technology procedures. Moreover, none give direct information about the status of viable sperm, nor would be able to evaluate its capacity to function properly and thus achieve pregnancy. Few studies used Raman spectroscopy to evaluate sperm DNA fragmentation (Huser *et al*., 2009; Meister *et al*., 2010; Mallidis *et al*., 2011; Sanchez *et al*., 2012), and none of these studies investigated the ability of Raman spectroscopy to evaluate sperm chromatin condensation except Huser *et al*. (2009). They tested the ability of Raman spectroscopy to reveal any protein and DNA changes related to nucleus shape. But this study was based on single donor. In the current study, the ability of Raman spectroscopy to detect different

levels of sperm chromatin condensation was investigated. In addition, the consequences of sperm chromatin condensation on semen parameters and ICSI outcomes were analyzed.

5.1 Effect of chromatin condensation and DNA integrity on semen parameters

Spermatogenesis is a multistep process that turn the primary spermatogonia into fully developed sperm that occur in the testes. Several more remodeling processes happen during the passage of sperm through the epididymis that finally end up with sperm characterized by all the essential functional and morphological structures that allow the sperm to participate in the fertilization process effectively (Wistuba *et al*., 2007; Zhang *et al*., 2008). Generally, spermatogenesis is a complex process where numerous anomalies can and do occur. In some abnormal cases with an increased percentage of abnormal sperm, this may eventually lead to failure of the fertilization process, increased aneuploidy or pregnancy loss. These anomalies may include variation in sperm morphology, reduced motility, impaired DNA integrity and reduced chromatin condensation (Sivanarayana *et al*., 2012).

Sperm chromatin condensation, induced by substitution of histones by protamine, provides a special structural organization of the sperm chromatin. This organization protects sperm chromatin from nucleases and maintains its integrity (Ward and Coffey, 1991; Kazerooni *et al*., 2009). Any deviation in protamines content or ratio leads to abnormal chromatin condensation and affects normal sperm development, its fertilization capability and as a consequence normal fertilization and normal fetal development (Erenpreiss *et al*., 2006; Zini and Sigman, 2008). Loosely condensed chromatin and DNA fragmentation were observed in semen samples of poor quality (Saxena *et al*., 2008). Conventionally, male infertility is evaluated by sperm morphology, motility and concentration. Over the last 15 years the integrity of sperm DNA has been accepted as an essential factor in male fertility diagnosis (Lewis and Aitken, 2005; Ozmen *et al*., 2007; Tarozzi *et al*., 2007). The evaluation of sperm chromatin, including both chromatin condensation and DNA fragmentation, is now widely used as an additional diagnostic parameter providing more accurate diagnostic data than the traditional semen parameters evaluation. Several studies indicate that sperm with abnormal chromatin are more frequent in infertile men compared to fertile men (Machev *et al*., 2005; Zini and Libman, 2006; Larson *et al*., 2003). Additionally, the quality of sperm chromatin is negatively correlated with semen parameters including sperm morphology and motility (Sakkas *et al*., 1996; Giwercman *et al*., 2003). The occurrence of abnormal morphology sperm demonstrates that sperm often cannot complete the spermiogenesis process (Sakkas *et al*., 1999; Esteves and Agarwal, 2011).

In the current study, protamine deficiency evaluated by chromomycin A3 staining was significantly negatively correlated with sperm normal morphology ($r=-0.482$, $p<0.001$) and sperm concentration ($r=-0.388$, $p<0.001$), but it has not been significantly correlated with the total sperm motility ($r=-0.183$,

p=0.092). Histones retention evaluated by aniline blue staining was significantly negatively correlated with sperm concentration (r=-0.275, p=0.011), but it has not been significantly correlated with total sperm motility (r=-0.055, p=0.611) and sperm normal morphology (r=-0.049, p=0.654). DNA fragmentation evaluated by acridine orange staining was significantly negatively correlated with sperm concentration (r=-0.359, p<0.001), total sperm motility (r=-0.249, p=0.021) and sperm normal morphology (r=-0.328, p=0.002). The result of the current study indicates that there are negative correlations between the sperm chromatin related factors chromatin condensation and DNA fragmentation and the conventional semen parameters (normal morphology and concentration).

These results are in agreement with that of Franken *et al*. (1999) who found the chromomycin A3 and aniline blue positivity percentage in severe abnormal morphology donors were significantly higher compared to the normal morphology donors. Iranpour *et al*. (2000) found the chromomycin A3 positivity percentage was significantly negatively correlated with conventional semen parameters including sperm morphology, count and motility. Hammadeh *et al*. (2001) found the aniline blue positivity and semen parameters including sperm morphology, count, and motility show significant differences between patients and normal donors. But they have not found any correlation between aniline blue staining and semen parameters. Morris *et al*. (2002) found the DNA fragmentation was significantly positively correlated with sperm motility, and sperm concentration was significantly negatively correlated with sperm concentration and morphology. Nijs *et al*. (2009) found the DNA fragmentation was significantly negatively correlated with conventional semen parameters including sperm morphology, concentration and good motility. They also found the chromomycin A3 was significantly negatively correlated with sperm concentration. Kazerooni *et al*. (2009) found the chromatin quality evaluated by both chromomycin A3 and aniline blue was significantly negatively correlated with sperm morphology and progressive motility. Tarozzi *et al*. (2009) found the chromomycin A3 positivity percentage was significantly negatively correlated with conventional semen parameters including sperm morphology, concentration and motility. Kazerooni *et al*. (2009) found the protamine deficiency was significantly negatively correlated with sperm morphology and sperm progressive motility. Smit *et al*. (2010) found the DNA fragmentation was significantly negatively correlated with semen parameters including normal morphology, sperm concentration, total sperm count, progressive motility, and sperm vitality. Manochantr *et al*. (2011) found both chromomycin A3 and DNA fragmentation evaluated by terminal deoxynucleotidyl transferase dUTP nick end labeling (TUNEL) were significantly negatively correlated with sperm normal morphology, concentration, motility. Kim *et al*. (2013) found the aniline blue positivity was significantly negatively correlated with strict morphology. García-Ferreyra *et al*. (2014) found the sperm concentration, motility and vitality show significant

differences between normal and abnormal morphology donors. They found the DNA fragmentation was significantly higher among the abnormal morphology donors.

In the current study also, by applying the samples grouping based on a single cutoff point, the sperm concentration, motility and normal morphology were higher in the low CMA3 positive group (CMA3≤41) compared to the high CMA3 positive group (CMA3>41), but this difference was only significant for sperm concentration and morphology (sperm concentration (CMA3≤41 (46±29.58), CMA3>41 (27±17.71), p<0.001), sperm normal morphology (CMA3≤41 (8.5±8.93), CMA3> 41 (5±4.23), p<0.001) and sperm motility (CMA3≤41 (65.5±15.21), CMA3>41 (61±24.9), p=0.056)). By applying the samples grouping based on two cutoff points, the sperm morphology, concentration and motility were higher in the low CMA3 positive group (CMA3<28) followed by medium CMA3 positive group (28≤CMA3≤50) then the high CMA3 group (CMA3>50). But this difference was only significant for sperm concentration and morphology (sperm motility (CMA3<28 (69.5±15.91), 28≤CMA3≤50 (62.5±19.83), CMA3>50 (62±24.63), p=0.340), sperm concentration (CMA3<28 (43±42.05), 28≤CMA3≤50 (40±18.41), CMA3>50 (25±16.52), p=0.007) and sperm normal morphology (CMA3<28 (11.5±9.03), 28≤CMA3≤50 (6±7.74), CMA3>50 (5±3.47), p<0.001)). By applying Dunn's Post Hoc test sperm concentration did not show significant differences between CMA3<28 and 28≤CMA3≤50 groups, while it is decreased dramatically in the CMA3>50. This result indicates that the sperm concentration starts to be affected by highly improper sperm chromatin condensation. This effect starts earlier (at lower CMA3 positive) on sperm morphology. no significant difference was found between 28≤CMA3≤50 and CMA3>50 groups, but both of them are decreased dramatically compared to the CMA3<28 group. This result indicates that the sperm morphology is highly affected by sperm chromatin condensation even at moderate percentage levels of CMA3 positive sperm. This result explains why many authors focused their attention on the prognostic value of the sperm morphology (Pousette *et al*., 1986; Bianchi *et al*., 1996; Franken *et al*., 1999; Iranpour *et al*., 2000; Manochantr *et al*., 2011), it is logical that normal morphology is indicative of normal function.

The association between abnormal chromatin condensation and reduced semen quality is not easily clear. Abnormal chromatin condensation may be caused by altered protamine expression. But in order to explain the reduction of semen quality, this should be linked to the control of the spermatogenesis process (Carrell *et al*., 2007). Carrell *et al*. (2007) discussed two proposed hypotheses about this manner. The first hypothesis proposed that the abnormal expression of protamine is indicative of an abnormal spermatogenesis process that may be resulting from the aberrant functioning of transcriptional or translational regulators. The second hypothesis proposed that protamine could act as a checkpoint controller during spermatogenesis, so irregular expression of protamines may lead to the generation of apoptosis that then may result in reduced semen quality.

5.2 Effect of chromatin condensation on DNA integrity

Chromatin condensation is critical to maintain the sperm DNA integrity and its reproductive potential. Sperm from patients with subfertility are characterized by a structural abnormality in their DNA organization including DNA fragmentation, epigenetic modifications, aneuploidy and Y chromosome microdeletion (Seli and Sakkas, 2005). Particularly, protamines abnormalities make the sperm DNA more subjected to DNA damaging factors such as oxidative stress (Ozmen *et al*., 2007). Protamines deficiency evaluation by chromomycin A3 test and DNA fragmentation evaluation by different assays were used to understand the association between DNA fragmentation and chromatin condensation (Aoki *et al*., 2006b; Nili *et al*., 2009). Several studies correlate the DNA fragmentation with protamines abnormality by indirect measurements using chromomycin A3 staining. These studies have provided evidence that suggests the protamines abnormality may be the origin of sperm DNA fragmentation based on the strong correlation between protamines deficiency and DNA fragmentation (Bianchi *et al*., 1993; Manicardi *et al*., 1995; Naser-Esfahani *et al*., 2005; Aoki *et al*., 2006b; Torregrosa *et al*., 2006; Carrell *et al*., 2007; Tarozzi *et al*., 2009). Deficiency in protamines and DNA fragmentation are associated with male infertility (Oliva, 2006).

In the current study, the protamine deficiency evaluated by chromomycin A3 staining was significantly positively correlated with DNA fragmentation evaluated by acridine orange staining ($r=0.449$, $p<0.001$), but it has not been significantly correlated with histones retention evaluated by aniline blue staining ($r=0.151$, $p=0.166$). Additionally, acridine orange staining was not significantly correlated with aniline blue staining ($r=0.195$, $p=0.072$). These results indicated that there is a strong positive association between sperm chromatin condensation represented by protamines deficiency and DNA fragmentation. This correlation was tested for linearity by Pearson's correlation and found to be highly correlated ($r=0.492$, $p<0.001$) indicating that a strong relation exists between protamines deficiency and DNA fragmentation. By applying a linear regression model DNA fragmentation can be predicted from the chromomycin A3 result. These results are in agreement with that of Manicardi *et al*. (1995). They found the chromomycin A3 positivity was significantly positively correlated with the endogenous nick. Tarozzi *et al*. (2009) found the chromomycin A3 positivity was significantly positively correlated with sperm DNA fragmentation (TUNEL). Manochantr *et al*. (2011) found the chromomycin A3 positivity was significantly positively correlated with DNA fragmentation (TUNEL). Kim *et al*. (2013) found the abnormal sperm chromatin condensation (aniline blue staining) was significantly positively correlated with sperm chromatin structure (toluidine blue staining).

In the current study, by applying the samples grouping based on a single cutoff point, the DNA fragmentation was significantly higher in the high CMA3 positive group (CMA3>41) compared to low CMA3 positive group (CMA3≤41) (CMA3≤41 (27±10.93), CMA3>41 (42±15.74), $p<0.001$). By applying

the samples grouping based on two cutoff points, the DNA fragmentation shows a significant difference among the three groups (CMA3<28 (31.5±12.05), 28≤CMA3≤50 (30.5±10.68), CMA3>50 (44±17.81), p<0.001). By applying Dunn's Post Hoc test DNA fragmentation did not show a significant difference between the CMA3<28 and 28≤CMA3≤50 groups, but a substantial increase was observed in the CMA3>50. This result indicates that the DNA fragmentation starts to be affected by highly improper sperm chromatin condensation. However, during spermiogenesis DNA strand nicks occur and are ligated by a specific enzyme called topoisomerase II in order to replace histones by transition proteins and finally by protamines (Sakkas *et al*., 1999; Henkel *et al*., 2004; McPherson and Longo, 1993). The improper repair of the DNA strand nicks that occurred during spermiogenesis may result in DNA fragmentation. Another proposed mechanism to explain the DNA fragmentation is defective apoptosis. Apoptosis naturally occurs in the testes, probably to reduce the germ cells number in order to be supported by Sertoli cells or to reduce the abnormal sperm number. It is known that abnormal sperm express apoptotic markers such as p53. Some of these cells may escape the apoptosis process and complete the spermiogenesis (Gorczyca *et al*., 1993; Sakkas *et al*., 1999; Evenson *et al*., 2002). Cho *et al*. (2011, 2003) investigated the importance of protamines content for normal chromatin condensation during spermiogenesis by protamine knockout mice. They found insufficient protamine 1 and 2 leads to infertility, and insufficient protamine 2 leads to DNA fragmentation in addition to embryo death. These results indicated that protamines are a critical factor for differentiation of normal spermatid and any abnormalities in the ratio of P1/P2 are associated with infertility and could lead to defect in spermiogenesis (Manochantr *et al*., 2011).

5.3 Effect of semen parameters on ICSI outcomes

Traditional semen parameters including sperm morphology, concentration and motility are widely considered as the key parameters in male fertility evaluation (Kruger *et al*., 1986; Martinez *et al*., 2000). The effect of semen parameters on ICSI outcomes were investigated in several studies and contradictory result were published (Jiaen *et al*., 1995; Hammadeh *et al*., 1996, 1998; Lolis *et al*., 1996; Nikolettos *et al*., 1999; Nasr-Esfahani *et al*., 2001; Loutradi *et al*., 2006; Karpuz *et al*., 2007).

In the current study, the fertilization rate was significantly positively correlated with sperm concentration (r=0.449, p<0.001) and sperm morphology (r=0.487, p<0.001), but it has not been significantly correlated with the total sperm motility (r=0.208, p=0.056). Cleavage score was significantly positively correlated with sperm concentration (r=0.34, p=0.002) and sperm morphology (r=0.222, p=0.042), but it has not been significantly correlated with the total sperm motility (r=0.042, p=0.701). Embryo quality score was significantly positively correlated with sperm morphology (r=0.299, p=0.006), but it has not been significantly correlated with sperm concentration (r=0.208, p=0.058) or total sperm motility (r=-0.036, p=0.741). Embryo development score was significantly positively correlated with sperm concentration

(r=0.325, p=0.003) and sperm morphology (r=0.299, p=0.006), but it has not been significantly correlated with total sperm motility (r=-0.018, p=0.869). Also, the fertilization rate among all ICSI outcomes shows a significant difference between the fertile and subfertile groups (fertile (73±19.02), subfertile (58.5±24.09), p=0.006).

The result of the current study indicates that both sperm concentration and morphology affect ICSI outcomes. Sperm morphology seems to be the most critical parameter because it was independently correlated to all investigated ICSI outcomes including fertilization rate, cleavage score, embryo quality score and embryo development score. But, investigating the effect of all WHO semen parameters together as fertile, subfertile groups, only fertilization rate was affected as demonstrated by substantial decrease in the subfertile group. These results are in agreement with that of Loutradi *et al*. (2006). They found that the fertilization rate, cleavage rates, embryo quality and blastocyst development rates were reduced significantly when semen quality diminished. Other studies found the fertilization rate was significantly correlated with sperm morphology (Hammadeh *et al*., 1998; Nasr-Esfahani *et al*., 2001). Lolis *et al*. (1996) found the fertilization rate was significantly correlated with sperm concentration. Ron-El *et al*. (1991) demonstrated the effect of sperm quality on the fertilization rate. They repeated the cycles with mature oocytes that yielded low quality embryos by secondary insemination using high quality sperm donor and good quality embryos were obtained. They interpret these results with the presence of a high percentage of bad morphology sperm and the presence of sperm with autoantibodies that may interfere with attachment and penetration of oocytes. The effect of semen quality on ICSI outcomes may be explained based on the correlation between semen parameters and chromatin quality. The DNA fragmentation that may have evolved as a result of protamines deficiency during spermiogenesis could affect semen quality and consequently affecting ICSI outcomes (Sakkas *et al*., 1999; Evenson *et al*., 2002). Also, protamines deficiency may result in improper sperm chromatin condensation and consequently affecting abnormal decondensation at fertilization (Sakkas *et al*., 1999).

On the other hand, several studies demonstrated that no correlations were found between ICSI outcomes and semen parameters (Jiaen *et al*., 1995; Hammadeh *et al*., 1996; Nikolettos *et al*., 1999; Karpuz *et al*., 2007). The results of these studies are based on the fact that fertilization in ICSI procedure can be succeeded even when few normal sperm are available because the ICSI procedure bypasses the sperm natural selection steps (Palermo *et al*., 1992). In other studies, they explain the independency of ICSI outcomes from the quality of semen parameters, especially motility and morphology, with three possible reasons. First, all requirements in normal sperm (count, morphology and motility) to cross the zona pellucida and all barriers through the female reproductive tract are bypassed by injecting the sperm inside the oocytes during ICSI procedure (Nikolettos *et al*., 1999; Kahraman *et al*., 1999). Second, low quality sperm neither the abnormal

morphology nor the immotile sperm are usually selected by the embryologists during the ICSI procedure (Nikolettos *et al*., 1999). Third, sperm selection under low magnification power during ICSI procedure cannot detect the clear morphology and minor defects cannot be recognized by the embryologists (Berkovitz *et al*., 1999).

5.4 Effect of chromatin condensation and DNA integrity on ICSI outcomes

The unique sperm chromatin condensation is essential to protect sperm DNA from nucleases and polymerases (Ward and Coffey, 1991; Kazerooni *et al*., 2009). It is obvious that chromatin quality is important for normal fertilization and subsequently embryo cleavage and development during ICSI procedure because traditional semen parameters are bypassed by injecting a good quality sperm into the oocyte (Sakkas *et al*., 1998; Esterhuizen *et al*., 2000a; Iranpour, 2014). Indeed, sperm that bind to the oocytes are reported to have higher chromatin integrity than sperm that do not bind to oocytes, suggesting that sperm with higher chromatin quality can be naturally selected during natural reproduction or IVF procedure (Ellington *et al*., 1999; Nasr-Esfahani *et al*., 2005). But, during ICSI procedure the selection of sperm is mainly based on morphology and motility, in this manner sperm with poor chromatin quality may be used inadvertently, especially in case of low quality of semen parameters and sperm chromatin (Nasr-Esfahani *et al*., 2005). Sperm chromatin quality can be estimated using a wide range of staining methods, and these methods can detect sperm chromatin abnormalities that may have occurred during spermiogenesis (Balhorn, 1989; Iranpour, 2014). The effects of sperm chromatin quality on ICSI outcomes were investigated based on three sperm functional staining procedures including aniline blue (histone retention), chromomycin A3 (protamine deficiency) and acridine orange (DNA fragmentation).

In the current study, chromomycin A3 staining was significantly negatively correlated with the fertilization rate ($r=-0.626$, $p<0.001$), cleavage score ($r=-0.386$, $p<0.001$), embryo quality score ($r=-0.319$, $p=0.003$) and embryo development score ($r=-0.388$, $p<0.001$). Acridine orange staining was significantly negatively correlated with the fertilization rate ($r=-0.466$, $p<0.001$), cleavage score ($r=-0.238$, $p=0.029$), embryo quality score ($r=-0.254$, $p=0.019$) and embryo development score ($r=-0.284$, $p=0.009$). Aniline blue staining was not significant correlated with the fertilization rate ($r=-0.207$, $p=0.057$), cleavage score ($r=-0.181$, $p=0.098$), embryo quality score ($r=-0.099$, $p=0.368$) and embryo development score ($r=-0.156$, $p=0.156$).

The result of the current study indicates that both chromatin condensation evaluated by chromomycin A3 and DNA fragmentation evaluated by acridine orange, but not aniline blue, affects all the investigated ICSI outcomes. These result are in agreement with that of several studies in which they found the DNA fragmentation was significantly negatively correlated with the fertilization rate and embryo cleavage (Host *et al*., 2000; Morris *et al*., 2002; Benchaib *et al*., 2003; Agarwal and Allamaneini, 2004). Other studies

demonstrated that chromatin condensation evaluated by chromomycin A3 was significantly negatively correlated with the fertilization rate during ICSI procedure (Lolis *et al*., 1996; Nasr-Esfahani *et al*., 2001, 2005, 2008; Razavi *et al*., 2003; Bakos *et al*., 2008). Several studies demonstrated that chromatin condensation evaluated by chromomycin A3 was significantly negatively correlated with embryo development (Lolis *et al*., 1996; Esterhuizen *et al*., 2000a; Benchaib *et al*., 2003; Razavi *et al*., 2003; Nasr-Esfahani *et al*., 2005, 2008; Bakos *et al*., 2008). Tavalaee *et al*. (2009) found both chromomycin A3 positivity and DNA fragmentation was significantly negatively correlated with fertilization rate (ICSI). Henkel *et al*. (2003 and 2004) and Nasr-Esfahani *et al*. (2005) found that the DNA fragmentation (TUNEL) was significantly negatively correlated with embryo cleavage. Hammadeh *et al*. (1996) found that histone retention was not correlated with fertilization rate and cleavage score during ICSI procedure.

Also, the results of the current study demonstrated that all the investigated ICSI outcomes were higher in the low chromomycin A3 group (CMA3≤41) and decreased significantly in the high chromomycin A3 group (CMA3>41). The median fertilization rates were (CMA3≤41 (82±15.5), CMA3>41 (57±19.73), $p<0.001$), cleavage scores (CMA3≤41 (3.66±0.44), CMA3>41 (3.25±0.78), $p=0.009$), embryo quality scores (CMA3≤41 (2.47±0.35), CMA3> 41 (2.33±0.57), $p=0.014$) and embryo development scores (CMA3≤41 (6.06±0.71), CMA3>41 (5.61±1.28), $p=0.006$). The fertilization rate shows the highest difference between the studied groups indicating that fertilization rate is highly affected by sperm chromatin condensation compared to the other ICSI outcomes. The embryo quality score represents the least affected outcomes.

By applying the samples grouping based on two cutoff points, the medians of the fertilization rate, cleavage score, embryo quality score and embryo development score were significantly higher in the low CMA3 positive group (CMA3<28) followed by medium CMA3 positive group (28≤CMA3≤50) and then the high CMA3 group (CMA3>50). ((CMA3<28 (88±13.27), 28≤CMA3≤50 (70±16.83), CMA3>50 (56±22.6), $p<0.001$), cleavage score (CMA3<28 (3.84±0.46), 28≤CMA3≤50 (3.53±0.41), CMA3>50 (3.24±0.65), $p=0.003$), embryo quality score (CMA3<28 (2.64±0.43), 28≤CMA3≤50 (2.33±0.31), CMA3>50 (2.39±0.52), $p=0.018$) and embryo development score (CMA3<28 (6.51±0.83), 28≤CMA3≤50 (5.78±0.57), CMA3>50 (5.5±1.12), $p=0.007$)). All the studied ICSI outcomes were significantly correlated with chromatin condensation. Applying Dunn's Post Hoc test revealed that fertilization rate is the only outcome that differs significantly between the three groups. Cleavage score did not show a significant difference between the low CMA3 (CMA3<28) and the middle CMA3 (28≤CMA3≤50) groups. Embryo quality score did not show a significant difference between the middle CMA3 (28≤CMA3≤50) and the high CMA3 (CMA3>50) groups. For the embryo development score the only significant difference was found between the low CMA3 (CMA3<28) and the high CMA3 (CMA3>50) groups. These results indicate that

chromatin condensation may affect ICSI outcomes in different ways. The correlation between chromomycin A3 and fertilization rate was tested for linearity by Pearson's correlation and found to be highly correlated ($r=0.652$, $p<0.001$). This indicates that a strong relation exists between protamines deficiency and fertilization rate. By applying a linear regression model the fertilization rate can be predicted from the chromomycin A3 result.

The effect of chromatin condensation and DNA fragmentation on ICSI outcomes could be explained based on the following mechanism. During ICSI procedure, if the oocyte is fertilized by sperm characterized by abnormal chromatin condensation and DNA fragmentation, this may interfere with the normal decondensation process. This process involves protamines degradation and histones resynthesis that leads to the reestablishment of the sperm genome into its transcriptionally active state. The fertilization process and the subsequent embryo development may essentially not proceed normally (Sakkas *et al*., 1996; Esterhuizen *et al*., 2000b, 2002; Razavi *et al*., 2003). Sakkas *et al*. (1998) reported that a high level of sperm chromatin abnormalities including both chromatin condensation and DNA fragmentation in the selected sperm during ICSI procedure may inhibit the initiation or the completion of the decondensation process and subsequently leads to fertilization failure. Chromatin condensation could have a direct consequence on the fertilization rate because of the co-existence of protamines deficiency with other disorders in the late spermiogenesis events (Manicardi *et al*., 1995). These events include the formation of the acrosome, remodeling of membranes and other important biochemical and morphological events that are essential for sperm normal functioning (Carrell and Liu, 2001; Nasr-Esfahani *et al*., 2005). The decreased fertilization rate in sperm with abnormal chromatin condensation could also be explained by the premature chromosomal condensation. Premature chromosomal condensation induced by protamines deficiency is considered as a common cause of fertilization failure (Tejada *et al*., 1992; Schmiady *et al*., 1996; Mozdarani and Aghdaei, 2001). Nasr-Esfahani *et al*. (2004) reported that the premature chromosomal condensation is significantly higher in samples with high chromomycin A3 compared to low chromomycin A3 samples.

On the other hand, several studies reported some contradictory results. Tarozzi *et al*. (2009) did not find a correlation between the fertilization rate and chromomycin A3 in ICSI cases. Tesarik *et al*. (2004) found the DNA fragmentation (TUNEL) was not correlated with zygote morphological abnormalities and embryo cleavage. Henkel *et al*. (2003 and 2004) found the DNA fragmentation evaluated by TUNEL was not significantly correlated with the fertilization rate (ICSI). Benchaib *et al*. (2003) found the DNA fragmentation having no correlation with embryo quality. Karydis *et al*. (2005) found that the chromatin condensation evaluated by chromomycin A3 was not correlated with fertilization rate and embryo quality. Nasr-Esfahani *et al*. (2005) did not find significant correlations between protamine deficiency evaluated by chromomycin A3 and embryo cleavage and quality scores. Hammadeh *et al*. (1998) found the fertilization

rate (IVF) was significantly higher in the high condensed chromatin group (aniline blue positivity<20%) compared to the poor condensed chromatin group (aniline blue positivity >20%). Nasr-Esfahani *et al*. (2001) found a significant correlation between fertilization rate and aniline blue, but not with the DNA fragmentation (acridine orange).

These contradictory results could be explained based on the effect of the preparation methods usually employed during the ICSI procedure. It is reported that these preparation methods increase the percentage of sperm with normally condensed chromatin in low quality semen samples (Golan *et al*., 1997; Sakkas *et al*., 2000). As a result of using these preparation methods, the probability to select sperm with low chromatin quality will be decreased. Also, the selection of the most morphologically normal and good motility sperm decreases the probability of injecting the oocyte with low chromatin quality sperm (Tarozzi *et al*., 2009). The result of Tarozzi *et al*. (2009) supports this. They found that the fertilization rate was not correlated with chromatin condensation in ICSI cases, but this correlation is found in IVF cases that still depend on the natural selection of sperm. As mentioned before, the result of the current study and several other studies found a significant correlation between DNA fragmentation and chromatin condensation. But, the correlation of these two parameters with ICSI outcomes shows highly variable results. These variabilities demonstrated that chromatin condensation and DNA fragmentation affect ART in different means (Tarozzi *et al*., 2009). This might be explained based on the differences in the nature of DNA fragmentation and improper chromatin condensation and their effect on sperm quality. DNA fragmentation occurs as a result of protamines deficiency (Carrell *et al*., 2007), but the opposite is not true. Additionally, DNA fragmentation can be occurred by other intrinsic or extrinsic factors such as oxidative stress, storage temperature, abnormal nuclease activity and apoptosis (González-Marín *et al*., 2012).

Also, these contradictory results could be explained by the oocyte ability to repair the damaged sperm DNA (Brandriff and Pedersen, 1981; Ashwood-Smith and Edwards, 1996). It is suggested that oocyte can repair the sperm's fragmented DNA if it not exceeds 8% (Ahmadi and Ng, 1999). The ability of oocytes to repair the fragmented DNA depends on the nature of the DNA fragmentation, single or double-stranded. Generally, the single-stranded type is more readily to repair compared to the double-stranded one (González-Marín *et al*., 2012). It could be concluded that the DNA fragmentation test may not reflect the final paternal genome integrity. Finally, contradictory results could be explained based on the procedures that are used to evaluate the DNA fragmentation and the principles of these methods. Sperm chromatin structure assay requires a denaturalization step to detect the fragmented DNA under acidic pH, while TUNEL or comet assay at neutral pH, the denaturalization step is not required. They measure the actual DNA damage in one or both strands (González-Marín *et al*., 2012; Zidi-Jrah *et al*., 2016). This explanation could be confirmed by the result of a meta-analysis study that investigated the effect of DNA fragmentation

on ICSI and IVF indicated that different conclusions could be drawn when results are pooled based on the methods that are used to evaluate the DNA fragmentation (Li *et al*., 2006).

5.5 Raman spectral analysis

To establish a new diagnostic technique based on the Raman spectroscopy that is able to distinguish between sperm with normal and abnormal chromatin condensation it is essential to understand the Raman spectra of the sperm components and Raman spectral differences between normal sperm and sperm with chromatin condensation abnormalities. It is reported that each specific region of the sperm is characterized by specific Raman spectral features that reflect the biochemical components of these regions (Meister *et al*., 2010; De Luca *et al*., 2014; Amaral *et al*., 2018). In order to obtain the Raman spectral features that may reflect the sperm chromatin condensation, all spectra in this study were acquired from normal morphology sperm heads (post-acrosomal region). The following Raman peaks were recognized in the sperm head: 670 cm^{-1}, 731 cm^{-1}, 785 cm^{-1}, 1062 cm^{-1}, 1098 cm^{-1}, 1185 cm^{-1}, 1334 cm^{-1}, 1372 cm^{-1}, 1424 cm^{-1}, 1450 cm^{-1}, 1532 cm^{-1}, 1618 cm^{-1} and 1673 cm^{-1}. These peaks represent the functional groups or the backbones of the major macromolecules (DNA, proteins and lipids) that constitute the sperm head (De Mul *et al*., 1984; Peticolas *et al*., 1996; Thomas, 1999; Huser *et al*., 2009; Geldr *et al*., 2007; Luca *et al*., 2014; Talari *et al*., 2014; Ferrara *et al*., 2015; Angelis *et al*., 2017; Amaral *et al*., 2018; Nazarenko *et al*., 2018; Angelis *et al*., 2019). It is reported that the analysis of Raman spectral parameters such as Raman peaks intensities and Raman peak intensities ratio is a useful differentiating technique (Huser *et al*., 2009; Huang *et al*., 2013).

Previous studies analyzed some of these Raman peaks and correlated them to various properties. The presence of the Raman peak around 670 cm^{-1} represents the ring breathing mode of guanine, indicates that the DNA backbone was in B-form conformation (Benevides and Thomas, 1983). Raman peaks around 731 cm^{-1} and 785 cm^{-1}, which are the ring breathing modes of the nitrogen bases in the DNA nucleotides, are correlated to the DNA content and can be used to differentiate between sperm with X- or Y-chromosome (De Luca *et al*., 2014; Ferrara *et al*., 2015).

The results of the current study showed a significant difference in the Raman peaks median intensities of 731 cm^{-1} and 785 cm^{-1} that were significantly higher in the low chromomycin A3 (CMA3≤41) group compared to the high chromomycin A3 (CMA3>41) group (731 cm^{-1} (CMA3≤41 (0.479±0.029), CMA3>41 (0.462±0.028), p=0.002), 785 cm^{-1} (CMA3≤41 (0.763±0.05), CMA3>41 (0.691±0.064), p=0.015)) with medium effect size of r=0.34 for 731 cm^{-1} and small effect size of r=0.26 for 785 cm^{-1}. This indicates that chromatin condensation quality could affect the sperm's relative DNA content. The highly condensed chromatin in the low chromomycin A3 (CMA3≤41) group produces more intense DNA Raman

signals due to the presence of highly compacted DNA in the laser beam path compared to the high chromomycin A3 (CMA3>41) group in which the loosely compacted DNA produces less intense DNA Raman signals. The highly compacted chromatin protects the sperm DNA against DNA fragmentation factors such as nucleases and polymerases (Ward and Coffey, 1991; Kazerooni *et al*., 2009) or oxidative stress (Ozmen *et al*., 2007) and this could be confirmed by the significant difference of the DNA fragmentation between the two groups (CMA3≤41 (27±10.93), CMA3>41 (42±15.74), $p<0.001$). It is obvious that the highly condensed chromatin in the low chromomycin A3 (CMA3≤41) group seems to be more protected compared to the high chromomycin A3 (CMA3>41) group. The symmetric stretching vibration of the phosphate (PO_4) peak around 1098 cm^{-1} showed the same trend and confirmed the previous finding. It was significantly higher in the low chromomycin A3 (CMA3≤41) group compared to the high chromomycin A3 (CMA3>41) group (CMA3≤41 (0.594±0.031), CMA3>41 (0.553±0.033), $p<0.001$) with a large effect size $r=0.6$. It was reported that Raman peaks intensity and position are affected by nucleotide composition and sequence (Deng *et al*., 1999), and the Raman phosphate (PO_4) peak around 1098 cm^{-1} is the least affect one (Guan and Thomas, 1996). Therefore, this peak is often used to estimate DNA content (Okotrub *et al*., 2014). Based on these grounds and the large effect size of the phosphate peak, the DNA contents dramatically differ between the low and the high chromomycin A3 groups. Therefore, the low chromomycin A3 (CMA3≤41) group has more DNA occupied in the irradiated zone indicating that the DNA is denser and more compacted compared to the high chromomycin A3 (CMA3>41) group. Regarding the Raman peak intensity of adenine vibration mode around 731cm^{-1}, it was significantly higher in the low chromomycin A3 positive group compared to the high chromomycin A3 positive group. A similar finding was reported by Hud *et al*. (1994) in which they found the intensity of this Raman peak being significantly higher in the salmine- and polyarginine-DNA complexes compared to the native B-form DNA. The increased intensity was higher in the salmine-DNA complex than the polyarginine-DNA complex. This is not surprising and indicates that the packaging efficiency of protamines is higher compared to polyarginine. Also, this provides evidence that naturally occurring chromatin condensation during spermiogenesis results in more compacted chromatin compared to that produced by incorporating protamines or polyarginine to DNA in vitro (Huser *et al*., 2009).

The same trend was observed in the Raman peaks around 1185 cm^{-1} and 1372 cm^{-1} in which the median intensities of these Raman peaks were significantly higher in the low chromomycin A3 (CMA3≤41) group compared to the high chromomycin A3 (CMA3>41) group (1185 cm^{-1} (CMA3≤41 (0.251±0.015), CMA3>41 (0.238±0.015), $p=0.007$) and 1372 cm^{-1} (CMA3≤41 (0.763±0.0123), CMA3>41 (0.748±0.0171), $p<0.001$)) with medium effect size $r=0.3$ for 1185 cm^{-1} and $r=0.42$ for 1372 cm^{-1}. Several studies identify these Raman peaks and assigned them to ring breathing modes of DNA nitrogen bases (De

Mul *et al*., 1984; Peticolas *et al*., 1996; Thomas, 1999; Huser *et al*., 2009; Luca *et al*., 2014; Talari *et al*., 2014; Angelis *et al*., 2017; Amaral *et al*., 2018; Nazarenko *et al*., 2018). These results confirmed the effect of chromatin condensation quality on the sperm relative DNA content. These changes in the Raman activities of these DNA nitrogen bases could be caused by DNA damage (Li *et al*., 2014).

On the other hand, Huser *et al*. (2009) linked the highly intense Raman peak (which is very weak in their result) at 785 cm^{-1} with protamines packaging efficiency. With low intensity indicating highly packaged chromatin. The result of the current study showed a significant negative correlation (r=-0.234, p=0.030) between this peak and the chromomycin A3 positivity indicating that the intensity of this peak is significantly decreased in poorly condensed chromatin (785 cm^{-1} (CMA3≤41 (0.763±0.05), CMA3>41 (0.691±0.064), p=0.015)). This result is in the same line as Hud *et al*. (1994) in which they found the intensity of 785 cm^{-1} Raman peak being higher in the salmine-DNA complex compared to the native B-form DNA. This peak results from the contribution of cytosine and sugar-phosphate backbone vibrational modes. The increased intensity could be explained by the disturbance of the vibrational modes that occur as a result of binding to arginine residues in the protamine (Hud *et al*., 1994). Amaral *et al*. (2018) found the intensity of this peak is the lowest in sea urchin compared to the other studied species. Protamines are absent in sea urchin (Poccia *et al*., 1987).

The Raman peak of the methylene deformation mode around 1450 cm^{-1} was significantly higher in the high chromomycin A3 (CMA3>41) group compared to the low chromomycin A3 (CMA3≤41) group (CMA3≤41 (0.715±0.0137), CMA3>41 (0.719±0.0213), p=0.028) with medium effect size r=0.34. This peak is associated with the protein and lipids content in the cell (Huser *et al*., 2009; Sanchez *et al*., 2012; Huang *et al*., 2013). This can be further confirmed by the absence of this peak in the Raman spectrum of purified salmon sperm DNA compared to that of the intact salmon sperm (Kubasek *et al*., 1986). A similar finding was observed in this peak by Sanchez *et al*. (2012). They found the intensity of this Raman peak increased with oxidatively induced DNA fragmentation. This is not surprising, because DNA fragmentation is one of the main consequences of the abnormal chromatin condensation, and chromatin condensation evaluated by chromomycin A3 is highly correlated with the oxidative DNA fragmentation (De Iuliis *et al*., 2009; Aitken and De Iuliis, 2010). Also, the result of the current study showed that DNA fragmentation evaluated by acridine orange was significantly positively correlated with the Raman peak intensity around 1450 cm^{-1} (r=0.315, p=0.003). Two possible explanations could be offered here. The first one is based on the lipids contribution in this peak. Unsaturated fatty acids are the main component of the biological membranes and are very vulnerable to oxidative attack. Therefore, alteration in the lipids content can be associated or may be caused by lipid peroxidation, which is a well-recognized indicator of oxidative DNA fragmentation (Aitken and De luliis, 2010; Sanchez *et al*., 2012). The second explanation is based on the

protein contribution in this peak. As indicated in the result, sperm with low chromatin condensation quality (CMA3>41) have a higher relative protein content compared to sperm with high chromatin condensation quality (CMA3≤41). This could be explained by the presence of other nuclear proteins such as histones or transition proteins. These proteins are more loosely bound to the DNA compared to protamines resulting in less condensed chromatin (Huser *et al*., 2009). They are also less efficient in protecting the DNA against damaging factors. This could be partially confirmed by the result of aniline blue test, in which the retained histone was higher in CMA3>41 group compared to the CMA3≤41 group, but not significantly (CMA3≤41 (35±11.66), CMA3>41 (42±14.41), p=0.058). As the effect size is rather large (Cohen's d = 0.53), the observed difference might become statistically significant at larger sample numbers.

The same trend was observed in the Raman peaks around 1424 cm^{-1}, 1532 cm^{-1}, 1618 cm^{-1} and 1673 cm^{-1} in which the median intensities of these Raman peaks were significantly higher in the high chromomycin A3 (CMA3>41) group compared to the low chromomycin A3 (CMA3≤41) group (1424 cm^{-1} (CMA3≤41 (0.444±0.019), CMA3>41 (0.462±0.017), p=0.001), 1532 cm^{-1} (CMA3≤41 (0.0864±0.0153), CMA3>41 (0.0998±0.0139), p=0.003), 1618 cm^{-1} (CMA3≤41 (0.295±0.025), CMA3>41 (0.332±0.031), p<0.001) and 1673 cm^{-1} (CMA3≤41 (0.643±0.027), CMA3>41 (0.694±0.041), p<0.001)) with medium effect sizes r=0.36 for 1424 cm^{-1}, r=0.32 for 1532 cm^{-1}, r=0.4 for 1618 cm^{-1} and r=0.42 for 1673 cm^{-1}. Several studies identify these Raman peaks and assigned them to protein (De Mul *et al*., 1984; Thomas, 1999; Gelder *et al*., 2007; Luca *et al*., 2014; Talari *et al*., 2014; Amaral *et al*., 2018; Nazarenko *et al*., 2018; Angelis *et al*., 2019). The elevated intensities of these protein Raman peaks confirmed the previously discussed idea about the presence of other proteins in the low quality condensed group such as histone and transition proteins that bound to the DNA more loosely than protamines.

Huser *et al*. (2009) plotted two-dimensional distribution of the Raman peaks intensities ratio 785 cm^{-1}/1098 cm^{-1} and 1445 cm^{-1}/1098 cm^{-1} in order to discriminate between normal morphology sperm from abnormal sperm. The ratio distribution was not accurate and most abnormal morphology sperm were found in the normal morphology range. Mallidis *et al*. (2011) and Huang *et al*. (2013) in addition to the current study similar plots were drawn but, no similar results were observed. As a reminder, all spectra in the current study were acquired from normal morphology sperm and it is therefore expected to did not find any pattern based on the same hypothesis. Raman spectroscopy is an accurate technique, and these obvious variations in the result could be caused by the preparation method employed by Huser *et al*. (2009), in which they used a chemically treated amembranous sperm, in addition to extremely low sample size (n=1).

The results of the current study showed that the Raman peak intensities ratio (1050 cm^{-1}/1098 cm^{-1}) was significantly positively correlated with the percentage of the chromomycin A3 positivity (r=0.273, p=0.011) and this ratio was significantly higher in high chromomycin A3 (CMA3>41) group compared to the low

chromomycin A3 (CMA3≤41) group (CMA3≤41 (0.544±0.036), CMA3>41 (0.561±0.05), p=0.039). A similar trend was found for DNA fragmentation evaluated by acridine orange. DNA fragmentation was significantly correlated with Raman peak intensities ratio (1050 cm^{-1}/1098 cm^{-1}) (r=0.227, p=0.036). This result is in agreement with that of Sanchez *et al*. (2012). They found the Raman peak intensities ratio (1050 cm^{-1}/1098 cm^{-1}) being correlated with induced oxidative DNA fragmentation evaluated by flow cytometry also based on acridine orange. The same trend was observed by Mallidis *et al*. (2011). They reported that the Raman peak intensities ratio (1050 cm^{-1}/1098 cm^{-1}) was increased with UV-induced DNA fragmentation. As mentioned before, the phosphate (PO_4) Raman peak around 1098 cm^{-1} is the least variable DNA peak and is assumed not to be affected by nucleotide composition or sequence (Guan and Thomas, 1996). As a consequence, this spectral ratio difference represents a distortion in the chemical bonds between DNA bases and consequently affecting conformation and chromatin condensation (Ke *et al*., 1999; Meister *et al*., 2010). The increased intensity of the C–O stretching vibration of deoxyribose peak around 1050 cm^{-1} could be due to the changes in the groups and their force-bearing environment resulting from covalent bonds breakages between the deoxyribose and phosphate groups (Yiming *et al*., 1999). The results of Sanchez *et al*. (2012) and Mallidis *et al*. (2011) have a main difference compared to the current study. Their data show a highly elevated intensity around 1050 cm^{-1} and it appears as a separated peak. In the current study and other several studies (Meister *et al*., 2010; Huang *et al*., 2013; De Luca *et al*., 2014; Amaral *et al*., 2018) this peak is actually rather small and shows as a shoulder of the major phosphate peak as illustrated in Figure 4.25. The separate peak around 1050 cm^{-1} they observed could be caused by the extensive DNA fragmentation caused by their sample preparation methods or could alternatively be explained by the substrate used during the spectral acquisition. They used quartz and it is obvious that quartz contributes in the intensity of this Raman peak Figure 4.20. This spectral background contribution might not have been fully corrected by the authors.

In summary, the spectral analysis of Raman peaks indicates that the Raman DNA related peaks intensities decrease when chromatin condensation quality decreased, while the Raman proteins related peaks intensities increase when the chromatin condensation quality decreased. The effect of the relative total DNA, relative total protein and the DNA/protein ratio on the chromatin condensation will be discussed later with the spectral fitting model result.

5.6 Raman quantitative parameters

In order to investigate if the estimated relative total DNA and proteins contents and their ratio have an effect on sperm chromatin integrity either on chromatin condensation or DNA fragmentation and consequently on the ICSI outcomes, these contents were estimated based on the Raman spectral fitting model. The model applied to all the acquired spectra and peaks assignment was based on literature assignment (Table 4.5) and

confirmed by correlating the peaks that were assigned to the same molecule class (DNA or proteins). Six Raman spectral parameters were extracted and correlated to all studied parameters including: protamine deficiency, DNA fragmentation and all ICSI outcomes.

Alteration in sperm nuclear proteins content of subfertile men and its effect on chromatin condensation, DNA fragmentation and ICSI outcomes had been investigated in several studies (Lolis *et al*., 1996; Sakkas *et al*., 1996; Nasr-Esfahani *et al*., 2001, 2005, 2008; Razavi *et al*., 2003; Bakos *et al*., 2008; Velez *et al*., 2008; Tavalaee *et al*., 2009), but these studies focused on measuring either protamines and/or histones using direct biochemical methods or estimating methods based on staining protocols. Estimating the amount of separate sperm nuclear proteins by applying Raman spectroscopy is still difficult as most proteins look very similar from a Raman spectroscopy perspective. They are after all made up from almost the same types and numbers of chemical bonds. On the other side, Raman spectroscopy can compensate this limitation by being able to estimate the amount of DNA and protein from an individual cell or even subcellular structures. The direct (bio)chemical methods measure the desired molecules from pooled samples that could contain several contaminant cells such as epithelial cells, leukocytes, abnormal sperm, supporting testicular cells or arrested spermatids (Bench *et al*., 1998). Therefore, during the current study Raman spectroscopy was used to estimate the relative total nuclear proteins content including both protamines and histones in addition to sperm relative DNA content from individual cells.

It is known that chromatin condensation is unique and highly condensed in sperm compared to chromatin condensation in the somatic cells (Ward, 1993; Haaf and Ward, 1995; Evenson *et al*., 2002). This highly condensed chromatin is due to the presence of basic arginine rich proteins called protamines (Meistrich, 1989; Barratt, 1995; Kistler *et al*., 1996; Prigent *et al*., 1996; Steger, 1999; Kierszenbaum, 2001; Zhao *et al*., 2001). Protamines constitute about 85% of the sperm nuclear proteins. The remaining 15% are histones (Gatewood *et al*., 1987, Li *et al*., 2008). Histones are essential in reducing the compaction of sperm chromatin and initiate the decondensation of the sperm chromatin after the fertilization. Therefore, the retained histones are essential for sperm functioning and early embryo development (Wykes and Krawetz, 2003; Rajender *et al*., 2011). Protamines function is not fully understood (Carrell *et al*., 2007), but three proposed functions have been postulated: nucleus condensation, male genome protection and parental genome imprinting (Oliva and Dixon, 1991; Balhorn, 2007).

The result of the current study showed that the relative total protein content was significantly increased when the sperm chromatin condensation quality decreased. This was indicated by the significant positive correlation between the protamine deficiency evaluated by chromomycin A3 and the relative protein content ($r=0.444$, $p<0.001$) and the significant difference in the median relative protein content (CMA3≤41 (51.18±0.9), CMA3>41 (52.25±1.62), $p<0.001$) with a medium effect size $r=0.41$. The same positive

correlation was found between DNA fragmentation and the relative protein content ($r=0.469$, $p<0.001$). This is not surprising and supports the DNA protection function of protamines. The correlation between the relative protein content and both protamines deficiency and DNA fragmentation were tested for linearity by Pearson's correlation and were found to be highly correlated ($r=0.483$, $p<0.001$) for chromomycin A3 and ($r=0.469$, $p<0.001$) for acridine orange. This indicates that a strong relation exists between the relative protein content and both protamines deficiency and DNA fragmentation. By applying linear regression models both protamines deficiency and DNA fragmentation can be predicted from the Raman estimated relative protein content. As mentioned before, the elevated relative protein content in donors with low protamine content indicates the presence of other nuclear protein such as histone, and these proteins bind more loosely to the DNA than protamines resulting in less condensed chromatin (Huser *et al*., 2009). This could be confirmed by the increased number of sperm with histone retention as indicated by the significant positive correlation between the relative protein content and aniline blue staining ($r=0.231$, $p=0.033$). This result is in agreement with the result of other studies that associate the low protamine content with histones retention. This indicates that the combination of both low protamines and retained histones results in a low protection efficiency against oxidative DNA damage (Aoki *et al*., 2006b; Zhang *et al*., 2006; Tarozzi *et al*., 2009). Actually, the chromomycin A3 test evaluates the chromatin condensation by binding to the sperm DNA not bound to protamines. It competes with protamines to bind to the same binding sites in the DNA sequence. Therefore, the probability of the presence of unbound protamines and/or histones could explain the elevated relative protein content in the poor condensed chromatin donors. Thus, any factors affecting the binding of protamine to the DNA could negatively affect the chromatin condensation even when the protamines are normally synthesized. Oliva and Dixon (1991) reported that protamines phosphorylation is an essential factor to facilitate DNA-protamines binding. Quintanilla *et al*. (2000) reported that the toxic metal lead can induce conformational changes in protamines affecting its binding abilities to the DNA. Additionally, the presence of protamine 2 precursors could explain the elevated relative protein content in the poor condensed chromatin donors. It is reported that high amounts of protamine 2 precursors were found in sperm nuclear proteins extracted from infertile donors (Bench *et al*., 1998). Similarly, De Yebra *et al*. (1997) found elevated levels of protamine 2 precursors in infertile donors who have reduced level of protamine 2.

Regarding the ICSI outcomes, the estimated relative protein content was significantly negatively correlated with the fertilization rate ($r=-0.569$, $p<0.001$) and embryo development score ($r=-0.216$, $p=0.048$). These results indicate that the elevated sperm relative protein content affects the sperm fertilizing capability due to the distortion of the normal sperm protamines and histones content. Both are essential for normal decondensation and reestablishment of the sperm genome to its transcriptionally active state at fertilization

and consequently affect embryo development (Sakkas *et al*., 1996; Esterhuizen *et al*., 2000b, 2002; Razavi *et al*., 2003). A similar trend was observed in several studies in which they found protamines deficiency being significantly correlated with the fertilization rate (Lolis *et al*., 1996; Nasr-Esfahani *et al*., 2001, 2005, 2008; Razavi *et al*., 2003; Bakos *et al*., 2008), and embryo development (Lolis *et al*., 1996; Esterhuizen *et al*., 2000a; Benchaib *et al*., 2003; Razavi *et al*., 2003; Nasr-Esfahani *et al*., 2005, 2008; Bakos *et al*., 2008). The correlation between relative protein content and the fertilization rate was tested for linearity by Pearson's correlation and found to be highly correlated ($r=-0.654$, $p<0.001$), indicating that a strong relation exists between the relative protein content and the fertilization rate. By applying a linear regression model the fertilization rate can be predicted from the Raman estimated relative protein content.

The result of the current study showed that sperm relative DNA content declines significantly in poorly condensed chromatin donors as indicated by the significant negative correlation between the protamine deficiency evaluated by chromomycin A3 and the relative DNA content ($r=-0.485$, $p<0.001$) and the significant difference in the median relative DNA content (CMA3≤41 (63.98±1.13), CMA3>41 (62.36±1.81), $p<0.001$) with medium effect size $r=0.45$. The same significant negative correlation was observed with DNA fragmentation and histone retention ($r=-0.330$, $p=0.002$ and $r=-0.380$, $p<0.001$, respectively). The correlation between the relative DNA content and both protamines deficiency and DNA fragmentation were tested for linearity by Pearson's correlation and found they are highly correlated ($r=-0.522$, $p<0.001$) for chromomycin A3 and ($r=-0.426$, $p<0.001$) for acridine orange, indicating that a strong relations exist between the relative DNA content and both protamines deficiency and DNA fragmentation. By applying linear regression models both protamines deficiency and DNA fragmentation can be predicted from the Raman estimated relative DNA content.

The decreased relative DNA content in the protamines deficient donors could be explained with the protective function of the protamines. It is known that protamines provide a high compaction that protects the sperm DNA against DNA fragmentation factors such as nucleases (Ward and Coffey, 1991; Kazerooni *et al*., 2009). This is consistent with the results of the acridine orange test. The other factor that could affect the relative DNA content in the sperm is that in addition to 22 autosomal chromosomes sperm either have a X or Y chromosome that are of different size and DNA content. As mentioned before, two previous studies used Raman spectroscopy to differentiate between bull sperm with X or Y chromosome based on the differences in the Raman peak intensities around 731 cm^{-1}, 785 cm^{-1} and 1575 cm^{-1} (De Luca *et al*., 2014; Ferrara *et al*., 2015). In the current study, the Raman peak intensities of both 731 cm^{-1} and 785 cm^{-1} were significantly different between low and high chromomycin A3 groups, but this difference cannot be explained based on the sex-chromosome differences because the data points in this study are derived from 50 sperm per donor, and these data points represent the median value of the 50 selected sperm. The main

factor that could affect the sperm DNA content is chromosomal abnormalities that could result from mitotic or meiotic non-disjunction during spermatogenesis. It is reported that anomalies occurring during spermatogenesis are associated with the increased incidence of aneuploid gametes among the subfertile men (Moosani *et al*., 1995; Machev *et al*., 2005). It is reported that chromosomal abnormalities are associated with the reduced ICSI outcomes (Rubio *et al*., 2001; Burrello *et al*., 2003; Nicopoullos *et al*., 2008). Therefore, DNA fragmentation and chromosomal abnormalities could explain the reduced relative DNA content in donors with poorly condensed chromatin. These findings are consistent and could be confirmed by the significant correlation between the relative DNA content and ICSI outcomes. The relative DNA content was significantly positively correlated with the fertilization rate ($r=0.525$, $p<0.001$), cleavage score ($r=0.295$, $p=0.006$) and embryo development score ($r=0.257$, $p=0.018$). The correlation between relative DNA content and the fertilization rate was tested for linearity by Pearson's correlation and found to be highly correlated ($r=0.618$, $p<0.001$). This indicates that a strong relation exists between the relative DNA content and the fertilization rate. By applying a linear regression model fertilization rate can be predicted from the Raman estimated relative DNA content.

The result of the current study showed that the sperm DNA/protein ratio significantly declines in the poorly condensed chromatin donors. This is indicated by the significant negative correlation between the protamine deficiency evaluated by chromomycin A3 and the DNA/protein ratio ($r=-0.469$, $p<0.001$) and the significant difference in the median DNA/protein ratio of the two donor groups (CMA3≤41 (1.24±0.039), CMA3>41 (1.19±0.068), $p<0.001$) with a medium effect size $r=0.43$. During spectral acquisition, the laser beam always irradiates approximately the same volume of the sperm head. Sperm with low chromomycin A3 positivity that represent fully developed sperm with highly condensed chromatin showed a high DNA/protein ratio with more DNA and less proteins within a constant volume. These results indicate that the DNA is highly compacted and denser as indicated by the larger DNA spectral signals and the smaller proteins spectral signals. These findings are consistent with the chromatin condensation protection function in which the DNA seem to be protected in the donors with a high DNA/protein ratio as indicated by the significant correlation between the DNA/protein ratio and acridine orange result ($r=-0.425$, $p<0.001$). Sperm with high chromomycin A3 positivity represent the not fully developed sperm with poorly condensed chromatin showed a low DNA/protein ratio with smaller DNA spectral signals and larger proteins spectral signals. This indicates that the chromatin is less condensed, less DNA is occupied in the same volume. This could be explained with the presence of proteins other than protamines such as histones. Histones are less efficient in chromatin packaging compared to protamines. These findings were further confirmed by the elevated retained histone levels determined by aniline blue staining. High levels of histone retention were observed in low DNA/protein ratio donors as indicated by the significant correlation between

aniline blue staining and the DNA/protein ratio (r=-0.313, p=0.003). In summary, if the DNA/protein ratio is high, the chromatin is denser, the compaction is higher and the DNA is more protected. If the DNA/protein ratio is low, the chromatin is less dense, the compaction is poor and the DNA is less protected. The correlation between the DNA/protein ratio and both protamines deficiency and DNA fragmentation were tested for linearity by Pearson's correlation and found to be highly correlated (r=-0.516, p<0.001) for chromomycin A3 and (r=-0.515, p<0.001) for acridine orange. This points towards a strong relations exist between the DNA/protein ratio and both protamines deficiency and DNA fragmentation. By applying linear regression models both protamines deficiency and DNA fragmentation can be predicted from the Raman estimated DNA/protein ratio.

The highly condensed DNA-protamines complex is maintained by the inter-molecular attraction between the negatively charged DNA and the positively charged protamines molecules (Aoki and Carrell, 2003). Therefore, any DNA/protamine content abnormalities can increase the susceptibility of DNA to damage (Aoki *et al*., 2006b). This negative correlation between the DNA fragmentation and DNA/protein ratio is consistent with the result of a former study that found the DNA fragmentation was significantly negatively correlated with DNA/protamine ratio measured by biochemical methods (Castillo *et al*., 2011). Similar studies also observed a correlation between protamine content and DNA fragmentation (Aoki *et al*., 2005). All these observations support the idea of the protective function of protamines. Further evidence is the results of Suzuki *et al*. (2009) in which they found that the DNA condensation induced by protamine offers protection against DNA fragmentation. Moreover, in a protamine knockout mice model, it was demonstrated that insufficient levels of protamine 2 lead to DNA fragmentation (Cho *et al*., 2011, 2003). These findings fit with the strong correlation between the fertilization rate and the DNA/protein ratio (r=0.576, p<0.001). Donors with high DNA/protein ratios have highly condensed and protected chromatin that is required to achieve successful fertilization. The correlation between the DNA/protein ratio and the fertilization rate was tested for linearity by Pearson's correlation and found to be highly correlated (r=0.674, p<0.001). This indicates that a strong relation exists between the DNA/protein ratio and the fertilization rate. By applying a linear regression model fertilization rate can be predicted from the Raman estimated DNA/protein ratio. No previous studies directly correlated the DNA/protein ratio (total protein) with the fertilization rate, but Simon *et al.* (2011) found that the total protamines/DNA ratio was significantly correlated with the fertilization rate. Several factors affect the DNA/protein ratio such as protamine deficiency, histone retention, DNA fragmentation and chromosomal abnormalities. All these factors as previously discussed have a direct effect on sperm fertilization capability.

The DNA/protein ratio was significantly different between the fertile and subfertile donors (fertile (1.24±0.054), subfertile (1.2±0.069), p=0.046). This result is consistent with Bench *et al*. (1998) finding,

they estimated the DNA/total protamine ratio of a single sperm. The measurement was based on determining the phosphor and sulfur contents using Particle Induced X-ray Emission (PIXE) technique. They found this ratio to differ between fertile and subfertile donors (Bench *et al*., 1998). Bench *et al*. (1996) used the same technique (PIXE) to measure the DNA/total protamine ratio in human fertile donors and found it to be 1.37±0.04. This value is close to the fertile donor ratio derived from the spectral fitting model in the current study with 1.24±0.054. The difference between these ratios might be explained by this study's measurement of total protein including histones and any other proteins. Recalculating this ratio based on that protamines constitute 85% of the total nuclear proteins in fertile human, this ratio become 1.4±0.06 and it is more closed to the ratio reported by Bench *et al*. (1996).

The main objective of the current study was to investigate the ability of Raman spectroscopy to detect different levels of chromatin condensation. The obtained spectra were analyzed both by individual spectral analysis and by a quantitative parameter based Raman spectral fitting model. As seen in the result of Dunn's Post Hoc test, no individual Raman peak can be used to differentiate between the three studied groups. These results indicate that chromatin condensation cannot be predicted based on any individual Raman peaks. By incorporating almost, the entire complex spectrum into the quantitative parameter based Raman spectral fitting model, quantitative parameters including relative protein content, relative DNA content and DNA/protein ratio showed a significant difference among all the studied groups as indicated in the Dunn's Post Hoc test results. These findings reflect the strength of the spectral fitting model and its ability to detect different levels of chromatin condensation compared to individual spectral analysis. The computerized model can batch process and analyze thousands of sperm spectra at a time.

The result of the current study showed that the relative DNA content, relative proteins content and DNA/protein ratio show high variability among the studied samples and their standard deviations were significantly positively correlated with functional sperm staining tests and significantly negatively correlated with the ICSI outcomes. These findings indicate that samples with poorly condensed chromatin and low fertilization rate show high variations in their estimated parameters. It is known that sperm either possess a X-chromosome or a Y-chromosome that contain different amounts of DNA. Although this difference is small, it is reported that Raman spectroscopy can differentiate between X or Y bearing chromosome sperm (De Luca *et al*., 2014; Ferrara *et al*., 2015). These generally observed variations could be partially explained by the type of sex chromosome. But, the main difference could be resulting from the presence of subpopulations of sperm in the samples under analysis. These variations indicate that these samples contain sperm that have different chemical compositions. This is most likely caused by different maturation levels reflecting some hidden anomalies in spermatogenesis that could produce normal morphology sperm with immature chromatin.

The estimated Raman parameters were applied to see if these parameters can discriminate between donors based on the WHO classification. Fertile versus subfertile classification shows significant differences in the relative DNA content, DNA/protein ratio and protein standard deviation. Normal count versus oligozoospermia show significant differences in the relative protein content, protein standard deviation, DNA standard deviation and DNA/protein ratio standard deviation. Normal motility versus asthenozoospermia show significant differences in protein standard deviation and DNA/protein ratio standard deviation. Normal morphology versus teratozoospermia did not show any difference in all the investigated Raman quantitative parameters. These results generally indicate that Raman spectroscopy cannot distinguish between sperm samples obtained from donors with different abnormal semen parameters such as oligozoospermia and asthenozoospermia. But, it can detect the variation between these spemiogram abnormalities as indicated in the significant difference in their standard deviations. The absence of any significant differences between normal morphology and teratozoospermia donors is logical because all spectra in this study were acquired from normal morphology sperm. A previous study based on few sperm showed that Raman spectra of normal morphology sperm differ from that of abnormal one, in addition to spectral variability between normal morphology sperm (Huser *et al*., 2009; Huang *et al*., 2013; Nazarenko *et al*., 2018).

6 Conclusion

The result of the current study indicates that among the three evaluated sperm functional tests (CMA3, AO and AB), chromatin condensation and DNA fragmentation evaluated by chromomycin A3 and acridine orange staining, respectively, were related to semen parameters quality, histones retention evaluated by aniline blue was not. Also, both chromatin condensation and DNA fragmentation affect all the investigated ICSI outcomes including, fertilization rate, embryo cleavage score, embryo quality score and embryo developmental score. These result indicate that both chromomycin A3 and acridine orange staining are a potential prognostic tests for ICSI patients.

The result of the current study indicates that Raman quantitative parameters (relative protein content, relative DNA content and DNA/protein ratio), estimated by a spectral fitting model, are related to all chromatin integrity parameters including protamine deficiency, histones retention and DNA fragmentation. Additionally, these Raman quantitative parameters were related to ICSI outcomes.

Also, the result of the current study indicates that Raman spectroscopic measurements, either individual Raman peaks or Raman quantitative parameters, represent a promising diagnostic tool. Raman spectroscopy has the ability to detect sperm with chromatin abnormalities such as improper chromatin condensation and DNA fragmentation to a similar degree than the existing staining techniques at the individual cell level. These capabilities also enable its use to predict ICSI outcomes.

The Raman spectroscopy result, both the spectral analysis and Raman quantitative parameters, obtained from normal morphology sperm showed great differences. These results indicated that Raman spectroscopy has the ability to detect the presence of immature sperm and some hidden abnormalities resulting from disturbances during spermatogenesis.

Unlike the currently used chromatin integrity tests that destroy the sample under analysis, Raman spectroscopy also has the ability to noninvasively detect chromatin integrity in living sperm. Therefore, Raman spectroscopy represents a promising system that could accompany the ICSI procedure to select sperm with proper chromatin condensation and intact DNA. But this ultimate goal still needs further optimization, especially regarding laser power density and its effects on the living sperm. Therefore, starting with animal models is recommended. Besides this application, Raman spectroscopy could be developed into a pre-diagnostic tool to predict ICSI outcomes or to optimize currently employed sperm processing techniques prior ICSI such as density gradient centrifugation or swim-up.

7 References

Agarwal A, Allamaneni SS (2004) The effect of sperm DNA damage on assisted reproduction outcomes. A review. Minerva Ginecologica 56:235–245.

Ahmadi A, Ng S-C (1999) Fertilizing ability of DNA-damaged spermatozoa. The Journal of Experimental Zoology 284:696–704.

Ainsworth C, Nixon B, Aitken RJ (2005) Development of a novel electrophoretic system for the isolation of human spermatozoa. Human Reproduction 20:2261–2270.

Aitken RJ, De luliis GN (2010) On the possible origins of DNA damage in human spermatozoa. Molecular Human Reproduction 16:3–13.

Amaral S, Costa RD, Wübbeling F, Redmann K, Schlatt S (2018) Raman micro-spectroscopy analysis of different sperm regions: a species comparison. Molecular Human Reproduction 24:185–202.

Angelis AD, Ferrara MA, Coppola G, Matteo LD, Siani L, Dale B, Coppola G, De Luca AC (2019) Combined Raman and polarization sensitive holographic imaging for a multimodal label-free assessment of human sperm function. Scientific Reports 9:1–15.

Angelis AD, Managò S, Ferrara MA, Napolitano M, Coppola G, De Luca AC (2017) Combined Raman spectroscopy and digital holographic microscopy for sperm cell quality analysis. Journal of Spectroscopy 2017:1–14.

Angelopoulos T, Moshel YA, Lu L, Macanas E, Grifo JA, Krey LC (1998) Simultaneous assessment of sperm chromatin condensation and morphology before and after separation procedures: effect on the clinical outcome after in vitro fertilization. Fertility and Sterility 69:740–747.

Anifandis G, Dafopoulos K, Messini C, Chalvatzas N, Messinis I (2010) Effect of the position of the polar body during ICSI on fertilization rate and embryo development. Reproductive Sciences 17:849–853.

Aoki VW, Liu L, Jones K, Hatasaka H, Gibson M, Peterson C, Carrell D (2006a) Sperm protamine 1/protamine 2 ratios are related to in vitro fertilization pregnancy rates and predictive of fertilization ability. Fertility and Sterility 86:1408–1415.

Aoki VW, Emery BR, Liu L, Carrell DT (2006b) Protamine levels vary between individual sperm cells of infertile human males and correlate with viability and DNA integrity. Journal of Andrology 27:890–898.

Aoki VW, Moskovtsev SI, Willis J, Liu L, Mullen JB, Carrell DT (2005) DNA integrity is compromised in protamine-deficient human sperm. Journal of Andrology 26:741–748.

Aoki VW, Carrell DT (2003) Human protamines and the developing spermatid: their structure, function, expression and relationship with male infertility. Asian Journal of Andrology 5:315–324.

Asher SA (1993) UV resonance Raman spectroscopy for analytical, physical, and biophysical chemistry. Analytical Chemistry 65:201–210.

Ashwood-Smith MJ, Edwards RG (1996) DNA repair by oocytes. Molecular Human Reproduction 2:46–51.

Atkins PW (2002) Atkins physical chemistry. Oxford University Press, Oxford.

Baker K, Sabanegh E (2013) Obstructive azoospermia: reconstructive techniques and results. Clinics 68:61–73.

Bakos H, Thompson J, Feil D, Lane M (2008) Sperm DNA damage is associated with assisted reproductive technology pregnancy. International Journal of Andrology 31:518–526.

Balhorn R (2011) "Sperm chromatin: an overview." In sperm chromatin, pp. 3-18. Springer, New York, NY, 2011.

Balhorn R (2007) The protamine family of sperm nuclear proteins. Genome Biology 8:1–8.

Balhorn R, Cosman M, Thornton K, Krishnan VV, Corzett M, Bench G, Kramer C, Lee J, Hud NV, Allen MJ (1999) In the male gamete: from basic science to clinical applications. Gagnon C (eds.). Cache River Press, Vienna, IL.

Balhorn R (1989) Mammalian protamines: structure and molecular interactions. In Molecular biology of chromosome function (366-395). Springer, New York, NY.

Banwell CN, McCash EM (2013) Fundamentals of molecular spectroscopy. McGraw-Hill Education, New Delhi.

Barone JG, De Lara J, Cummings KB, Ward WS (1994) DNA organization in human spermatozoa. Journal of Andrology 15:139–144.

Barratt C L (2007) Semen analysis is the cornerstone of investigation for male infertility. The Practitioner 8-8.

Bartoov B, Berkovitz A, Eltes F, Kogosowski A, Menezo Y, Barak Y (2002) Real-time fine morphology of motile human sperm cells is associated with IVF-ICSI outcome. Journal of Andrology 23:1–8.

Bastiaan HS, Windt ML, Menkveld R, Kruger TF, Oehninger, Franken DR (2003) Relationship between zona pellucida-induced acrosome reaction, sperm morphology, sperm-zona pellucida binding, and in vitro fertilization. Fertility and Sterility 79:49–55.

Bench G, Corzett M, Yebra LD, Oliva R, Balhorn R (1998) Protein and DNA contents in sperm from an infertile human male possessing protamine defects that vary over time. Molecular Reproduction and Development 50:345–353.

Bench G, Friz A, Corzett M, Morse DH, Balhorn R (1996) DNA and total protamine masses in individual sperm from fertile mammalian subjects. Cytometry 23:263–271.

Benchaib M, Braun V, Lornage J Hadj S, Salle B, Lejeune H, Guérin JF (2003) Sperm DNA fragmentation decreases the pregnancy rate in an assisted reproductive technique. Human Reproduction 18:1023–1028.

Benevides JM, Thomas Jr GJ (1983) Characterization of DNA structures by Raman spectroscopy: high-salt and low-salt forms of double helical poly (dG-dC) in H2O and D2O solutions and application to B, Z and A-DNA. Nucleic acids research 11:5747–5761.

Bergholt MS, Lin K, Zheng W, Huang Z, Lau D (2012) In vivo, real-time, transnasal, image-guided Raman endoscopy: defining spectral properties in the nasopharynx and larynx. Journal of biomedical optics 17:0770021.

Berkovitz A, Eltes F, Lederman H, Peer S, Ellenbogen A, Feldberg B, Bartoov B (2006) How to improve IVF–ICSI outcome by sperm selection. Reproductive BioMedicine Online 12:634–638.

Berkovitz A, Eltes F, Soffer Y, Zabludovsky N, Beyth Y, Farhi J, Levran D, Bartoov B (1999) ART success and in vivo sperm cell selection depend on the ultramorphological status of spermatozoa. Andrologia 31:1–8.

Bianchi F, Rousseauxprevost R, Bailly C, Rousseaux J (1994) Interaction of human P1 and P2 protamines with DNA. Biochemical and Biophysical Research Communications 201:1197–1204.

Bianchi PG, Manicardi GC, Urner F, Campana A, Sakkas D (1996) Chromatin packaging and morphology in ejaculated human spermatozoa: evidence of hidden anomalies in normal spermatozoa. Molecular Human Reproduction 2:139–144.

Bianchi PG, Manicardi GC, Bizzaro D, Bianchi U, Sakkas D (1993) Effect of deoxyribonucleic acid protamination on fluorochrome staining and in situ nick-translation of murine and human mature spermatozoa. Biology of Reproduction 49:1083–1088.

Black M, Liu de Y, Bourne H, Baker HW (2010) Comparison of outcomes of conventional intracytoplasmic sperm injection and intracytoplasmic sperm injection using sperm bound to the zonapellucida of immature oocytes. Fertility and Sterility 93:672–674.

Boe-Hansen GB, Fedder J, Ersboll AK, Christensen P (2006) The sperm chromatin structure assay as a diagnostic tool in the human fertility clinic. Human Reproduction 21:1576–1582.

Bonde JPE, Ernst E, Jensen TK, Hjollund N, Kolstad H, Scheike T, Giwercman A, Skakkebæk N, Henriksen T, Olsen J (1998) Relation between semen quality and fertility: a population-based study of 430 first-pregnancy planners. The Lancet 352:1172–1177.

Bonnier F, Meade AD, Merzha S, Knief P, Bhattacharya K, Lyng F, Byrne H (2010) Three dimensional collagen gels as a cell culture matrix for the study of live cells by Raman spectroscopy. The Analyst 135:1697–1703.

Braga DPAF, Iaconelli A, Figueira RDCS, Madaschi C, Semião-Francisco L, Borges E (2009) Outcome of ICSI using zona pellucida-bound spermatozoa and conventionally selected spermatozoa. Reproductive BioMedicine Online 19:802–807.

Brandriff B, Pedersen RA (1981) Repair of the ultraviolet-irradiated male genome in fertilized mouse eggs. Science 211:1431–1433.

Braun RE (2001) Packaging paternal chromosomes with protamine. Nature Genetics 28:10–12.

Brewer L, Corzett M, Lau EY, Balhorn R (2003) Dynamics of protamine 1 binding to single DNA molecules. Journal of Biological Chemistry 278:42403–42408.

Brewer L, Corzett M, Balhorn R (2002) Condensation of DNA by spermatid basic nuclear proteins. Journal of Biological Chemistry 277:38895–38900.

Bulkin BJ (1972) Raman spectroscopic study of human erythrocyte membranes. Biochimica et Biophysica Acta (BBA)-Protein Structure 274:649–651.

Bungum M, Humaidan P, Axmon A, Spano M, Bungum L, Erenpreiss J, Giwercman A (2007) Sperm DNA integrity assessment in prediction of assisted reproduction technology outcome. Human Reproduction 22:174–179.

Burrello N, Vicari E, Shin P, Agarwal A, De Palma A, Grazioso C, D'Agata R, Calogero AE (2003) Lower sperm aneuploidy frequency is associated with high pregnancy rates in ICSI programmes. Human Reproduction 18:1371–1376.

Carrell DT, Emery BR, Hammoud S (2007) Altered protamine expression and diminished spermatogenesis: what is the link? Human Reproduction Update 13:313–327.

Carrell DT, Liu L (2001). Altered protamine 2 expression is uncommon in donors of known fertility, but common among men with poor fertilizing capacity, and may reflect other abnormalities of spermiogenesis. Journal of Andrology 22:604–610.

Castillo J, Simon L, Mateo SD, Lewis S, Oliva R (2010) Protamine/DNA ratios and DNA damage in native and density gradient centrifuged sperm from infertile patients. Journal of Andrology 32:324–332.

Cebesoy FB, Aydo K, Unlu C (2006) Effect of sperm chromatin damage on fertilization ratio and embryo quality post-ICSI. Archives of Andrology 52:397–402.

Chan PJ, Jacobson JD, Corselli JU, Patton WC (2006) A simple zeta method for sperm selection based on membrane charge. Fertility and Sterility 85:481–486.

Chan PJ, Corselli JU, Patton WC, Jacobson JD, Chana SR, King A (2001) A simple comet assay for archived sperm correlates DNA fragmentation to reduced hyperactivation and penetration of zona-free hamster oocytes. Fertility and Sterility 75:186–192.

Check JH, Katsoff D, Check ML, Choe JK. Swenson K (2001) In vitro fertilization with intracytoplasmic sperm injection is an effective therapy for male factor infertility related to subnormal hypo-osmotic swelling test scores. Journal of Andrology 22:261–265.

Chen D-L, Li N, Lin L, Long H, Lin H, Chen J, Zhang H, Zeng C, Liu S (2014) Confocal mirco-Raman spectroscopic analysis of the antioxidant protection mechanism of the oligosaccharides extracted from Morinda officinalis on human sperm DNA. Journal of Ethnopharmacology 153:119–124.

Cho C, Jung-Ha H, Willis WD, Goulding EH, Stein P, Xu Z, Schultz RM, Hecht NB, Eddy EM (2003). Protamine 2 deficiency leads to sperm DNA damage and embryo death in mice. Biology of reproduction 69:211–217.

Cho C, Willis WD, Goulding EH, Jung-Ha H, Choi YC, Hecht NB, Eddy EM (2001) Haploinsufficiency of protamine-1 or -2 causes infertility in mice. Nature Genetics 28:82–86.

Conwell CC, Vilfan ID, Hud NV (2003) Controlling the size of nanoscale toroidal DNA condensates with static curvature and ionic strength. Proceedings of the National Academy of Sciences 100:9296–9301.

Cooper TG, Neuwinger J, Bahrs S, Nieschlag E (1992) Internal quality control of semen analysis. Fertility and Sterility 58:172–178.

D’Occhio M, Hengstberger K, Johnston S (2007) Biology of sperm chromatin structure and relationship to male fertility and embryonic survival. Animal Reproduction Science 101:1–17.

Dadoune JP (2003) Expression of mammalian spermatozoal nucleoproteins. Microscopy Research and Technique 61:56–75.

D'Auria G, Paolillo L, Sartorio R, Wurzburger S (1993) Structure and function of protamines: an 1H nuclear magnetic resonance investigation of the interaction of clupeines with mononucleotides. Biochimica et Biophysica Acta (BBA) - Protein Structure and Molecular Enzymology 1162:209–216.

Day JP, Domke KF, Rago G, Kano H, Hamaguchi HO, Vartiainen EM, Bonn M (2011) Quantitative coherent anti-Stokes Raman scattering (CARS) microscopy. The Journal of Physical Chemistry B 115:7713–7725.

De Iuliis GN, Thomson LK, Mitchell LA, Finnie JM, Koppers AJ, Hedges A, Nixon B, Aitken RJ (2009) DNA damage in human spermatozoa is highly correlated with the efficiency of chromatin remodeling and the formation of 8-hydroxy-2′-deoxyguanosine, a marker of oxidative stress. Biology of reproduction 81:517–524.

De Jong BW, Schut TC, Maquelin K, Kwast TV, Bangma CH, Kok D, Puppels GJ (2006) Discrimination between nontumor bladder tissue and tumor by Raman spectroscopy. Analytical Chemistry 78:7761–7769.

De Jong BW, De Gouveia Brazao CA, Stoop H, Wolffenbuttel KP, Oosterhuis JW, Puppels GJ, Weber RF, Looijenga LH, Kok DJ (2004) Raman spectroscopic analysis identifies testicular microlithiasis as intratubular hydroxyapatite. The Journal of Urology 171:92–96.

De Kretser DM (1997) Male infertility. Lancet 34:787–790.

De Luca AC, Managó S, Ferrara MA, Rendina I, Sirleto L, Puglisi R, Balduzzi D, Galli A, Ferraro P, Coppola G (2014) Non-invasive sex assessment in bovine semen by Raman spectroscopy. Laser Physics Letters 11:055604.

De Mul FFM, Welie AGMV, Otto C, Mud J, Greve J (1984) Micro-Raman spectroscopy of chromosomes. Journal of Raman Spectroscopy 15:268–272.

De Rooij DG, Russell LD (2000) All you wanted to know about spermatogonia but were afraid to ask. Journal of Andrology 21:776–798.

De Yebra L, Ballesca JL, Vanrell JA, Corzett M, Balhorn R, Oliva R (1998) Detection of P2 precursors in the sperm cells of infertile patients who have reduced protamine P2 levels. Fertility and Sterility 69:755–759.

De Yebra L, Ballesca JL, Vanrell JA, Bassas L, Oliva R (1993) Complete selective absence of protamine P2 in humans. Journal of Biological Chemistry 268:10553–10557.

Deng H, Bloomfield VA, Benevides JM, Thomas GJ (1999) Dependence of the Raman signature of genomic B-DNA on nucleotide base sequence. Biopolymers 50:656–666.

Draux F, Jeannesson P, Beljebbar A, Tfayli A, Fourre N, Manfait M, Sulé-Suso J, Sockalingum G (2009) Raman spectral imaging of single living cancer cells: a preliminary study. The Analyst 134:542–548.

Duran EH, Gurgan T, Gunalp S, Enginsu ME, Yarali H, Ayhan A (1998) A logistic regression model including DNA status and morphology of spermatozoa for prediction of fertilization in vitro. Human Reproduction 13:1235–1239.

Ellington JE, Evenson DP, Wright Jr RW, Jones AE, Schneider CS, Hiss GA, Brisbois RS (1999) Higher-quality human sperm in a sample selectively attach to oviduct (fallopian tube) epithelial cells in vitro. Fertility and Sterility 71:924–929.

Eppelmann U, Gottardo F, Wistuba J, Ehmcke J, Kossack N, Westernstroeer B, Redmann K, Wuebbeling F, Burger M, Tuettelmann F, Kliesch S, Mallidis C (2013) Raman microspectroscopic discrimination of TCam-2 cultures reveals the presence of two sub-populations of cells. Cell and Tissue Research 354:623–632.

Erenpreiss J, Spano M, Erenpreisa J, Bungum M, Giwercman A (2006) Sperm chromatin structure and male fertility: biological and clinical aspects. Asian Journal of Andrology 8:11–29.

Erenpreiss J, Jepson K, Giwercman A, Tsarev I, Erenpreisa J, Spano M (2004) Toluidine blue cytometry test for sperm DNA conformation: comparison with the flow cytometric sperm chromatin structure and TUNEL assays. Human Reproduction 19:2277–2282.

Esterhuizen AD, Franken DR, Becker PJ, Lourens JG, Muller II, Rooyen LH (2002) Defective sperm decondensation: a cause for fertilization failure. Andrologia 34:1–7.

Esterhuizen AD, Franken DR, Lourens JG, Prinsloo E, Van Rooyen LH (2000a) Sperm chromatin packaging as an indicator of in-vitro fertilization rates. Human Reproduction. 15: 657–661.

Esterhuizen AD, Franken DR, Lourens JG, Van Zyl C, Müller II, Van Rooyen LH (2000b) Chromatin packaging as an indicator of human sperm dysfunction. Journal of Assisted Reproduction and Genetics 17:508–514.

Esteves SC, Agarwal A (2011) Novel concepts in male infertility. International Brazilian Journal of Urology 37:5–15.

Evenson DP, Larson KL, Jost LK (2002) Sperm chromatin structure assay: its clinical use for detecting sperm DNA fragmentation in male infertility and comparisons with other techniques. Journal of Andrology 23:25–43.

Evenson DP (1999) Loss of livestock breeding efficiency due to uncompensable sperm nuclear defects. Reproduction, Fertility and Development 11:1–16.

Evgeni E, Charalabopoulos K, Asimakopoulos B (2014) Human sperm DNA fragmentation and its correlation with conventional semen parameters. Journal of Reproduction and Infertility. 15:2–14.

Ewing LL, Keeney DS (1993) Leydig cells: structure and function. In: Cell and molecular biology of the testis. Oxford University Press, New York, pp 137–165.

Ferrara M, Caprio GD, Managò S, Angelis AD, Sirleto L, Coppola G, De Luca AC (2015) Label-free imaging and biochemical characterization of bovine sperm cells. Biosensors 5:141–157.

Ferraro JR, Nakamoto K (2012) Introductory Raman spectroscopy. Elsevier Science, Burlington.

Fode M, Krogh-Jespersen S, Brackett NL, Ohl DA, Lynne CM, Sønksen J (2012) Male sexual dysfunction and infertility associated with neurological disorders. Asian Journal of Andrology 14:61–68.

Franken DR, Bastiaan HS (2009) Can a cumulus cell complex be used to select spermatozoa for assisted reproduction? Andrologia 41:369–376.

Franken DR, Oehninger S (2006) The clinical significance of sperm-zona pellucida binding: 17 years later. Frontiers in Bioscience 11:1227–1233.

Franken DR, Franken CJ, de la Guerre H, de Villiers A (1999) Normal sperm morphology and chromatin packaging: comparison between aniline blue and chromomycin A3 staining. Andrologia 31:361–366.

Fuentes-Mascorro G, Serrano H, Rosado A (2000) Sperm chromatin. Archives of Andrology 45:215–225.

Gao X, Mirau P, Patel DJ (1992) Structure refinement of the chromomycin dimer-DNA oligomer complex in solution. Journal of Molecular Biology 223:259–279.

Gao X, Patel DJ (1990) Chromomycin dimer-DNA oligomer complexes. Sequence selectivity and divalent cation specificity. Biochemistry 29:10940–10956.

García-Ferreyra J, Villegas L, Obst RR, Obst PZ, Hilario R, Casafranca G, Dueñas-Chacón J (2014) Sperm DNA fragmentation is significantly increased in those men with morphologically abnormal spermatozoa. journal of fertilization: In Vitro - IVF-Worldwide, Reproductive Medicine, Genetics and Stem Cell Biology 2:131.

Gatewood JM, Cook GR, Balhorn R, Bradbury EM, Schmid CW (1987) Sequence-specific packaging of DNA in human sperm chromatin. Science 236:962–964.

Gelder JD, Gussem KD, Vandenabeele P, Moens L (2007) Reference database of Raman spectra of biological molecules. Journal of Raman Spectroscopy 38:1133–1147.

Giwercman A, Richthoff J, Hjøllund H, Bonde JP, Jepson K, Frohm B (2003) Correlation between sperm motility and sperm chromatin structure assay parameters. Fertility and Sterility 80:1404–1412.

Golan R, Shochat L, Weissenberg R, Soffer Y, Marcus Z, Oschry Y and Lewin LM (1997) Evaluation of chromatin condensation in human spermatozoa: a flow cytometric assay using acridine orange staining. Molecular Human Reproduction 13:47–54.

Goldberg RB, Geremia R, Bruce WR (1977) Histone synthesis and replacement during spermatogenesis in the mouse. Differentation 7:167–180.

González-Marín C, Gosálvez J, Roy R (2012) Types, causes, detection and repair of DNA fragmentation in animal and human sperm cells. International Journal of Molecular Sciences 13:14026–14052.

Gorczyca W, Gong J, Darzynkiewics Z (1993) Detection of DNA strand breaks in individual apoptotic cells by the in situ terminal deoxynucleotidyl transferase and nick translation assays. Cancer Research 53:1945–1951.

Gregoriou VG, Braiman MS (2006) Vibrational spectroscopy of biological and polymeric materials. CRC Press/Taylor and Francis, Boca Raton, FL.

Griswold MD (1995) Interactions between germ cells and sertoli cells in the testis. Biology of Reproduction 52:211–216.

Guan Y, Thomas GJ (1996) Force field and conformation-dependent modes of the phosphodiester backbone modeled by diethyl phosphate. Biophysical Journal 71:3350–3360.

Gurunath S, Pandian Z, Anderson RA, Bhattacharya S (2011) Defining infertility-a systematic review of prevalence studies. Human Reproduction Update 17:575–588.

Guzick DS, Overstreet JW, Factor-Litvak P, Brazil C, Nakajima S, Coutifaris C, Carson S, Cisneros P, Steinkampf M, Hill J, Xu D, Vogel D (2001) Sperm morphology, motility, and concentration in fertile and infertile men. New England Journal of Medicine 345:1388–1393.

Haaf T, Ward DC (1995) Higher order nuclear structure in mammalian sperm revealed by in situ hybridization and extended chromatin fibers. Experimental Cell Research 219:604–611.

Hamada AJ, Esteves SC, Agarwal A (2013) A comprehensive review of genetics and genetic testing in azoospermia. Clinics 68:39–60.

Hammadeh ME, Zeginiadov T, Rosenbaum P, Georg T, Schmidt W, Strehler E (2001) Predictive value of sperm chromatin condensation (aniline blue staining) in the assessment of male fertility. Archives of Andrology 46:99–104.

Hammadeh ME, Stieber M, Haidl G, Schmidt W (1998) Association between sperm cell chromatin condensation, morphology based on strict criteria, and fertilization, cleavage and pregnancy rates in an IVF program. Andrologia 30:29–35.

Hammadeh ME, Al-Hasani S, Stieber M, Rosenbaum P, Küpker D, Diedrich K, Schmidt W (1996) Andrology: The effect of chromatin condensation (Aniline Blue staining) and morphology (strict criteria) of human spermatozoa on fertilization, cleavage and pregnancy rates in an intracytoplasmic sperm injection programme. Human Reproduction 11:2468–2471.

Hammoud S, Liu L, Carrell DT (2009) Protamine ratio and the level of histone retention in sperm selected from a density gradient preparation. Andrologia 41:88–94.

Harlev A, Agarwal A, Gunes SO, Shetty A, du Plessis SS (2015) Smoking and male infertility: an evidence-based review. The World Journal of Men's Health 33:143–160.

Hartman K, Clayton N, Thomas G (1973) Studies of virus structure by Raman spectroscopy I. R17 virus and R17 RNA. Biochemical and Biophysical Research Communications 50:942–949.

Haynes CL, McFarland AD, Duyne RPV (2005) Surface-enhanced Raman spectroscopy. Analytical Chemistry 77:338–346.

Hekmatdoost A, Lakpour N, Sadeghi MR (2009) Sperm chromatin integrity: etiologies and mechanisms of abnormality, assays, clinical importance, preventing and repairing damage. Avicenna Journal of Medical Biotechnology 1:147–160.

Henkel R, Hajimohammad M, Stalf T, Hoogendijk C, Mehnert C, Menkveld R, Gips H, Schill W, Kruger T (2004) Influence of deoxyribonucleic acid damage on fertilization and pregnancy. Fertility and Sterility 81:965–972.

Henkel R, Kierspel E, Hajimohammad M, Stalf T, Hoogendijk C, Mehnert C, Menkveld R, Schill WB, Kruger TF (2003) DNA fragmentation of spermatozoa and assisted reproduction technology. Reproductive BioMedicine Online 7:477–484.

Hodjat M, Akhondi MA, Al-Hasani S, Mobaraki M, Sadeghi MR (2008) Increased sperm ubiquitination correlates with abnormal chromatin integrity. Reproductive BioMedicine Online 17:324–330.

Hofmann N, Hilschler B (1991) Use of aniline blue to assess chromatin condensation in morphologically normal spermatozoa in normal and infertile men. Human Reproduction 6: 979–982.

Hong SJ, Chiu PC, Lee KF, Tse JM, Ho PC, Yeung WS (2004) Establishment of a capillary-cumulus model to study the selection of sperm for fertilization by the cumulus oophorus. Human Reproduction 19:1562–1569.

Host E, Lindenberg S and Smidt-Jensen S (2000) DNA strand breaks in human spermatozoa: correlation with fertilization in vitro in oligozoospermic men and in men with unexplained infertility. Acta Obstetricia Gynecologica Scandinavica 79:189–193.

Huang Z, Xiao H, Qi T, Hu Z, Li H, Chen D, Xu Y, Chen J (2014) Antioxidative protective effect of icariin on the FeSO4/H2O2-damaged human sperm based on confocal Raman micro-spectroscopy. Journal of Huazhong University of Science and Technology [Medical Sciences] 34:755–760.

Huang Z, Chen G, Chen X, Wang J, Chen J, Lu P, Chen R (2013) Rapid and label-free identification of normal spermatozoa based on image analysis and micro-Raman spectroscopy. Journal of Biophotonics 7:671–675.

Hud NV, Milanovich FP, Balhorn R (1994) Evidence of novel secondary structure in DNA-bound protamine is revealed by Raman spectroscopy. Biochemistry 33:7528–7535.

Hunter D, Anand-Ivell R, Danner S, Ivell R (2012) Models of in vitro spermatogenesis. Spermatogenesis 2:32–43.

Huser T, Orme CA, Hollars CW, Corzett M, Balhorn R (2009) Raman spectroscopy of DNA packaging in individual human sperm cells distinguishes normal from abnormal cells. Journal of Biophotonics 2:322–332.

Huszar G, Ozenci CC, Cayli S, Zavaczki Z, Hansch E, Vigue L (2003) Hyaluronic acid binding by human sperm indicates cellular maturity, viability, and unreacted acrosomal status. Fertility and Sterility 79:1616–1624.

Iranpour F (2014) Impact of sperm chromatin evaluation on fertilization rate in intracytoplasmic sperm injection. Advanced Biomedical Research 3:229.

Iranpour FG, Nasr-Esfahani MH, Valojerdi MR, Al-Taraihi TMT (2000) Chromomycin A3 staining as a useful tool for evaluation of male fertility. Journal of Assisted Reproduction and Genetics 17:60–66.

Ishijima SA, Okuno M, Mohri H (1991) Zeta potential of human X- and Y-bearing sperm. International Journal of Andrology 14:340–347.

Jensen TK, Bonde JP, Joffe M (2006) The influence of occupational exposure on male reproductive function. Occupational Medicine 56:544–553.

Jequier AM (2010) Semen analysis: a new manual and its application to the understanding of semen and its pathology. Asian Journal of Andrology 12:11–13.

Jeyendran RS, Van der Ven HH, Perez-Pelaez M, Crabo BG, Zaneveld LJD. (1984) Development of an assay to assess the functional integrity of the human sperm membrane and its relationship to other semen characteristics. Reproduction 70:219–228.

Jiaen L, Nagy, Joris H, Tournaye H, Smitz J, Camus M, Devroey P, Steirteghem AV. (1995) Analysis of 76 total fertilization failure cycles out of 2732 intracytoplasmic sperm injection cycles. Human Reproduction 10:2630–2636.

Jose-Miller AB, Boyden JW, Frey KA (2007) Infertility. American Family Physician 75:849–856.

Jung A, Schuppe HC (2006) Influence of genital heat stress on semen quality in humans. Andrologia 39:203–215.

Kahraman S, Akarsu C, Cengiz G, Dirican K, Sözen E, Can B, Güven C, Vanderzwalmen P (1999) Fertility of ejaculated and testicular megalohead spermatozoa with intracytoplasmic sperm injection. Human Reproduction 14:726–730.

Kao SH, Chao HT, Chen HW, Hwang TIS, Liao TL, Wei YH (2008) Increase of oxidative stress in human sperm with lower motility. Fertility and Sterility 89:1183–1190.

Karpuz V, Gokturk A, Koyuturk M (2007) The effects of sperm morphology and motility on the outcome of intracytoplasmic sperm injection. Marmara Medical Journal 20:92–97.

Karydis S, Asimakopoulos B, Papadopoulos N, Vakalopoulos I, Al-hasani SA, Nikolettos N (2005) ICSI outcome is not associated with the incidence of spermatozoa with abnormal chromatin condensation. In Vivo 19:921–925.

Katz A, Kruger EF, Minko G, Liu CH, Rosen RB, Alfano RR (2003) Detection of glutamate in the eye by Raman spectroscopy. Journal of Biomedical Optics 8:167–173.

Kazerooni T, Asadi N, Jadid L, Kazerooni M, Ghanadi A, Ghaffarpas F, Kazerooni Y, Zolghadr J (2009) Evaluation of sperm's chromatin quality with acridine orange test, chromomycin A3 and aniline blue staining in couples with unexplained recurrent abortion. Journal of Assisted Reproduction and Genetics 26:591–596.

Ke W, Yu D, Wu J (1999) Raman spectroscopic study of the influence on herring sperm DNA of heat treatment and ultraviolet radiation. Spectrochimica Acta Part A: Molecular and Biomolecular Spectroscopy 55:1081–1090.

Keller MD, Kanter EM, Lieber CA, Majumder SK, Hutchings J, Ellis DL, Beaven RB, Stone N, Mahadevan A (2008) Detecting temporal and spatial effects of epithelial cancers with Raman spectroscopy. Disease Markers 25:323–337.

Khalili MA, Aghaie-Maybodi F, Anvari M, Talebi AR (2009) Sperm nuclear DNA in ejaculates of fertile and infertile men: correlation with semen parameters. Urology journal 3:154–159.

Kheirollahi-Kouhestani M, Razavi S, Tavalaee M, Deemeh MR, Mardani M, Moshtaghian J, Nasr-Esfahani MH (2009) Selection of sperm based on combined density gradient and Zeta method may improve ICSI outcome. Human Reproduction 24:2409–2416.

Kierszenbaum AL (2001) Transition nuclear proteins during spermiogenesis: Unrepaired DNA breaks not allowed. Molecular Reproduction and Development 58:357–358.

Kim H-S, Kang MJ, Kim SA, Oh SK, Kim H, Ku S, Kim SH, Moon SY, Choi YM (2013) The utility of sperm DNA damage assay using toluidine blue and aniline blue staining in routine semen analysis. Clinical and Experimental Reproductive Medicine 40:23–28.

Kirchhoff C, Hale G (1996) Cell-to-cell transfer of glycosylphosphatidylinositol-anchored membrane proteins during sperm maturation. Molecular Human Reproduction 2:177–184.

Kistler W, Henriksén K, Mali P, Parvinen M (1996) Sequential expression of nucleoproteins during rat spermiogenesis. Experimental Cell Research 225:374–381.

Koljenović S, Choo-Smith L-P, Schut T, Kros J, Berge H, Puppels G (2002) Discriminating vital tumor from necrotic tissue in human glioblastoma tissue samples by Raman spectroscopy. Laboratory Investigation 82:1265–1277.

Kordus RJ, Price RL, Davis JM, Whitman-Elia GF (2008) Successful twin birth following blastocyst culture of embryos derived from the immotile ejaculated spermatozoa from a patient with primary ciliary dyskinesia: A case report. Journal of Assisted Reproduction and Genetics 25:437–443.

Krafft C, Sergo V (2006) Biomedical applications of Raman and infrared spectroscopy to diagnose tissues. Spectroscopy 20:195–218.

Kruger TF, Menkveld R, Stander FSH, Lombard CJ, Merwe JP, Zyl JA, Smith K (1986) Sperm morphologic features a prognostic factor in in vitro fertilization. Fertility and Sterility 46:1118–1123.

Kubasek WL, Wang Y, Thomas GA, Patapoff TW, Schoenwaelder KH, Van der Sande JH, Peticolas WL (1986) Raman spectra of the model B-DNA oligomer d(CGCGAATTCGCG)2 and of the DNA in living salmon sperm show that both have very similar B-type conformations. Biochemistry 25:7440–7445.

Kumar R (2013) Medical management of non-obstructive azoospermia. Clinics 68:75–79.

Kumaroo KK, Jahnke G, Irvin JL (1975) Changes in basic chromosomal proteins during spermatogenesis in the mature rat. Archives of Biochemistry and Biophysics. 168:413–424.

Lang T, Dechant M, Sanchez V, Wistuba J, Boiani M, Pilatz A, Stammler A, Middendorff R, Schuler G, Bhushan S, Tchatalbachev S, Wubbeling F, Burger M, Chakraborty T, Mallidis C, Meinhardt A (2013) Structural and functional integrity of spermatozoa is compromised as a consequence of acute uropathogenic E. coli-associated epididymitis. Biology of Reproduction 89:1–10.

Larson KL, Brannian JD, Hansen KA, Kasperson KM, Aamold ET, Evenson DP (2003) Relationship between the outcomes of assisted reproductive techniques and sperm DNA fragmentation as measured by the sperm chromatin structure assay. Fertility and Sterility 80:895–902.

Larson KL, De Jonge CJ, Barnes AM, Jost LK, Evenson DP (2000) Sperm chromatin structure assay parameters as predictors of failed pregnancy following assisted reproductive techniques. Human Reproduction 15:1717–1722.

Lewis SE, Aitken RJ (2005) DNA damage to spermatozoa has impacts on fertilization and pregnancy. Cell and Tissue Research. 322:33–41.

Li N, Chen D, Xu Y, Liu S, Zhang H (2014) Confocal Raman micro-spectroscopy for rapid and label-free detection of maleic acid-induced variations in human sperm. Biomedical Optics Express 5:1690–1699.

Li Y, Lalancette C, Miller D, Krawetz SA (2008) Characterization of nucleohistone and nucleoprotamine components in the mature human sperm nucleus. Asian Journal of Andrology 10:535–541.

Li Z, Wang L, Cai J, Huang H (2006) Correlation of sperm DNA damage with IVF and ICSI outcomes: A systematic review and meta-analysis. Journal of Assisted Reproduction and Genetics 23:367–376.

Lin MH, Kuo-Kuang Lee R, Li SH, Lu CH, Sun FJ, Hwu YM (2008) Sperm chromatin structure assay parameters are not related to fertilization rates, embryo quality, and pregnancy rates in in vitro fertilization and intracytoplasmic sperm injection, but might be related to spontaneous abortion rates. Fertility and Sterility 90:352–359.

Liu DY, Garrett C, Baker HW (2003) Low proportions of sperm can bind to the zona pellucida of human oocytes. Human Reproduction 18:2382–2389.

Liu F, Zhu Y, Liu Y, Wang X, Ping P, Zhu X, Hu H, Li Z, He L (2013) Real-time Raman microspectroscopy scanning of the single live sperm bound to human zona pellucida. Fertility and Sterility 99:684–689.

Liu F, Qiu Y, Zou Y, Deng ZH, Yang H, Liu de Y (2011) Use of zona pellucida-bound sperm for intracytoplasmic sperm injection produces higher embryo quality and implantation than conventional intracytoplasmic sperm injection. Fertility and Sterility 95:815–818.

Liu Y, Zhu Y, Li Z (2014) Application of Raman spectroscopy in andrology: non-invasive analysis of tissue and single cell. Translational Andrology and Urology 3:125–133.

Lolis D, Georgiou I, Syrrou M, Zikopoulos K, Konstantelli M, Messinis I (1996) Chromomycin A3-staining as an indicator of protamine deficiency and fertilization. International Journal of Andrology 19:23–27.

Long DA (2001) The Raman effect. Wiley, New York.

Lotti F, Corona G, Rastrelli G, Jannini E, Maggi M (2012) Clinical correlates of erectile dysfunction and premature ejaculation in men with couple infertility. The Journal of Sexual Medicine 9:2698–2707.

Loutradi KE, Tarlatzis BC, Goulis DG, Zepiridis L, Pagou T, Chatziioannou E, Grimbizis GF, Papadimas I, Bontis I (2006) The effects of sperm quality on embryo development after intracytoplasmic sperm injection. Journal of Assisted Reproduction and Genetics 23:69–74.

Love CC, Kenney RM (1999) Scrotal heat stress induces altered sperm chromatin structure associated with a decrease in protamine disulfide bonding in the stallion. Biology of Reproduction 60:615–620.

Ma M, Yang S, Zhang Z, Li P, Gong Y, Liu L, Zhu Y, Tian R, Liu Y, Wang X, Liu F (2013) Sertoli cells from non-obstructive azoospermia and obstructive azoospermia patients show distinct morphology, Raman spectrum and biochemical phenotype. Human Reproduction 28:1863–1873.

Ma Y, Yang H-Z, Xu L-M, Huang, YR, Dai HL, Kang XN (2015) Testosterone regulates the autophagic clearance of androgen binding protein in rat Sertoli cells. Scientific Reports 5:8894.

Machev N, Gosset P, Viville S (2005) Chromosome abnormalities in sperm from infertile men with normal somatic karyotypes: teratozoospermia. Cytogenetic and Genome Research 111:352–357.

Mallidis C, Sanchez V, Wistuba J, Wuebbeling F, Burger M, Fallnich C, Schlatt S (2013) Raman microspectroscopy: shining a new light on reproductive medicine. Human Reproduction Update 20:403–414.

Mallidis C, Wistuba J, Bleisteiner B, Damm O, Gross P, Wubbeling F, Fallnich C, Burger M, Schlatt S (2011) In situ visualization of damaged DNA in human sperm by Raman microspectroscopy. Human Reproduction 26:1641–1649.

Manicardi GC, Bianchi PG, Pantano S, Azzoni P, Bizzaro D, Bianchi U, Sakkas D (1995) Presence of endogenous nicks in DNA of ejaculated human spermatozoa and its relationship to chromomycin A3 accessibility. Biology of Reproduction 52:864–867.

Manochantr S, Chiamchanya C, Sobhon P (2011) Relationship between chromatin condensation, DNA integrity and quality of ejaculated spermatozoa from infertile men. Andrologia 44:187–199.

Mansy S, Engstrom S, Peticolas W (1976) Laser Raman identification of an interaction site on DNA for arginine containing histones in chromatin. Biochemical and Biophysical Research Communications 68:1242–1247.

Marcon L, Boissonneault G (2004) Transient DNA strand breaks during mouse and human spermiogenesis: new insights in stage specificity and link to chromatin remodeling. Biology of Reproduction 70:910–918.

Marquardt DW (1963) An algorithm for least-squares estimation of nonlinear parameters. Journal of the society for Industrial and Applied Mathematics 11:431–41.

Martin S, Reutelingsperger, CP, McGahon AJ, Rader JA, Van Schie RC, LaFace DM, Green DR (1995) Early redistribution of plasma membrane phosphatidylserine is a general feature of apoptosis regardless of the initiating stimulus: inhibition by overexpression of Bcl-2 and Abl. Journal of Experimental Medicine 182:1545–1556.

Martinez C, Marc C, Azcarate M, Pascual P, Aritzeda JMA (2000) Sperm motility index: a quick screening parameter from sperm quality analyser-IIB to rule out oligo- and astenozoospermia in male fertility study. Human Reproduction 15:1727–1733.

Mcpherson SM, Longo FJ (1993) Nicking of rat spermatid and spermatozoa DNA: possible involvement of DNA topoisomerase II. Developmental Biology 158:122–130.

Meister K, Schmidt DA, Bründermann E, Havenith M (2010) Confocal Raman microspectroscopy as an analytical tool to assess the mitochondrial status in human spermatozoa. Analyst 135:1370–1374.

Moosani N, Pattinson HA, Carter MD, Cox DM, Rademaker AW, Martin RH (1995) Chromosomal analysis of sperm from men with idiopathic infertility using sperm karyotyping and fluorescence in situ hybridization. Fertility and Sterility 64:811–817.

Morris I, Ilott S, Dixon L, Brison DR (2002) The spectrum of DNA damage in human sperm assessed by single cell gel electrophoresis (Comet assay) and its relationship to fertilization and embryo development. Human Reproduction 17:990–998.

Mozdarani H, Aghdaei F (2001) Cytogenetic analysis of failed fertilized oocytes from Iranian infertile women after in vitro fertilization (IVF) and intracytoplasmic sperm injection (ICSI) procedures. Middle East Fertility Society Journal 6:216–225.

Nadalini M, Tarozzi N, Distratis V, Scaravelli G, Borini A (2009) Impact of intracytoplasmic morphologically selected sperm injection on assisted reproduction outcome: a review. Reproductive BioMedicine Online 19:45–55.

Nardelli AA, Stafinski T, Motan T, Klein K, Menon D (2014) Assisted reproductive technologies (ARTs): Evaluation of evidence to support public policy development. Reproductive Health. 11:76.

Nasr-Esfahani MH, Deemeh MR, Tavalaee M (2011) New era in sperm selection for ICSI. International Journal of Andrology 35:475–484.

Nasr-Esfahani MH, Razavi S, Travalaee M (2008) Failed fertilization after ICSI and spermiogenic defects. Fertility and Sterility 89:892–898.

Nasr-Esfahani MH, Razavi S, Mardani M, Shirazi R, Javanmardi S (2007) Effects of failed oocyte activation and sperm protamine deficiency on fertilization post-ICSI. Reproductive BioMedicine Online 14:422–429.

Nasr-Esfahani MH, Salehi M, Razavi S, Anjomshoa M, Rozbahani S, Moulavi F, Mardani M (2005) Effect of sperm DNA damage and sperm protamine deficiency on fertilization and embryo development post-ICSI. Reproductive BioMedicine Online 11:198–205.

Nasr-Esfahani MH, Razavi S, Mozdarani H, Mardani M, Azvagi H (2004) Relationship between protamine deficiency with fertilization rate and incidence of sperm premature chromosomal condensation post-ICSI. Andrologia 36:95–100.

Nasr-Esfahani MH, Razavi S, Mardani M (2001) Relation between different human sperm nuclear maturity tests and in vitro fertilization. Journal of Assisted Reproduction and Genetics 18:221–227.

Naz M, Kamal M (2017) Classification, causes, diagnosis and treatment of male infertility: a review. Oriental Pharmacy and Experimental Medicine 17:89–109.

Nazarenko R, Irzhak A, Pomerantsev A, Rodionova OY (2018) Confocal Raman spectroscopy and multivariate data analysis for evaluation of spermatozoa with normal and abnormal morphology. A feasibility study. Chemometrics and Intelligent Laboratory Systems 182:172–179.

Neuwinger J, Behre HM, Nieschlag E (1990) External quality control in the andrology laboratory: an experimental multicenter trial. Fertility and Sterility 54:308–314.

Nicopoullos J, Gilling-Smith C, Almeida P, Homa S, Nice L, Tempest H, Ramsay JW (2008) The role of sperm aneuploidy as a predictor of the success of intracytoplasmic sperm injection? Human Reproduction 23:240–250.

Nijs M, Creemers E, Cox A, Franssen K, Janssen M, Vanheusden E, De Jonge C, Ombelet W (2009) Chromomycin A3 staining, sperm chromatin structure assay and hyaluronic acid binding assay as predictors for assisted reproductive outcome. Reproductive BioMedicine Online 19:671–684.

Nikolettos N, Kupker W, Demirel C, Schöpper B, Blasig C, Sturm R, Felberbaum R, Bauer O, Diedrich K, Al-Hasani S (1999) Fertilization potential of spermatozoa with abnormal morphology. Human Reproduction 14:47–70.

Nili HA, Mozdarani H, Aleyasin A (2009) Correlation of sperm DNA damage with protamine deficiency in Iranian subfertile men. Reproductive BioMedicine Online 18:479–485.

Okotrub KA, Surovtsev NV, Semeshin VF, Omelyanchuk LV (2014) Raman spectroscopy for DNA quantification in cell nucleus. Cytometry Part A 87:68–73.

Oliva R (2006) Protamines and male infertility. Human Reproduction Update 12:417–435.

Oliva R, Dixon GH (1991) Vertebrate protamine genes and the histone-to-protamine replacement reaction. Progress in Nucleic Acid Research and Molecular Biology 40:25–94.

Oshima Y, Shinzawa H, Takenaka T, Furihata C, Sato H (2010) Discrimination analysis of human lung cancer cells associated with histological type and malignancy using Raman spectroscopy. Journal of biomedical optics 15:017009.

Ozmen B, Koutlaki N, Youssry M, Diedrich K, Al-Hasani S (2007) DNA damage of human spermatozoa in assisted reproduction: origins, diagnosis, impacts and safety. Reproductive BioMedicine Online 14:384–395.

Painter PC, Koenig JL (1975) Raman spectroscopic study of the structure of antibodies. Biopolymers 14:457–468.

Palermo G, Joris H, Devroey P, Van Steirteghem AC (1992) Pregnancies after intracytoplasmic injection of single spermatozoon into an oocyte. The Lancet 340:17–18.

Pappas D, Benjamin W. Smith, James D. Winefordner (2000) Raman spectroscopy in bioanalysis. Talanta 51:131–144.

Parmegiani L, Cognigni GE, Bernardi S, Troilo E, Ciampaglia W, Filicori M (2010) "Physiologic ICSI": Hyaluronic acid (HA) favors selection of spermatozoa without DNA fragmentation and with normal nucleus, resulting in improvement of embryo quality. Fertility and Sterility 93:598–604.

Patil P, Humbarwadi R, Gune A, Patil A (2013) Immature germ cells in semen - correlation with total sperm count and sperm motility. Journal of Cytology 30:185–189.

Payne AH, Downing JR, Wong KL (1980) Luteinizing hormone receptors and testosterone synthesis in two distinct populations of Leydig cells. Endocrinology 106:1424–1429.

Peticolas WL, Patapoff TW, Thomas GA, Postlewait J, Powell JW (1996) Laser Raman microscopy of chromosomes in living eukaryotic cells: DNA polymorphism in vivo. Journal of Raman Spectroscopy 27:571–578.

Pizent A, Tariba B, Živković T (2012) Reproductive toxicity of metals in men. Archives of Industrial Hygiene and Toxicology 63:35–46.

Poccia DL, Simpson MV, Green GR (1987) Transitions in histone variants during sea urchin spermatogenesis. Developmental Biology 121:445–453.

Poccia DL (1986) Remodelling of nucleoproteins during gametogenesis fertilization and early development. International Reviews in Cytology 105:1–65.

Pogany GC, Corzett M, Weston S, Balhorn R (1981) DNA and protein content of mouse sperm. Implications regarding sperm chromatin structure. Experimental Cell Research 136:127–136.

Pousette Å, Åkerlöf E, Rosenborg L, Fredricsson B (1986) Increase in progressive motility and improved morphology of human spermatozoa following their migration through Percoll gradients. International Journal of Andrology 9:1–13.

Prigent Y, Muller S, Dadoune J (1996) lmmunoelectron microscopical distribution of histones H2B and H3 and protamines during human spermiogenesis. Molecular Human Reproduction 2:929–935.

Quintanilla-Vega B, Hoover D, Bal W, Silbergeld EK, Waalkes MP, Anderson LD (2000) Lead effects on protamine-DNA binding. American Journal of Industrial Medicine 38:324–329.

Rahman MS, Lee JS, Kwon WS, Pang MG (2013) Sperm proteomics: road to male fertility and contraception. International Journal of Endocrinology 2013:1–11.

Rajender S, Avery K, Agarwal A (2011) Epigenetics, spermatogenesis and male infertility. Mutation Research/Reviews in Mutation Research 727:62–71.

Raman CV, Krishnan KS (1928) A New type of secondary radiation. Nature 121:501–502.

Razavi SH, Nasr-Esfahani MH, Deemeh MR, Shayesteh M, Tavalaee M (2010) Evaluation of zeta and HA-binding methods for selection of spermatozoa with normal morphology, protamine content and DNA integrity. Andrologia 42:13–19.

Razavi SH, Nasr-Esfahani MH, Mardani M, Mafi A, Moghdam A (2003) Effect of human sperm chromatin anomalies on fertilization outcome post-ICSI. Andrologia 35:238–243.

Rijsdijk M, Franken DR (2007) Use of the capillary-cumulus oophorus model for evaluating the selection of spermatozoa. Fertility and Sterility 88:1595–1602.

Ron-El R, Nachum H, Herman A, Golan A, Caspi E, Soffer Y (1991) Delayed fertilization and poor embryonic development associated with impaired semen quality. Fertility and Sterility 55:338–344.

Rubio C, Gil-Salom M, Simon C, Vidal F, Rodrigo L, Minguez Y, Remohi J, Pellicer A (2001) Incidence of sperm chromosomal abnormalities in a risk population: relationship with sperm quality and ICSI outcome. Human Reproduction 16:2084–2092.

Sadeghi MR, Hodjat M, Lakpour N, Arefi S, Amirjannati N, Modarresi T, Jadda HH, Akhondi MM (2009) Effects of sperm chromatin integrity on fertilization rate and embryo quality following intracytoplasmic sperm injection. Avicenna Journal of Medical Biotechnology 1:173–180.

Said T, Agarwal A, Grunewald S, Rasch M, Glander HJ, Paasch U (2006a) Evaluation of sperm recovery following annexin V magnetic-activated cell sorting separation. Reproductive BioMedicine Online 13:336–339.

Said T, Agarwal A, Grunewald S, Rasch M, Baumann T, Kriegel C, Li L, Glander HJ, Thomas AJ Jr, Paasch U (2006b) Selection of non apoptotic spermatozoa as a new tool for enhancing assisted reproduction outcomes: an in vitro model. Biology of Reproduction 74:530–537.

Sakkas D, Moffatt O, Manicardi GC, Mariethoz E, Tarozzi N, Bizzaro D (2002) Nature of DNA damage in ejaculated human spermatozoa and the possible involvement of apoptosis. Biology of Reproduction 66:1061–1067.

Sakkas D, Manicardi GC, Tomlinson M, Manicardi M, Bizzaro D, Bianchi PG and Bianchi U (2000) The use of two density gradient centrifugation techniques and the swim-up method to separate spermatozoa with chromatin and nuclear DNA anomalies. Human Reproduction 15: 1112–1116.

Sakkas D, Mariethoz E, Manicardi G, Bizzaro D, Bianchi PG, Bianchi U (1999) Origin of DNA damage in ejaculated human spermatozoa. Reviews of Reproduction 4:31–37.

Sakkas D, Urner F, Bizzaro D, Manicardi G, Bianchi PG, Shoukir Y, Campana A (1998) Sperm nuclear DNA damage and altered chromatin structure: effect on fertilization and embryo development. Human Reproduction 13:11–19.

Sakkas D, Urner F, Bianchi P, Bizzaro D, Wagne I, Jaquenoud N, Manicardi G, Campana A (1996) Sperm chromatin anomalies can influence decondensation after intracytoplasmic sperm injection. Human Reproduction 11:837–843.

Sanchez V, Redmann K, Wistuba J, Wubbeling F, Burger M, Oldenhof H, Wolkers WF, Kliesch S, Schlatt S, Mallidis C (2012) Oxidative DNA damage in human sperm can be detected by Raman microspectroscopy. Fertility and Sterility 98:1124–1129.

Saxena P, Misro MM, Chaki SP, Chopra K, Roy S, Nandan D (2008) Is abnormal sperm function an indicator among couples with recurrent pregnancy loss? Fertility and Sterility 90:1854–1858.

Schlicker M, Schnulle V, Schneppel L, Vorob'ev VI, Engel W (1994) Disturbances of nuclear condensation in human spermatozoa: search for mutations in the genes for protamine 1, protamine 2 and transition protein 1. Human Reproduction 9:2313–2317.

Schmiady H, Tandler-Schneider A, Kentenich H (1996) Premature chromosome condensation of the sperm nucleus after intracytoplasmic sperm injection. Human Reproduction 11:2239–2245.

Scott L, Alvero R, Leondires M, Miller B (2000) The morphology of human pronuclear embryos is positively related to blastocyst development and implantation. Human Reproduction 15:2394–2403.

Seli E, Sakkas D (2005) Spermatozoal nuclear determinants of reproductive outcome: implications for ART. Human Reproduction Update 11:337–349.

Settle FA (1997) Handbook of instrumental techniques for analytical chemistry. Prentice Hall, Upper Saddle River, NJ.

Sharma KR (2007) Physiology of male gametogenesis. In: Clinical reproductive medicine and surgery: a practical guide. Springer, Cham, pp 73–83.

Shoukir Y, Chardonnens D, Campana A, Sakkas D (1998) Blastocyst development from supernumerary embryos after intracytoplasmic sperm injection: a paternal influence? Human Reproduction 13:1632–1637.

Sills ES, Fryman JT, Perloe M, Michels KB, Tucker M (2004) Chromatin fluorescence characteristics and standard semen analysis parameters: correlations observed in andrology testing among 136 males referred for infertility evaluation. Journal of Obstetrics and Gynaecology 24:74–77.

Simon L, Castillo J, Oliva R, Lewis SE (2011) Relationships between human sperm protamines, DNA damage and assisted reproduction outcomes. Reproductive BioMedicine Online 23:724–734.

Singh K, Jaiswal D (2011) Human male infertility: a complex multifactorial phenotype. Reproductive Sciences 18:418–425.

Sivanarayana T, Krishna CR, Prakash GJ, Krishna KM, Madan K, Rani BS, Sudhakar G, Raju GA (2012) CASA derived human sperm abnormalities: correlation with chromatin packing and DNA fragmentation. Journal of Assisted Reproduction and Genetics 29:1327–1334.

Smit M, Romijn JC, Wildhagen MF, Weber RFA, Dohle GR (2010) Sperm chromatin structure is associated with the quality of spermatogenesis in infertile patients. Fertility and Sterility 94: 1748–1752.

Smith GD, Clark RJ (2004) Raman microscopy in archaeological science. Journal of Archaeological Science 31:1137–1160.

Spiro TG and Strekas TC (1972) Resonance Raman spectra of hemoglobin and cytochrome c: inverse polarization and vibronic scattering. Proceedings of the National Academy of Sciences 69:2622–2626.

Stanger JD, Vo L, Yovich JL, Almahbobi G (2010) Hypo-osmotic swelling test identifies individual spermatozoa with minimal DNA fragmentation. Reproductive BioMedicine Online 21:474–484.

Steger K (1999) Transcriptional and translational regulation of gene expression in haploid spermatids. Anatomy and Embryology 199:471–487.

Stone N, Matousek P (2008) Advanced transmission Raman spectroscopy: a promising tool for breast disease diagnosis. Cancer Research 68:4424–4430.

Strekas TC and Spiro TG (1972) Hemoglobin: resonance Raman spectra. Biochimica et Biophysica Acta (BBA)-Protein Structure 263:830–833.

Suzuki M, Crozatier C, Yoshikawa K, Toshiaki M, Yoshikawa Y (2009) Protamine-induced DNA compaction but not aggregation shows effective radioprotection against double-strand breaks. Chemical Physics Letters 480:113–117.

Szymanski HA (1967) Raman spectroscopy: theory and practice. Plenum Pr., New York.

Talari ACS, Movasaghi Z, Rehman S, Rehman IU (2014) Raman spectroscopy of biological tissues. Applied Spectroscopy Reviews 50:46–111.

Tarlatzis BC, Bili H (1998) Survey on intracytoplasmic sperm injection: report from the ESHRE ICSI Task Force. Human Reproduction 13:165–177.

Tarozzi N, Nadalini M, Stronati A, Bizzaro D, Prato LD, Coticchio G, Borini A (2009) Anomalies in sperm chromatin packaging: implications for assisted reproduction techniques. Reproductive BioMedicine Online 18:486–495.

Tarozzi N, Bizzaro D, Flamigni C, Borini A (2007) Clinical relevance of sperm DNA damage in assisted reproduction. Reproductive BioMedicine Online 14:746–757.

Tavalaee M, Razavi S, Nasr-Esfahani MH (2009) Influence of sperm chromatin anomalies on assisted reproductive technology outcome. Fertility and Sterility 91:1119–1126.

Teh SK, Zheng W, Ho KY, Teh M, Yeoh K G, Huang Z (2008) Diagnostic potential of near-infrared Raman spectroscopy in the stomach: differentiating dysplasia from normal tissue. British Journal of Cancer 98:457–465.

Tejada MI, Mendoza MR, Corcostegui B, Benito JA (1992) Factors associated with premature chromosome condensation (PCC) following in vitro fertilization. Journal of Assisted Reproduction Genetics 9:61–67.

Tejada RI, Mitchell JC, Norman A, Marik JJ, Friedman S (1984) A test for the practical evaluation of male fertility by acridine orange (AO) fluorescence. Fertility and Sterility 42:87–91.

Tesarik J, Greco E, Mendoza C (2004) Late, but not early, paternal effect on human embryo development is related to sperm DNA fragmentation. Human Reproduction 19:611–615.

Thomas GJ (1999) Raman spectroscopy of protein and nucleic acid assemblies. Annual Review of Biophysics and Biomolecular Structure 28:1–27.

Torregrosa N, Domínguez-Fandos D, Camejo MI, Shirley CR, Meistrich ML, Ballescà JL, Oliva R (2006) Protamine 2 precursors, protamine 1/protamine 2 ratio, DNA integrity and other sperm parameters in infertile patients. Human Reproduction 21:2084–2089.

Tseden K, Topaloglu Ö, Meinhardt A, Dev A, Adham I, Müller C, Wolf S, Böhm T, Schlüter G, Engel W, Nayernia K (2007) Premature translation of transition protein 2 mRNA causes sperm abnormalities and male infertility. Molecular Reproduction and Development 74:273–279.

Vargis E, Kanter EM, Majumder SK, Keller MD, Beaven RB, Rao GG, Mahadevan-Jansen A (2011) Effect of normal variations on disease classification of Raman spectra from cervical tissue. Analyst 136:2981–2987.

Vasan S (2011) Semen analysis and sperm function tests: How much to test? Indian Journal of Urology 27:41–48.

Vašková H (2011) A powerful tool for material identification: Raman spectroscopy. International journal of mathematical models and methods in applied sciences 5:1205–1212.

Velez de la Calle JF, Muller A, Walschaerts M, Clavere JL, Jimenez C, Wittemer C, Thonneau P (2008) Sperm deoxyribonucleic acid fragmentation as assessed by the sperm chromatin dispersion test in assisted reproductive technology programs: results of a large prospective multicenter study. Fertility and Sterility 90:1792–1799.

Ward WS (2011) Regulating DNA supercoiling: sperm points the way. Biology of Reproduction 84:841–843.

Ward WS (1993) Deoxyribonucleic acid loop domain tertiary structure in mammalian spermatozoa. Biology of Reproduction 48:1193–1201.

Ward WS, Coffey DS (1991) DNA packaging and organization in mammalian spermatozoa: comparison with somatic cell. Biology of Reproduction 44:569–574.

Wartewig S, Neubert RH (2005) Pharmaceutical applications of Mid-IR and Raman spectroscopy. Advanced Drug Delivery Reviews 57:1144–1170.

Wistuba J, Stukenberg JB, Luetjens CM. (2007) Mammalian spermatogenesis. Functional development and embryology. Functional and Development Embryology 1:99–117.

World Health Organization (2010) WHO Laboratory Manual for the Examination and Processing of Human Semen. 5th ed. World Health Organization Press, Geneva.

Wosnitzer M, Goldstein M, Hardy MP (2014) Review of azoospermia. Spermatogenesis 4:28218.

Wykes SM, Krawetz SA (2003) The structural organization of sperm chromatin. Journal of Biological Chemistry 278:29471–29477.

Xu Z, He Z, Song Y, Fu X, Rommel M, Luo X, Hartmaier A, Zhang J, Fang F (2018) Topic review: application of Raman spectroscopy characterization in micro/nano-machining. Micromachines 9:361.

Yeo B S, Stadler J, Schmid T, Zenobi R, Zhang W (2009) Tip-enhanced Raman spectroscopy–Its status, challenges and future directions. Chemical Physics Letters 472:1–13.

Yiming X, Zhixiang Z, Hongying Y, Yan X, Zhiyi Z (1999) Raman spectroscopic study of microcosmic photodamage of the space structure of DNA sensitized by Yangzhou haematoporphyrin derivative and Photofrin II. Journal of Photochemistry and Photobiology B: Biology 52:30–34.

Yu C, Gestl E, Eckert K, Allara D, Irudayaraj J (2006) Characterization of human breast epithelial cells by confocal Raman microspectroscopy. Cancer Detection and Prevention 30:515–522.

Zegers-Hochschild F, Adamson GD, De MJ, Ishihara O, Mansour R, Nygren K, Sullivan E, Poel SV (2009) International committee for monitoring assisted reproductive technology (ICMART) and the world health organization (WHO) revised glossary of ART terminology. Fertility and Sterility 92:1520–1524.

Zhang X, Gabriel MS, Zini A (2006) Sperm nuclear histone to protamine ratio in fertile and infertile men: evidence of heterogeneous subpopulations of spermatozoa in the ejaculate. Journal of Andrology 27:414–420.

Zhang Y, Wang H, Wang L, Zhou Z, Sha J, Mao Y, Cai L, Feng T, Yan Z, Ma L, Liu J. (2008) The clinical significance of sperm DNA damage detection combined with routine semen testing in assisted reproduction. Molecular Medicine Reports 1:617–24.

Zhao M, Shirley CR, Yu YE, Mohapatra B, Zhang Y, Unni E, Deng JM, Arango NA, Terry NHA, Weil MM, Russell LD, Behringer RR, Meistrich ML (2001) Targeted disruption of the transition protein 2 gene affects sperm chromatin structure and reduces fertility in mice. Molecular and Cellular Biology 21:7243–7255.

Zidi-Jrah I, Hajlaoui A, Mougou-Zerelli S, Kammoun M, Meniaoui I, Sallem A, Brahem S, Fekih M, Bibi M, Saad A, Ibala-Romdhane S (2016) Relationship between sperm aneuploidy, sperm DNA integrity, chromatin packaging, traditional semen parameters, and recurrent pregnancy loss. Fertility and Sterility 105:58–64.

Zini A, Sigman M (2008) Are tests of sperm DNA damage clinically useful? pros and cons. Journal of Andrology 30:219–229.

Zini A, Libman J (2006) Sperm DNA damage: clinical significance in the era of assisted reproduction. Canadian Medical Association Journal 175:495–500.

Zumbusch A, Holtom GR, Xie XS (1999) Three-dimensional vibrational imaging by coherent anti-stokes Raman scattering. Physical Review Letters 82:4142–4145.

Acknowledgement

I would like to express my sincere thanks and deep appreciation to my dear supervisor Prof. Dr. Dr. Mohammad Eid Hammadeh for the support he provided me at all levels. He gave me the opportunity to be a member of his laboratory and provided me with all the assistance required to write this thesis and finishing this stage of my academic career. He was characterized by endless patience and kindness.

I would like to express my sincere thanks and deep appreciation to my dear supervisor Prof. Dr. Marko Baller for the support he provided me at all levels. He provided me with all the assistance required to finish this stage of my academic career. He helped me in the writing of this thesis in addition to providing motivation and continuous assistance in expanding the content of this research. He was patient, kind with infinite knowledge. Actually, I could not have wished for a better supervisor than him.

I would like to express my sincere thanks and deep appreciation to many wonderful people in the Department of Informatics and Microsystems Technology, University of Applied Sciences Kaiserslautern, Campus Zweibrueken for their support and contribution during the optimization and the measurement processes, especially Mr. Rainer Lilischkis.

I would like to express my sincere thanks and deep appreciation to many wonderful people in in the Assisted Reproduction and Andrology Laboratory, Department of Obstetrics and Gynecology, University of Saarland for their support with staining techniques and invaluable contribution, especially Dr. Mariz Kasoha and Mrs. S. Saifryed.

I would like to thank my friend Mr. Mohammad Al-Smadi for his continuous support throughout my PhD project especially samples collection. Without him I have no chance to be a PhD candidate in this laboratory.

I would like to express my sincere thanks and deep appreciation to Yarmouk University for the financial support for me and my family during my PhD study.

I would like to express my sincere thanks and deep appreciation to all my family members, my parents, my brothers and sisters, for their continuous support and encouragement throughout my study.

And last but not least, I would like to express my sincere love and gratitude to my wife *Rana* and my children *Malak*, *Ahmad* and *Tasneem* for all moral support they provided me during my study. For their continuous support and encouragement and their patience during my long stay abroad.